1-1-2014

An Atomic Force Microscopy Nanoindentation Study of Size Effects in Face-Centered Cubic Metal and Bimetallic Nanowires

Erin Leigh Wood
University of Vermont, ewood1@uvm.edu

AN ATOMIC FORCE MICROSCOPY NANOINDENTATION STUDY OF SIZE EFFECTS IN FACE-CENTERED CUBIC METAL AND BIMETALLIC NANOWIRES

A Dissertation Presented

by

Erin Leigh Wood

to

The Faculty of the Graduate College

of

The University of Vermont

In Partial Fulfillment of the Requirements
for the Degree of Doctor of Philosophy Specializing in Mechanical Engineering

October, 2014

Accepted by the Faculty of the Graduate College, The University of Vermont, in partial fulfillment of the requirements for the degree of Doctor of Philosophy specializing in Mechanical Engineering

Dissertation Examination Committee:

_____ Advisor
Frederic Sansoz, Ph.D.

_____
Dryver Huston, Ph.D.

_____
Rachael Oldinski, Ph.D.

_____ Chairperson
John Hughes, Ph. D.

_____ Dean, Graduate College
Cynthia Forehand, Ph.D.

Date: May 1st, 2014

ABSTRACT

The enhancement of strength of nanoscale materials such as face-centered cubic metal nanowires is well known and arises largely from processes mediated by high energy surface atoms. This leads to strong size effects in nanoscale plasticity; *smaller is stronger*. Yet, other factors, such as crystalline defects also contribute greatly to the mechanical properties. In particular, twin boundaries, which are pervasive and energetically favorable defects in face-centered cubic metal nanowires, have been shown to greatly enhance the strength, furthermore this increase in strength has been shown to be directly influenced by the twin density. However, attempts to control the introduction of beneficial defects remains challenging. Additionally, even minor local variations in the crystalline structure or size of metal nanowires may have drastic effects on the yielding of metal nanowires, which are difficult to measure through tensile and bending tests.

In this study, atomic force microscopy based nanoindentation techniques are used to measure the local plasticity of Ni-Au bimetallic as well as Cu and Ag metallic nanowires. In the first part of the thesis the hardness of bimetallic nanowires synthesized through template-assisted electrodeposition is measured and found to show significant size-effects. It was found that the nanoindentation hardness was governed by materials properties, the observed indentation size effects were dependent on geometrical factors.

The second part of this thesis presents a methodology to control the crystal structure of Ag and Cu nanowires through direct electrodeposition techniques, which were tested directly as grown on the substrate to limit effects of pre-straining. Ag nanowires showed marked size-effects as well as two distinct modes of deformation which we attribute to the defects that arise during crystalline growth. We also show control of the surface microstructure in Cu nanowires which leads to strengths that are more than doubled compared to single crystalline Cu nanowires. Finally, we present support from classic crystal growth theory to justify that the observed plasticity in Ag and Cu nanowires is largely dependent on defects that are nucleated through changes in the growth environment.

CITATIONS

Material from this dissertation has been published in the following form:

Wood, E. L., and Sansoz, F.. (2012). Growth and Properties of Coherent Twinning Superlattice Nanowires. Nanoscale, 4, 5268-5276

Wood, E. L., Avant, T., Kim, G.S., Lee, S.K., Burchman, Z., Hughes, J.M., Sansoz, F.., (2014). Size Effects in Bimetallic Nickel-Gold Nanowires: Insight from Atomic Force Microscopy. Acta Materialia, 66, 32-34

ACKNOWLEDGEMENTS

Firstly, I would like to thank my advisor, Dr. Frederic Sansoz and my dissertation committee comprised of Drs. Huston, Oldinski and Hughes. They have been a source of inspiration and helpful beyond measure throughout this process. Their belief in my abilities has carried me through this journey. Of course, no acknowledgements section would be complete without thanking my family for their both financial and emotional support throughout the graduate school process. I would also thank my previous academic advisors for helping to shape me into the scientist that I've become today.

I am especially indebted to Ti Kawamoto (and our cat Nano!) for always being there for me on good days and bad. I truly could not have accomplished half of what I have without their love and support. Ti's family has also been a constant source of encouragement to me, and of course I am grateful to that.

The UVM support staff has been exceptionally helpful, and CEMS is lucky to have each and every person working there from the Dean's office to the custodians. The Graduate College has also been remarkably helpful in guiding me through this dissertation. Of course, I gratefully acknowledge the Sansoz group members I worked with over the years, Chuang, Jessie, Trevor, Evan, Dan and Aaron, for helpful discussions along the way. Finally, this work was supported through the NSF CAREER grant DMR-0747658 as well as graduate teaching assistantships from UVM's mechanical engineering program, to which I am grateful for the support. Finally, I'm indebted to lab mates past and present and

my Vermont friends for their helpful suggestions throughout my stay at UVM

TABLE OF CONTENTS

List of Tables

List of Figures

CHAPTER 1: LITERATURE REVIEW

1.1 Introduction

Face-centered cubic (FCC) metals such as Ag, Au, Ni and Cu, show enhanced mechanical strength and novel properties when one or more dimensions approaches 100 nm (10^{-9}m), enabling new applications such as high throughput sensors , nanoscale devices and memory . In particular, one-dimensional metal nanowires (NWs) have been of interest due to their enhanced strength while maintaining conductivity. However the plastic behavior of these NWs has been shown through experiment and atomistic simulations to be dependent on the material properties, size, geometry, and presence of defects

This chapter will present an overview of significant findings from theory and experiment with focus on the effects of size and microstructure. A very brief overview of the theoretical studies that motivated this work will be presented, followed by a discussion of twinning in metal nanowires that was published as part of a larger review on superlattice twinning in semiconductor and metallic nanowires. Finally, an overview of contemporary experimental techniques and findings will be presented, followed by a plan for this dissertation.

1.2 Atomistic Investigations of Face-Centered Cubic Metal Nanowire Plasticity

Molecular dynamics simulations have provided a wealth of insight into the yield behavior of FCC metal NWs. It seems that size effects are nearly universally reported in atomistic studies due to the more dominant effects from high energy surface atoms.

Furthermore, atomistic studies have been utilized to measure the effects of shape on the yield stress and orientation . Significant findings from some of these studies are presented in Fig. 1.1, below. In Fig. 1.1a, Gall et al. found significant increase in strength accompanied with changes in yield mechanism as the gold nanowires approach the diameter of single atom chains whereas Cao and Ma predicted that circular Cu NWs exhibit higher yield stresses than similarly sized square NWs, as shown in Fig. 1b Weinberger and Cai also have found that twisting gold NWs with different orientations resulted in either heterogeneous or homogenous deformation that was entirely dependent on the NWs orientation[22]

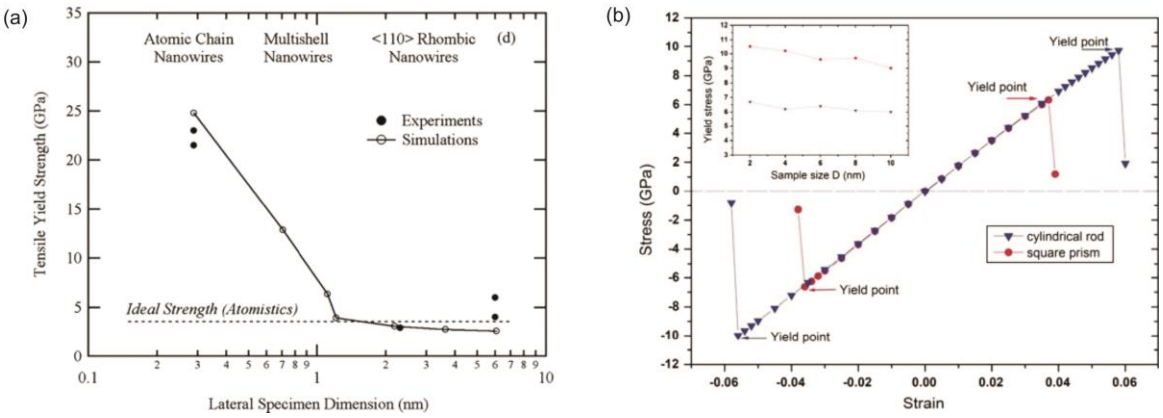

Figure 1.1: Molecular dynamics studies of the yielding behavior perfect FCC metal NWs, investigating the influence of (a) the size, [35] the (b) shape, [25].

Molecular dynamics simulations often model perfect nanowires, with no defects. Experimentally, however, NWs are frequently found to exist with grain boundaries or twin defects. Cao et al. found that polycrystalline Cu NWs deform with lower yield stressed due to dislocation emission from grain boundaries, rather than the free surfaces. Yet, molecular dynamics simulations have shown that some defects can actually enhance the mechanical behavior of metal NWs. The presence of coherent twin boundaries (TBs) has

been noted experimentally in FCC metal NWs with low stacking fault energies, as discussed below, and have been shown to strengthen Cu NWs as dislocations interact with TBs. This was further supported by Deng and Sansoz , who found a linear strengthening with increasing twin density as well as marked sample size effects (Fig. 1.2) A brief overview of twinning phenomena is presented in the following section with a particular focus on electrodeposited FCC metal nanowires

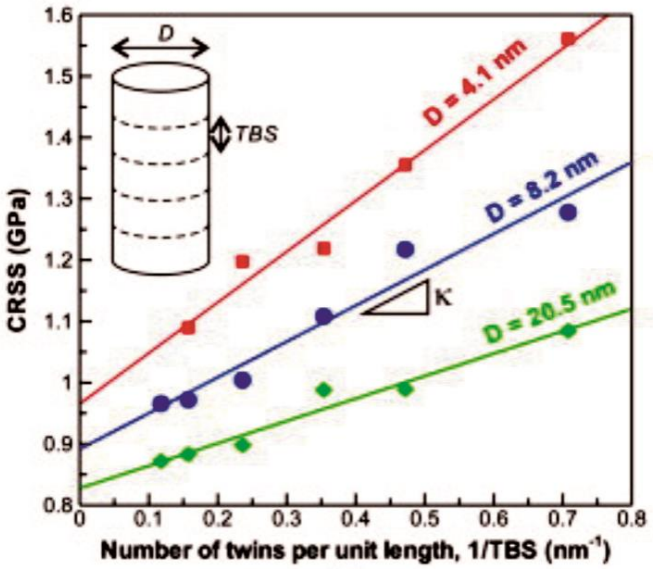

Figure 1.2: Molecular dynamics simulation of the tensile yielding in a twinned [111] Ag NW. [40]

1.3 Excerpt from "Growth and Properties of Coherent Twinning Superlattice Nanowires"

The following section an excerpt from an invited review to the journal Nanoscale, published in by Wood and Sansoz, prior to this thesis .

1.3.1 Twinning in Electrodeposited Nanowires

Electrodeposition (ED) is a well-established technique for the fabrication of metallic NWs with submicron diameters. Size reduction in ED NWs is obtained by directly

electroplating metals inside a solid template containing nanoscale cylindrical pores. Standard templates are either anodized aluminum oxide films with dense, hexagonally-arranged pores, or track-etched polycarbonate membranes with smaller porosities. Microstructure, morphology, and texture of ED NWs are generally controlled by the applied potential or current density, the bath composition, and the pore size and shape.

Twinning has been observed in ED NWs primarily made of Cu, Au and Ag. Evidence of twinning was reported as early as 2001 in Cu NWs produced by direct-current ED. Twin boundaries were observed with a salt bath consisting only of CuSO4·H2O and H2SO4, which exhibited increased conductivity in comparison to the other electrolytes used. However, these authors speculated that twins could be due to plastic deformation and slip, not growth twins, which agreed well with their observations of surface steps formed on the NWs. More recently, optimizing both the bath composition and the applied current density via pulsed ED was found to be successful in synthesizing twinned ED Cu nanopillars with a diameter of 500 nm. These nanopillars featured a [111] growth orientation and dense distributions of planar twins (TBS ~ 9 nm). Similarly occasional twinning has been observed in Ag NWs with certain electrolytes under alternating-current ED. Ag NWs with a [220] growth direction and lengthwise (111)[112] twins were also observed by Wang et al. However, the properties for this type of lengthwise twinning are not part of this review. In Au NWs, Tian et al. used 1-2% gelatin as an additive to increase pore wetting, and observed [111]-oriented Au NWs with occasional lamellar twinning. After further investigation by Wang et al. these NWs were found to present both primary $(111)[11\bar{2}]$ and secondary $(\bar{1}\,\bar{1}\,1)[112]$ twin boundaries. It can also be mentioned that Karim et al. found (111) twins in single-crystalline [110] Au NWs grown under potentiostatic

conditions.

To this date, however, significantly higher densities of twins have been observed in metallic NWs synthesized by non-templated ED, or direct ED method. Remarkably, Zhong et al. recently reported Cu NWs grown by direct ED on a glass substrate with TBS as small as 0.5 nm and an average diameter > 100 nm (Fig. 1.3a). Although direct ED makes the control of diameter more elusive, the lack of post-synthesis processing steps such as template dissolution assure that these twins are all growth twins.

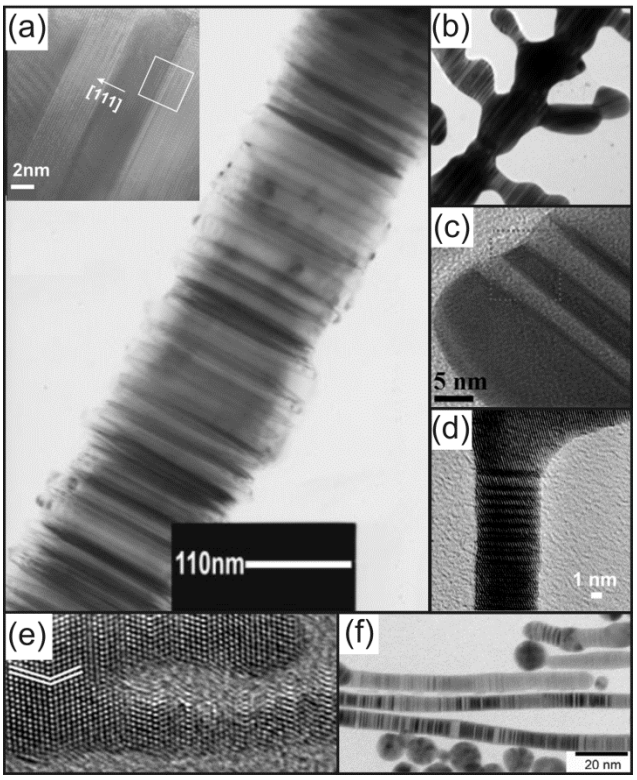

Figure 1.3: Coherent twinning superlattices in FCC metal NWs formed by different methods. (a) Cu NW obtained by binary interface stress during planar non-templated electrodeposition, a magnified view of twin boundaries is shown in inset (reprinted with permission from reference ©Wiley-VHC 2009). (b) Ag nanostructure obtained through ion migrational-transport-controlled 3D electrodeposition with (c) magnified view of twinning (reproduced from reference). Au NWs obtained through (d) mechanical disturbance (reprinted with permission from reference ©American Chemical Society 2010), (e) oriented-attachment of nanoparticles. (reprinted with permission from reference ©Wiley-VHC 2007), and (f) surface ligand rearrangement (reprinted with permission from reference).

There is also some experimental evidence of growth twins in Ag NWs obtained by direct ED . Such Ag NWs were initially grown as dendrite structures as shown in Fig. 1.3b-c. Upon relaxation, however, the dendrite arms fell off through a possible electrochemical Ostwald ripening process. Bamboo-like twinned Ag NWs were also produced by the same approach under high DC potentials and uniform magnetic fields .While no branching was visible, the NWs exhibited twinning in the narrowest areas.

1.3.2 Twinning via Other Synthetic Methods

Chemical reduction techniques are also increasingly popular for producing metallic NWs. A five-fold twinning about the axis of growth is a common twinning motif in FCC NWs, and has been observed in Au, Ag, Pd, Cu, and Fe . Evidence of twinning superlattices obtained by wet chemical methods or physical vapor deposition is more limited, but the number is growing in the literature. Several representative examples are shown in Fig. 4d-f. Au NW networks grown in microemulsions have been shown to have lamellar twinning characteristics, although these are not truly singular straight wires . Also, ultrathin (< 10 nm) Au NWs synthesized through a variation of the oleylamine reduction technique exhibited lamellar twinning. Halder and Ravinshankar first reported twinning in ultrathin Au NWs (Fig. 1.3e). Later, Bernardi et al. reported a method modification producing straight NWs with no branching and extensive twin boundaries (Fig. 1.3f). Twinning was also observed in similarly synthesized NWs, but under mechanical disturbance through stirring which promoted a bent structure . Twin boundaries were exclusively seen near the elbows (Fig. 1.3d), which therefore makes it unclear whether they were growth twins or deformation twins. Other types of twinned structures in Ag such as Ag rice-shaped nanoparticles with a high density of lattice defects were synthesized by Liang et al. through a polyol process with poly(ethylene glycol) used to reduce the Ag salt. These consisted predominately of FCC structure with some HCP phases near the tips. The FCC phase exhibited dense lamellar twins along the [111] direction. A similar structure was found in Ag heterostructures reported by Shen et al formed in the presence of a surfactant (sodium dodecyl sulfate) and a mild reducing agent (ascorbic acid). The reaction produced a wire like needle section conjoined with a much thicker rod like section. The silver

heterostructure also contained both FCC and HCP phases, with a higher density of lattice defects in the needle section. Furthermore, it is common to find Cu NWs produced by physical vapor deposition easily forming twin boundaries and flat {100} and facets.

1.3.4 Proposed Growth Mechanisms

Although there exists no general consensus to comprehensively explain the process governing twin nucleation in metallic NWs, two possible mechanisms have been envisioned so far. On one side, Halder and Ravishankar proposed the oriented attachment of nanoparticles for the growth of twinned Au NWs by oleylamine reduction. These authors suggested that Au cations are first reduced with an amine to form Au nanoparticles with {111} and {100} facets. These faceted nanoparticles are capped with the amine group; however preferential binding to the {100} facets takes place. When ascorbic acid is added to the growth solution, the {111} facets are deprotected and {111} facets from two particles can bind together and fuse in a chain-like manner to build NWs. The formation of twin boundaries during the fusion of {111} facets is energetically possible, and consistent with the creation of {111} /{100} sawtooth facets. This hypothesis is also supported by the existence of branched NWs and NWs with zigzag morphology. Oriented attachment of nanoparticles is also alluded for the twinning structures seen in Ag nano-rice . Sun et al. also suggested that, based on observations of the irregular cross-sectional shape and polyhedral surface morphology, twinned Ag NWs grown through direct ED process under a magnetic field could result from the aligned attachment of smaller Ag nanoparticles building blocks.

On the other side, Bernardi et al. proposed a layer-by-layer growth model with ligand rearrangement at the free surface. This mechanism is shown to be favored when twin

boundary formation is less than the energy for ligand rearrangement, which could occur in systems with low stacking-fault energy such as Au, when coupled with large, bulky asymmetric ligands such as oleylamine. In ED NWs, Wang et al. also alluded that during deposition with a correct stacking sequence of ABCABCABC, adatoms will preferentially seek to deposit on the next correct plan. Thus, if an A plane was last formed, adatoms will seek a B site; however additives do not have this preference and may force the adatom to bind instead to a C site. The energy difference between the B and C sites is small, so this process is not detrimental energetically. Furthermore, Zhong et al. have suggested in their direct ED experiments that perhaps twinning is dependent on an ionic flux causing energy changes at the liquid-solid interface which is "mapped" onto the wire. Formation of twins or stacking faults could then be a way of relaxing the excess energy.

1.3.5 Mechanical Properties

Metallic NWs are central building blocks in photonic and electronic nanodevice fabrication because of their unique electrical and optical properties at the nanoscale. Yet it is imperative for device reliability to employ materials with excellent mechanical properties without sacrificing their desired function, which is made possible with nanotwinned materials. For example, past studies on bulk metals have proved that nanoscale twins can significantly increase mechanical strength and plasticity without disrupting electrical conductivity in the same way that other types of grain boundaries do . Also, past reports in the literature tend to indicate that twinning does not change the plasmonic response of NWs, which agrees with the trend that the plasmonic resonance bands of metals such Au and Ag is mostly size-related. Also, early experimental studies showed that twin planes do not significantly affect the Young's modulus of metallic NWs and nanorods . Nevertheless,

examining the role of nanoscale twins on mechanical strength and plastic deformation in metallic NWs has become a focal point of research over the last few years, primarily because past experimental and theoretical studies in FCC metal NWs have shown clear evidence that, among all types of microstructures (e.g. nanocrystalline, polycrystalline with twins, etc.), twinning superlattice NWs are the strongest. For example, pronounced increases in strength were measured in direct ED Cu NWs and ED Cu nanopillars with lamellar twinning. Even with large diameters (> 200 nm), ED Cu NWs and nanopillars exhibited a three-fold increase in ultimate tensile strength compared to bulk Cu materials, with no significant change in electrical properties . Bernardi et al. also measured the yield strength of ultrathin Au NWs with twins by using ultrasonication, and estimated their tensile strength to be ~1.63 GPa, much higher than that of single-crystalline Au NWs with an equivalent diameter (600 MPa). However experimental strength measurements in twinned NWs are scarce because it is, in general, extremely challenging experimentally to characterize the mechanical properties of NWs with small diameters .

Surprisingly, past atomistic simulation studies on the plasticity of metallic NWs under uniform deformation revealed that twin boundaries do not always strengthen NWs compared to twin-free NWs. Our previous computer simulations using classical molecular dynamics have shown, in particular, that several factors such as TBS, the ratio of diameter over TBS, the stacking-fault energy of the metal, and the surface morphology such as surface facets must be carefully designed to produce strengthening in periodically twinned metallic NWs. In particular, pronounced strain-hardening effects and plastic deformation due to the blockage of dislocations by twin boundaries was seen in Au NWs as TBS decreases, which differs markedly from the brittle failure in twin-free Au NWs of same

diameter (Fig. 1.4a) .

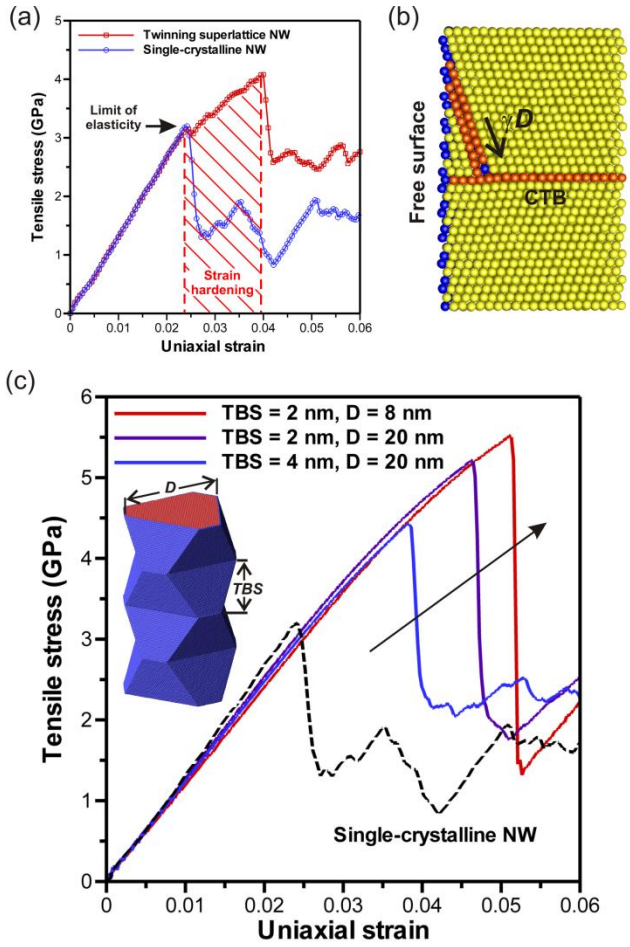

Figure 1.4: Mechanical behavior of twinning superlattice NWs in Au predicted by molecular dynamics computer simulations. (a) Tensile stress-strain curves in twinned and twin-free Au NWs with a diameter of 12 nm. (b) Strain-hardening effects obtained by the blockage of partial dislocations emitted from the free surface by coherent twin boundaries (CTB). (c) Giant size-dependent strengthening due to synergistic effects between CTB and zigzag surface facets in Au NWs. The ultimate strength achieved in twinned zigzag Au NWs approaches the ideal strength of Au.

Computer simulations also showed that the failure mode in circular Au NWs changes fundamentally from brittle-like to extended plasticity with strain hardening when a critical ratio of diameter over TBS is exceeded. Such noticeable increase in ductility could serve an important role as a fail-safe approach to prevent catastrophic failure of NWs under

applied stresses. This phenomenon occurs because partial dislocations, which are usually emitted from the free surface in the absence of internal defects, are blocked by pre-existing twin boundaries, as shown in Fig. 1.4b. The blocked dislocations can only transmit through the twin when the stress is strong enough to activate trailing partial dislocations. Therefore, the stress required to emit surface dislocations must be lower than the stress necessary to transmit partial dislocations through twin interfaces in order to observe strain hardening. Interestingly, if the stress decreases before blocked dislocations can transmit through coherent twin boundaries, dislocations could be reabsorbed by the surface, and leave a pristine NW upon unloading, somewhat reminiscent to a self-healing process . Also, strengthening effects in twinned Au NWs can be very strong, because their unstable stacking energy and stress for dislocation nucleation are low. On the contrary, in metals with high unstable stacking energies such as Cu and Ni, twinned NWs remains brittle. Another salient feature is that the surface morphology such as {111} zigzag facets, can dramatically improve the strength of twinned Au NWs as shown by the results of Deng and Sansoz presented in Fig. 1.4c. It was shown that the stress to nucleate new surface dislocations rises more dramatically as TBS decreases with zigzag {111} facets, because of the nucleation of Lomer (001)[110] dislocations, instead of partial dislocation commonly observed in FCC metals . Ultimately, this synergistic influence of twin, size and surface faceting on plastic deformation mechanisms enables zigzag metallic NWs to approach the theoretical limit of strength, as shown for twinned Au NWs in Fig. 1.4c.

1.4 Metallic Electrocrystallization

Metallic electrocrystallization has been studied in detail over the past few decades and

offers some insight into possible mechanisms of 2-D NW network growth through direct electrodeposition techniques [87-96] Zinc [89-92,94] has been one of the more commonly studied materials, however, silver [59,88,97], and copper [11,93,100] have been recently studied along with a handful of other metals . However, the control of both branching and morphology has proven to be difficult. It seems that the concentration is one of the most important factors in controlling the rate of branching. Higher concentrations have been shown to promote larger electric bilayers during direct electrodeposition [59,91], which then encourages branching. Temperature has been shown to have an effect as well. Lower temperatures [11,93] promote dendritic growth, whereas temperatures closer to the freezing point suppress branching. While most of the literature has been focused on these two parameters and how they affect the ramification of NWs, neither control of the twin density, nor a mechanism of twin growth were presented. However, the authors of [95] do offer excellent discussion to the rise of "bead-like" morphology in hexagonal-close-packed (HCP) Zn nanowires. They suggest that as Zn ions are reduced, the drop in concentration causes a potential drop. If the equilibrium electrode potential drops below the reduction potential growth ceases. Zn^{+} is then replenished at the electrode and growth resumes, promoting growth interfaces. It then stands to reason that this could also be giving rise to the appearance of TBs as seen in copper [11]. In potentiostatically controlled experiments, the ohmic drop is very sensitive to many factors, such as temperature, potential and concentration. However, under galvanostatic control, the ohmic drop is more predictable. This would suggest that twins may not be seen under constant current direct electrodeposition, although it is possible to assume pulsed electrodeposition could produce twinned structures. This would also suggest that the resistivity of the electrolyte salt will

greatly influence the deposition parameters, because low resistive solutions may experience a greater ohmic drop. For example, potentiostatic control has only produced branched Ag NWs [58, 59, 91], yet produces straight Cu NWs [11] owing to the difference in solution resistivity.

1.5. Current Experimental Overview of the Mechanical Testing of FCC Metal NWs

The mechanical testing of NWs is still a challenging task, although significant progress has been made over the last decade. There are many approaches to this from measuring tensile properties in-situ , and NW bending, to specially made tension and compression specimens. Some of the mechanical studies even investigate the influence of the microstructure. Nanoindentation testing, though less common, is advantageous over tensile, compressive and bending tests because it is capable of measuring local plasticity.

1.6 Objectives:

The overall goal of this thesis is to study the effects of size and microstructure on the strength and plastic deformation in FCC metal NWs synthesized by both traditional template-assisted electrodeposition and a newly developed direct electrodeposition methods.

The specific objectives are two-fold: (1) to measure the hardness of electrodeposited FCC metal NWs by AFM nanoindentation, with special consideration to the effects of stacking-fault energy and shear modulus and (2)to find experimental conditions to control the microstructure of FCC metal NWs and measure its impact on the nanohardness in NWs. . Furthermore, this thesis aims to address possible mechanisms of plastic deformation at the nanoscale.

1.7 Plan of the Dissertation

Chapter 2 presents a published study on nanoindentation size effects of Ni-Au bimetallic NWs grown by templated electrodeposition. This study revealed strong indentation size effects in pristine Ni NWs, and suppressed size effects in pre-strained Au NWs. The role of material properties on the experimental yielding behavior is discussed with supplemental support from atomistic simulations supplied by colleagues. Chapter 3 presents an experimental study of the growth and plastic deformation of Cu and Ag NWs grown through direct electrodeposition, with particular focus on how the mechanism of crystallization can influence the plasticity in NWs. Chapter 4 summarizes the major conclusions from this thesis, and offers some suggestions for future research. .

References:

1. Walter EC, Zach MP, Favier F, et al. Metal Nanowire Arrays by Electrodeposition, ChemPhysChem 2003;4:131.
2. Walter E, Penner R, Liu H, et al. Sensors from Electrodeposited Metal Nanowires, Surface and interface analysis 2002;34:409.
3. Ramgir NS, Yang Y, Zacharias M. Nanowire-Based Sensors, Small 2010;6:1705.
4. Li Z, Chen Y, Li X, et al. Sequence-Specific Label-Free DNA Sensors Based on Silicon Nanowires, Nano Letters 2004;4:245.
5. Cui Y, Wei Q, Park H, et al. Nanowire Nanosensors for Highly Sensitive and Selective Detection of Biological and Chemical Species, Science 2001;293:1289.
6. Li Y, Qian F, Xiang J, et al. Nanowire Electronic and Optoelectronic Devices,

Materials today 2006;9:18.

7. Amir Parviz B, Ryan D, Whitesides GM. Using Self-Assembly for the Fabrication of Nano-Scale Electronic and Photonic Devices, IEEE Trans. Adv. Packag 2003;26:233.
8. Lee S-H, Jung Y, Agarwal R. Highly Scalable Non-Volatile and Ultra-Low-Power Phase-Change Nanowire Memory, Nature Nanotech. 2007;2:626.
9. Kovtyukhova NI, Mallouk TE. Nanowires as Building Blocks for Self-Assembling Logic and Memory Circuits, Chemistry-A European Journal 2002;8:4354.
10. Fu J, Singh N, Buddharaju K, et al. Si-Nanowire Based Gate-All-around Nonvolatile Sonos Memory Cell, Electron Device Letters, IEEE 2008;29:518.
11. Zhong S, Koch T, Wang M, et al. Nanoscale Twinned Copper Nanowire Formation by Direct Electrodeposition, Small 2009;5:2265.
12. Zhu T, Li J. Ultra-Strength Materials, Progress in Materials Science 2010;55:710.
13. Sun Y, Gates B, Mayers B, et al. Crystalline Silver Nanowires by Soft Solution Processing, Nano Letters 2002;2:165.
14. Zhu Y, Qin Q, Xu F, et al. Size Effects on Elasticity, Yielding, and Fracture of Silver Nanowires: In Situ Experiments, Physical Review B 2012;85:045443.
15. Zhu J, Shi D, Zhao J, et al. Coupled Effects of Size and Uniaxial Force on Phase Transitions in Copper Nanowires, Nanotechnology 2010;21:185703.
16. Zhang JJ, Yin JH, Ma XC. Molecular Dynamics Study of Size Effect on Uniaxial Tension of Single Crystal Cu Nanowires, Advanced Materials Research 2011;160:682.
17. Wood E, Avant T, Kim G, et al. Size Effects in Bimetallic Nickel–Gold Nanowires:

Insight from Atomic Force Microscopy Nanoindentation, Acta Materialia 2014;66:32.

18. Wen Y, Zhang Y, Zhu Z. Size-Dependent Effects on Equilibrium Stress and Strain in Nickel Nanowires, Physical Review B 2007;76:125423.
19. Wang XW, Fei GT, Xu XJ, et al. Size-Dependent Orientation Growth of Large-Area Ordered Ni Nanowire Arrays, Journal of Physical Chemistry B 2005;109:24326.
20. Shankar MR, King AH. How Surface Stresses Lead to Size-Dependent Mechanics of Tensile Deformation in Nanowires, Applied physics letters 2007;90:141907.
21. Liang H, Upmanyu M, Huang H. Size-Dependent Elasticity of Nanowires: Nonlinear Effects, Physical Review B 2005;71:241403.
22. Weinberger CR, Cai W. Orientation-Dependent Plasticity in Metal Nanowires under Torsion: Twist Boundary Formation and Eshelby Twist, Nano Letters 2009;10:139.
23. Pan H, Sun H, Poh C, et al. Single-Crystal Growth of Metallic Nanowires with Preferred Orientation, Nanotechnology 2005;16:1559.
24. Ji C, Park HS. The Coupled Effects of Geometry and Surface Orientation on the Mechanical Properties of Metal Nanowires, Nanotechnology 2007;18:305704.
25. Cao A, Ma E. Sample Shape and Temperature Strongly Influence the Yield Strength of Metallic Nanopillars, Acta Materialia 2008;56:4816.
26. Weinberger CR, Cai W. Surface-Controlled Dislocation Multiplication in Metal Micropillars, Proc. Natl. Acad. Sci. USA 2008;105:14304.
27. Cao A, Wei Y, Ma E. Grain Boundary Effects on Plastic Deformation and Fracture

Mechanisms in Cu Nanowires: Molecular Dynamics Simulations, Physical Review B 2008;77:195429.

28. Zhang Y, Huang H. Do Twin Boundaries Always Strengthen Metal Nanowires?, Nanoscale Research Letters 2008;4:34
29. Wang JW, Sansoz F, Huang JY, et al. Near-Ideal Theoretical Strength in Gold Nanowires Containing Angstrom Scale Twins, Nat. Commun. 2013;4.
30. Wang J, Sansoz F, Huang J, et al. Near-Ideal Theoretical Strength in Gold Nanowires Containing Angstrom Scale Twins, Nature communications 2013;4:1742.
31. Wang J, Huang H. Novel Deformation Mechanism of Twinned Nanowires, Applied physics letters 2006;88:203112.
32. Marco B, Shilpa NR, Sung Keun L. Nanotwinned Gold Nanowires Obtained by Chemical Synthesis, Nanotechnology 2010;21:285607.
33. Jang D, Li X, Gao H, et al. Deformation Mechanisms in Nanotwinned Metal Nanopillars, Nature nanotechnology 2012;7:594.
34. Peng C, Zhan Y, Lou J. Size-Dependent Fracture Mode Transition in Copper Nanowires, Small 2012;8:1889.
35. Gall K, Diao J, Dunn ML. The Strength of Gold Nanowires, Nano Letters 2004;4:2431.
36. Diao J, Gall K, Dunn ML, et al. Atomistic Simulations of the Yielding of Gold Nanowires, Acta Mater. 2006;54:643.
37. Diao J, Gall K, Dunn ML. Yield Strength Asymmetry in Metal Nanowires, Nano Letters 2004;4:1863.

38. Hyde B, Espinosa HD, Farkas D. An Atomistic Investigation of Elastic and Plastic Properties of Au Nanowires, JOM 2005;57:62.
39. Chen Z, Jin Z, Gao H. Repulsive Force between Screw Dislocation and Coherent Twin Boundary in Aluminum and Copper, Physical Review B 2007;75:212104.
40. Deng C, Sansoz F. Repulsive Force of Twin Boundary on Curved Dislocations and Its Role on the Yielding of Twinned Nanowires, Scripta Mater. 2010;63:50.
41. Wood EL, Sansoz F. Growth and Properties of Coherent Twinning Superlattice Nanowires, Nanoscale 2012;4:5268.
42. Martin CR. Nanomaterials: A Membrane-Based Synthetic Approach, Science 1994;266:1961.
43. Maurer F, Brötz J, Karim S, et al. Preferred Growth Orientation of Metallic FCC Nanowires under Direct and Alternating Electrodeposition Conditions, Nanotechnology 2007;18:135709.
44. Tan M, Chen X. Growth Mechanism of Single Crystal Nanowires of FCC Metals (Ag, Cu, and Ni) and HCP Metal (Co) Electrodeposited, J. Electrochem. Soc. 2012;159:K15.
45. Motoyama M, Fukunaka Y, Sakka T, et al. Initial Stages of Electrodeposition of Metal Nanowires in Nanoporous Templates, Electrochimica Acta 2007;53:205.
46. Hui P, Han S, Cheekok P, et al. Single-Crystal Growth of Metallic Nanowires with Preferred Orientation, Nanotechnology 2005;16:1559.
47. Tian M, Wang J, Kurtz J, et al. Electrochemical Growth of Single-Crystal Metal Nanowires Via a Two-Dimensional Nucleation and Growth Mechanism, Nano Letters 2003;3:919.

48. Toimil-Molares ME, Buschmann V, Dobrev D, et al. Single-Crystalline Copper Nanowires Produced by Electrochemical Deposition in Polymeric Ion Track Membranes, Advanced Materials 2001;13:62.
49. Jang D, Cai C, Greer JR. Influence of Homogeneous Interfaces on the Strength of 500 Nm Diameter Cu Nanopillars, Nano Letters 2011;11:1743.
50. Sauer G, Brehm G, Schneider S, et al. Highly Ordered Monocrystalline Silver Nanowire Arrays, Journal of Applied Physics 2002;91:3243.
51. Wang B, Fei GT, Zhou Y, et al. Controlled Growth and Phase Transition of Silver Nanowires with Dense Lengthwise Twins and Stacking Faults, Crystal Growth & Design 2008;8:3073.
52. Wang J, Tian M, Mallouk TE, et al. Microtwinning in Template-Synthesized Single-Crystal Metal Nanowires, The Journal of Physical Chemistry B 2003;108:841.
53. Karim S, Toimil-Molares ME, Maurer F, et al. Synthesis of Gold Nanowires with Controlled Crystallographic Characteristics, Applied Physics A: Materials Science & Processing 2006;84:403.
54. Ding C, Tian C, Krupke R, et al. Growth of Non-Branching Ag Nanowires via Ion Migrational-Transport Controlled 3d Electrodeposition, Crystengcomm 2012;14.
55. Wang C, Wei Y, Jiang H, et al. Bending Nanowire Growth in Solution by Mechanical Disturbance, Nano Letters 2010;10:2121.
56. Halder A, Ravishankar N. Ultrafine Single-Crystalline Gold Nanowire Arrays by Oriented Attachment, Advanced Materials 2007;19:1854.
57. Bernardi M, N. Raja S, Lim SK. Nanotwinned Gold Nanowires Obtained by

Chemical Synthesis, Nanotechnology 2010;21:285607.

58. Fang J, Hahn H, Krupke R, et al. Silver Nanowires Growth via Branch Fragmentation of Electrochemically Grown Silver Dendrites, Chemical Communications 2009.
59. Sun S, Deng D, Kong C, et al. Magnetic Field Driven Assembly of 1d-Aligned Silver Superstructures, CrystEngComm 2011;13:4827.
60. Wu H-Y, Chu H-C, Kuo T-J, et al. Seed-Mediated Synthesis of High Aspect Ratio Gold Nanorods with Nitric Acid, Chemistry of Materials 2005;17:6447.
61. Sun Y, Mayers B, Herricks T, et al. Polyol Synthesis of Uniform Silver Nanowires: A Plausible Growth Mechanism and the Supporting Evidence, Nano Letters 2003;3:955.
62. Huang X, Zheng N. One-Pot, High-Yield Synthesis of 5-Fold Twinned Pd Nanowires and Nanorods, Journal of the American Chemical Society 2009;131:4602.
63. Zhao Y, Zhang Y, Li Y, et al. Soft Synthesis of Single-Crystal Copper Nanowires of Various Scales, New Journal of Chemistry 2012;36:130.
64. Ling T, Yu H, Liu X, et al. Five-Fold Twinned Nanorods of FCC Fe: Synthesis and Characterization, Crystal Growth & Design 2008;8:4340.
65. Shen M, Du Y, Yang P, et al. Morphology Control of the Fabricated Hydrophobic Gold Nanostructures in W/O Microemulsion under Microwave Irradiation, Journal of Physics and Chemistry of Solids 2005;66:1628.
66. Hong X, Wang D, Li Y. Kinked Gold Nanowires and Their SPR/SERS Properties, Chemical Communications 2011;47.

67. Liang H, Yang H, Wang W, et al. High-Yield Uniform Synthesis and Microstructure-Determination of Rice-Shaped Silver Nanocrystals, Journal of the American Chemical Society 2009;131:6068.
68. Shen XS, Wang GZ, Hong X, et al. Anisotropic Growth of One-Dimensional Silver Rod−Needle and Plate−Belt Heteronanostructures Induced by Twins and HCP Phase, Journal of the American Chemical Society 2009;131:10812.
69. Lu L, Shen Y, Chen X, et al. Ultrahigh Strength and High Electrical Conductivity in Copper, Science 2004;304:422.
70. Lu L, Chen X, Huang X, et al. Revealing the Maximum Strength in Nanotwinned Copper, Science 2009;323:607.
71. Pérez-Juste J, Pastoriza-Santos I, Liz-Marzán LM, et al. Gold Nanorods: Synthesis, Characterization and Applications, Coordination Chemistry Reviews 2005;249:1870.
72. Sun XM, Li YD. Cylindrical Silver Nanowires: Preparation, Structure, and Optical Properties, Advanced Materials 2005;17:2626.
73. Petrova H, Perez-Juste J, Zhang Z, et al. Crystal Structure Dependence of the Elastic Constants of Gold Nanorods, Journal of Materials Chemistry 2006;16.
74. Sansoz F, Huang H, Warner DH. An Atomistic Perspective on Twinning Phenomena in Nano-Enhanced FCC Metals, JOM 2008;9:79.
75. Deng C, Sansoz F. Near-Ideal Strength in Gold Nanowires Achieved through Microstructural Design, ACS Nano 2009;3:3001.
76. Sansoz F, Dupont V. Nanoindentation and Plasticity in Nanocrystalline Ni Nanowires: A Case Study in Size Effect Mitigation, Scripta Materialia

2010;63:1136.

77. Lu Y, Lou J. Quantitative in-Situ Nanomechanical Characterization of Metallic Nanowires, JOM Journal of the Minerals, Metals and Materials Society 2011;63:35.
78. Hyde B, Espinosa H, Farkas D. An Atomistic Investigation of Elastic and Plastic Properties of Au Nanowires, JOM 2005;57:62.
79. Afanasyev KA, Sansoz F. Strengthening in Gold Nanopillars with Nanoscale Twins, Nano Letters 2007;7:2056.
80. Cao AJ, Wei YG, Mao SX. Deformation Mechanisms of Face-Centered-Cubic Metal Nanowires with Twin Boundaries, Appl. Phys. Lett. 2007;90:151909.
81. Deng C, Sansoz F. Repulsive Force of Twin Boundary on Curved Dislocations and Its Role on the Yielding of Twinned Nanowires, Scripta Materialia 2010;63:50.
82. Deng C, Sansoz F. Enabling Ultrahigh Plastic Flow and Work Hardening in Twinned Gold Nanowires, Nano Letters 2009;9:1517.
83. Deng C, Sansoz F. Fundamental Differences in the Plasticity of Periodically Twinned Nanowires in Au, Ag, Al, Cu, Pb and Ni, Acta Mater. 2009;57:6090.
84. Deng C, Sansoz F. Effects of Twin and Surface Facet on Strain-Rate Sensitivity of Gold Nanowires at Different Temperatures, Phys. Rev. B 2010;81:155430.
85. Zheng H, Cao A, Weinberger CR, et al. Discrete Plasticity in Sub-10-Nm-Sized Gold Crystals, Nat Commun 2010;1:144.
86. Lu Y, Song J, Huang J, et al. Surface Dislocation Nucleation Mediated Deformation and Ultrahigh Strength in Sub-10-Nm Gold Nanowires, Nano Research 2011;4:1261.

87. Astley D, Harrison J, Thirsk H. Electrocrystallization of Mercury, Silver and Palladium, Trans. Faraday Soc. 1968;64:192.
88. Bostanov V, Staikov G, Roe D. Rate of Propagation of Growth Layers on Cubic Crystal Faces in Electrocrystallization of Silver, Journal of The Electrochemical Society 1975;122:1301.
89. Chen CP, Jorné J. Fractal Analysis of Zinc Electrodeposition, Journal of The Electrochemical Society 1990;137:2047.
90. Grier D, Ben-Jacob E, Clarke R, et al. Morphology and Microstructure in Electrochemical Deposition of Zinc, Physical review letters 1986;56:1264.
91. Liu T, Wang S, Wang M, et al. Self-Organization of Periodically Structured Single-Crystalline Zinc Branches by Electrodeposition, Surface and interface analysis 2006;38:1019.
92. Matsushita M, Hayakawa Y, Sawada Y. Fractal Structure and Cluster Statistics of Zinc-Metal Trees De-Posited on a Line Electrode, Physical Review A 1985;32:3814.
93. Matsushita M, Sano M, Hayakawa Y, et al. Fractal Structures of Zinc Metal Leaves Grown by Electrodeposition, Physical review letters 1984;53:286.
94. Sawada Y, Dougherty A, Gollub JP. Dendritic and Fractal Patterns in Electrolytic Metal Deposits, Physical review letters 1986;56:1260.
95. Wang M, Zhong S, Yin X-B, et al. Nanostructured Copper Filaments in Electrochemical Deposition, Physical Review Letters 2001;86:3827.
96. Zhong S, Wang D, Koch T, et al. Growth and Branching Mechanisms of Electrochemically Self-Organized Mesoscale Metallic Wires, Crystal Growth &

Design 2010;10:1455.

97. Fang J, Hahn H, Krupke R, et al. Silver Nanowires Growth via Branch Fragmentation of Electrochemically Grown Silver Dendrites, Chemical Communications 2009:1130.
98. Lu Y, Huang JY, Wang C, et al. Cold Welding of Ultrathin Gold Nanowires, Nature Nanotech. 2010;5:218.
99. Wu B, Heidelberg A, Boland JJ, et al. Microstructure-Hardened Silver Nanowires, Nano letters 2006;6:468.
100. Burek MJ, Greer JR. Fabrication and Microstructure Control of Nanoscale Mechanical Testing Specimens Via Electron Beam Lithography and Electroplating, Nano Letters 2009;10:69.
101. Bansal S, Toimil-Molares E, Saxena A, et al. Nanoindentation of Single Crystal and Polycrystalline Copper Nanowires. ELEC COMP C, 2005. Proceedings. 55th: IEEE, 2005. p.71.

Acta Materialia, 66, 32-34, 2014

CHAPTER 2: SIZE EFFECTS IN BIMETALLIC NICKEL-GOLD NANOWIRES: INSIGHT FROM ATOMIC FORCE MICROSCOPY NANOINDENTATION

E. L. Wood[1], T. Avant[1], G.SKim[2], S.K. Lee[3], Z. Burchman[1], J.M. Hughes[4], F.Sansoz[1,5*]

[1]Mechanical Engineering Program, School of Engineering, The University of Vermont, Burlington, VT 05405 USA

[2]Department of Semiconductor Science and Technology, Chonbuk National University, Jeonju 561-756, Korea

[3] Department of Physics, Chung-Ang University, Seoul 156-756, Korea

[4]Department of Geology, The University of Vermont, Burlington, VT 05405, USA

[5]Materials Science Program, The University of Vermont, Burlington, VT 05405 USA

Abstract

The crucial role of slip events emitted from free surfaces in the overall plasticity and strength of low-dimensional crystals such as metallic nanowires (NWs) is well-documented; yet the influence of stacking-fault-energy (SFE) and sample diameter on these local deformation processes are not clearly established. Experimental characterization by nanomechanical bending or tensile testing of NWs, in particular, may not be applicable to NWs made of different metals or exhibiting non-uniform dimensions. In this study, atomic force microscopy nanoindentation is used to probe the local plastic behavior and hardness properties of electrodeposited bimetallic Ni-Au NWs ranging from 60 nm to 358 nm in

diameter and fixed on functionalized-glass substrates. Hardness measurements in individual NW segments are found larger in Ni than Au owing largely to the difference of SFE between these two metals. However, the characteristic length scale associated with indentation size effects is shown to be material-independent and directly linked to the NW diameter. Atomistic study of deformation mechanisms in single-crystalline NWs by molecular dynamics simulations further confirms that the interaction mechanisms between newly emitted dislocations and free surfaces are fundamentally different between Ni NWs and Au NWs during nanoindentation. By decoupling the intrinsic diameter dependence from indentation size effects in the hardness of bimetallic Ni-Au NWs, we find a marked reduction of size effects with a power-law scaling exponent of $n = 0.18$ during the incipient yielding of pristine NWs, in contrast to $n = 0.8$ in plastically pre-strained NWs.

2.1. Introduction

In the last decade, a large number of applications employing single-crystalline nanowires (NWs) have been realized for storage , sensors , gene therapy , and self-assembled devices . Progress in NW synthesis has made possible the design of heterojunctions with two or more metals in a variety of motifs such as core-shell, crown-jewel, and barcoded NWs, lending themselves for breakthroughs in catalysis , immunoassays , and optical tags . Likewise, bimetallic or striped NWs have been of particular interest as multiplexing detection systems.

It is well-established that functional properties in low-dimensional metallic materials are strongly size-dependent, e.g. the absorption of light by Au nanoparticles ; however, gaining fundamental understanding of size effects in plastic deformation of geometrically-confined metals remains an important challenge. Surface-mediated dislocation nucleation has been

shown to govern the plasticity in ultrathin metallic NWs in computer simulations and nanoscale experiments. Past atomistic simulation studies have predicted that surface-mediated plasticity is generally localized and strongly dependent on the NW diameter, the surface morphology, and the stacking-fault-energy (SFE) curve. Yet, these simulations rely on semi-empirical interatomic potentials, whereas direct experimental evidence of SFE and size effects on surface dislocation dynamics in NWs remains limited.

Furthermore, significant advances have been made in mechanical testing of low-dimensional nanostructures, such as nanomechanical tensile testing, nanocolumn compression and NW bending. Although these techniques are useful to gain quantitative insight into the mechanical behavior of single-crystalline NWs, they are not well-suited for characterization of mechanical properties in NWs with different metals, such as bimetallic NWs, or exhibiting non-uniform dimensions. Conversely, nanoindentation , which has been used extensively to investigate size-dependent plasticity in metallic thin films and other patterned quasi-one-dimensional metals , offers a unique advantage for characterization of bimetallic NWs by enabling local measures of plastic behavior in reduced specimen areas. However, nanoindentation of crystalline metals notoriously gives rise to indentation size effects (ISE) that make intrinsic sample size effects more difficult to analyze in metallic NW studies. Furthermore, there is a growing body of evidence confirming that hardness properties are diameter-dependent in metallic NWs and nanopillars, but the role of SFE on underlying plasticity mechanisms is still not fully understood.

This study presents a successful attempt to decouple ISE and diameter effects in the hardness and plasticity of electrodeposited bimetallic NWs by pairing AFM

nanoindentation experiments with atomistic simulations. Our combined experimental-atomistic simulation approach is deployed to examine the role of SFE in bimetallic NWs varying between 60 nm and 358 nm in diameter and constructed with segments of Ni and Au, two face-centered-cubic (FCC) metals with very different stacking fault energies, 124 $mJ \cdot m^{-2}$ and 42 $mJ \cdot m^{-2}$, respectively . Details of the methods are provided in Section 2. Section 3 presents the structure of electrodeposited bimetallic Ni-Au NWs and the hardness of individual NW segments as a function of contact depth and NW diameter. This section also presents the results of atomistic simulations aimed at understanding the effects of crystal orientation and SFE on slip activity in single-crystalline Ni and Au NWs subjected to AFM nanoindentation. The influence of SFE and plastic straining on size effects in bimetallic Ni-Au NWs is discussed in Section 4.

2.2. Methods

The methodology used to conduct molecular dynamics studies that support this work are not included in this manuscript, as they are not the original work of the author. They may be found in full from Wood, E.L., *et al.* Acta Materialia, 66, 32-34, 2014

2.2.1. Nanowire Fabrication

Bimetallic NWs containing two Ni-Au heterojunctions were created by electrodeposition into the pores of an anodized aluminum oxide (AAO) sacrificial template using a previously published method . 50-µm-thick AAO membranes with a nominal pore size of 200 nm, 100 nm (Whatman plc. Maidstone, England) and 55 nm (Synkera Technologies, Inc. Longmont, CO) were used in this study. An electrode was formed by sputter coating

of a thin Au layer (<100 nm) on the membrane side exhibiting the smallest pore size (we note here that the pore shape in these membranes was found to be slightly conical). Ni segments were obtained with a standard Watts bath (Transene, Danvers, CO) at 55°C against a 99.995% pure Ni electrode (Alfa Aesar, Ward Hill, MA) at a voltage of -1 V. These conditions were found to produce single-crystalline NWs in the existing literature . After Ni deposition, the template was immersed in a DI water solution at room temperature, followed by several DI water rinses to wash away the electrolyte solution. A commercially-available Au plating solution, Orotemp-24 (Technic, Inc., Cranston, RI) was used as a bath for deposition Au segments. A platinized titanium mesh (Rolling Thunder Pyrotechnics, Rhinelander, WI) was used as anode with a deposition voltage of -0.7 V . Following this step, the template was again rinsed several times and placed back into the Watts bath under the conditions described above, with care taken to not over-plate the template. The times of electrodeposition were equal to 20 min and 45 min for Ni and Au segments, respectively. Pure Ni NWs were also made to serve as a control.

The NWs were freed by dissolving the template in 25% sodium hydroxide (Alfa Aesar, Ward Hill, MA). The precipitate was collected at the bottom of a vial placed on top of a magnet, and washed several times with DI water followed by several washes in ethanol. The NWs were subsequently stored in pure ethanol. The NWs were characterized by tapping-mode topographical atomic force microscopy (AFM), scanning electron microscopy (SEM) using either secondary or backscattered electron imaging, and scanning transmission electron microscopy (STEM) with energy dispersive spectroscopy (EDS). X-ray diffraction (XRD) patterns were also acquired with a Rigaku MiniFlex II using a Cu Kα radiation. XRD was performed on both bimetallic NWs left in an AAO template, which

had been partially etched to expose the NW tips, and NWs released from the template and dispersed on a flat amorphous substrate to produce powder XRD patterns.

2.2.2. AFM Nanoindentation

Pure Ni NWs were drop-casted on a Si (111) wafer and aligned with a magnet before being allowed to dry in air. Bimetallic NWs were drop-casted on an amino-silanized glass (Sigma-Aldrich, St Louis, MO), taking advantage of the amine-aurophilic interaction (Fig. 1a) to mitigate the possibility of the NW rolling away upon scanning or indentation. Quantitative hardness measurements were carried using a universal scanning probe microscope with a *XYZ* close-loop scanner (Quesant, Santa Cruz, CA). Following the manufacturer's calibration procedure, positioning precisions of 6.5 nm, 9.6 nm, and 0.1 nm were measured along the *X*, *Y*, and *Z* directions, respectively, for a maximum *XY* scan size of 40×40 μm^2 and a vertical *Z* range of 6.11 μm. The AFM was fitted with a cube-corner diamond probe glued on a sapphire AFM cantilever (both the cantilever and the tip were assembled by Micro Star Technologies, Huntsville, TX). The cube-corner tip was scanned over a TGT1 grating with sharp silicon spikes in order to obtain a three-dimensional (3D) image of the tip. Using the tip identification package in the software SPIP, it was determined from this 3D image that the tip apex was 74.5 nm in radius with a half angle of 44.8°. The 3D image was also used to fit an area function associated with the diamond probe, $A_c = f(h_c)$, where h_c is the distance for the tip apex, i.e. equivalent to the contact depth in the following, and f is a second-order polynomial function. The cantilever spring constant was found equal to k = 906.4 N/m by linear elastic finite-element analysis . The force-voltage relation was calibrated before each new nanoindentation series by using the force-matching method with a polished fused-quartz substrate. Extreme care was taken to

ensure that there was no movement of the laser and detector in the AFM head when exchanging the calibration standard for the specimens covered by NWs.

A schematic of the AFM nanoindentation setup developed in this study is shown in Fig. 1a. The nanoindentation procedure on NWs was carried out as follows. The substrate was scanned with a rate between 0.5 Hz and 0.75 Hz at 300 lines resolution. After locating a single NW, a 2 μm × 2 μm scan was performed on an area of interest such that the symmetry axis of the cube-corner diamond probe was parallel to the NW axis. The AFM was then allowed to rest for at least 10 minutes, after which the area was scanned again to ensure that no significant creep effect was present. The bare substrate and the NW were indented subsequently by displacing the piezo-scanner toward the diamond tip at a constant rate of 1 $\mu m \cdot s^{-1}$, leading to a loading rate of ~10 $\mu N \cdot s^{-1}$, until a desired force was attained. In this study, the maximum applied force for nanoindentation F_{max} varied between 15 μN and 40 μN. Each indentation was ideally performed at the maximum height of the NW shown on the AFM scan, Fig. 1b. However, slight offsets as far as 30° from the NW apex were found to be acceptable in measuring the contact depth h_c. Here, h_c corresponds to the residual depth obtained by post-indentation AFM imaging after the diamond probe was withdrawn, and determined by measuring the height difference across the indentation with the grain measurement analysis in the software Gwyddion , Fig. 1c. We assumed that the difference between contact depth and residual depth was negligible for shallow indentations . The contact area A_c was calculated using the measured h_c value and the local hardness H was obtained by the equation:

$$H = \frac{F_{\max}}{A_c} \tag{1}$$

It is worth noting that by using the value of h_c to calculate A_c is valid despite any differences in the geometry of the plastic indent (Figs 3b and 3e).

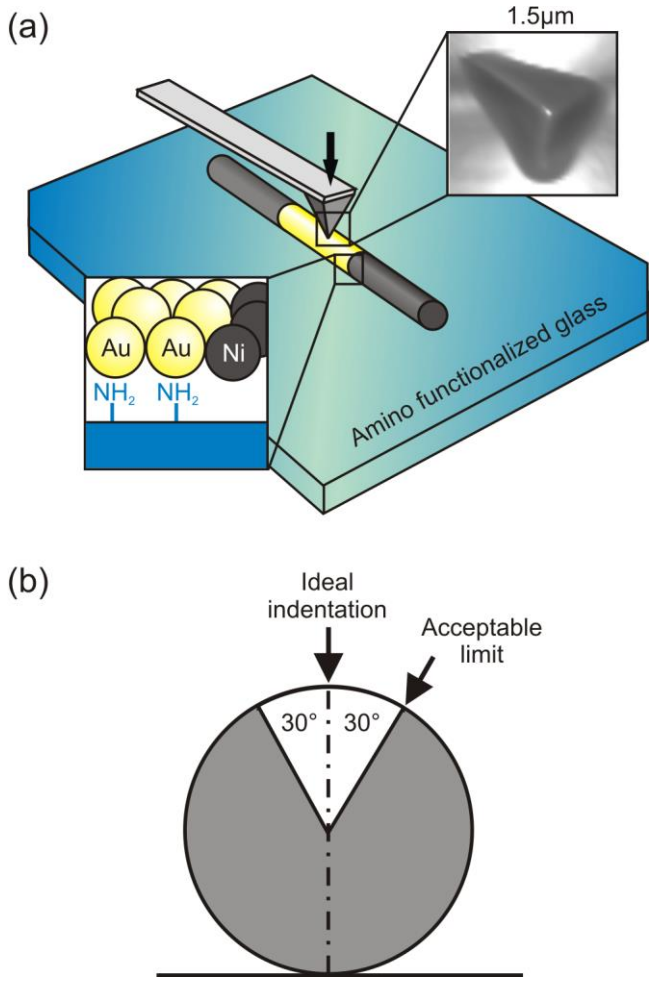

Figure 2.1: AFM nanoindention of bimetallic Ni-Au nanowires.(a) Schematic of experimental nanoindentation set-up showing a bimetallic nanowire with Au segment fixed to an amino-functionalized glass slide. Inset on the right-hand side shows a three-dimensional AFM image of the indenter tip obtained by scanning on a TGT1 Si grating. Illustration of nanowire cross-section (b) showing regions of acceptable and unacceptable indentations and (c) during deformation up to a contact depth h_c.

2.3. Results

The molecular dynamics results that were used to support the following discussions and conclusions are presented in Appendix A, as they were not contributed by the author of

this thesis, yet are required to support the conclusions of this study.

2.3.1. Nanowire Characterization

The bimetallic NWs synthesized in this study were found to be between 16 μm and 18 μm long with some areas of branches or irregular diameters due to imperfect pores in the template, as shown in Fig. 2a. Backscattered electron SEM imaging revealed brighter sections in the middle of the NWs compared to the ends, which made it possible to identify Au segments of ~6 μm in length sandwiched between two Ni segments of equivalent size. The XRD pattern of vertically-aligned bimetallic NWs embedded in the sacrificial template is shown in Fig. 2b. This spectrum displays strong Au(111) and Au(200) reflections, a moderate Ni(200) reflection and a weak Ni(220) reflection. The powder XRD pattern of freed NWs (not shown) revealed a lack of Ni(200) reflection at 51.8°, which conversely points to Ni segments with a preferential (200) growth direction. It is also important to note that the Au(200) and Ni(111) reflections are close in theory at 2 θ = 44.38° and 44.5°, respectively, and thus could likely overlap in our spectrum. Therefore, this analysis suggests that the NW segments were single-crystalline with a preferential growth parallel to either [111] or [001] crystallographic directions in both Au and Ni segments. However, we remained cautious that other NW orientations may have been possible in AFM nanoindentation of individual NW segments, because their crystal structure could not be directly ascertained by AFM imaging.

Furthermore, we observed that NWs released from the template exhibited several bent Au segments, Fig. 2c, possibly due to the NWs were put in an ultrasonic cleaner to break up any cluster, or the drop-casting of the NWs on the substrate. Also a few Au segments were also found to be broken near the Ni-Au heterojunction. The EDS analysis confirmed

that heterojunctions were clearly defined, as shown in inset of Fig. 2c, with little mixing of metals across the Ni-Au interfaces, Fig. 2d.

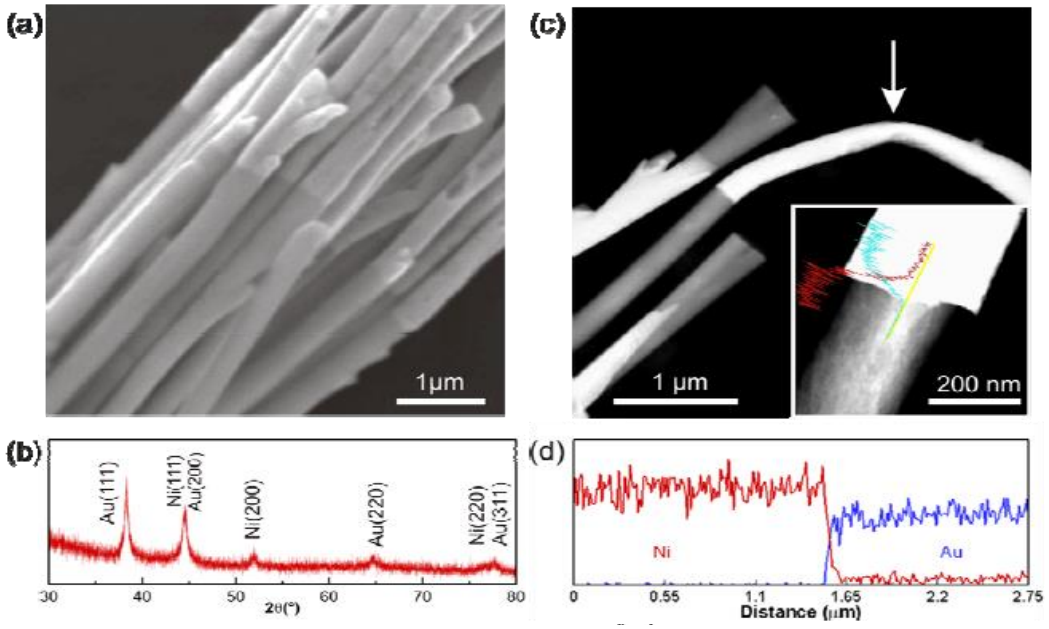

Figure 2.2: Bimetallic Ni-Au nanowires obtained by template-assisted electrodeposition. (a) Backscattered-electron SEM image of a bimetallic nanowire bundle. (b) XRD pattern of electrodeposited bimetallic nanowires inside the sacrificial AAO template. (c) STEM image of Ni and Au segments. Arrow points to a bent Au segment deformed during synthesis. Inset: Close-up view of a Ni-Au heterojunction. (d) EDS profiles for content in Ni and Au atoms showing no significant atom diffusion at the Ni-Au interface.

2.3.2. Experimental Hardness

A total of 41 individual indentations were performed including 7 indents on pure Ni NWs with 3 NWs each being indented one time and 1 NW being indented 4 times with each indent no closer than 1 μm. The remaining indents were obtained across different bimetallic NWs. A single bimetallic NW was typically indented at each end and in the middle to capture the plastic response of both metals. Because of the deposition motif, indents near the ends were most likely, though not necessarily, Ni. Identification of the metal was therefore verified using other factors: The indent appearance, the local hardness, and the

shape of the loading and unloading curves, as explained below. Of the 34 indents performed on bimetallic materials, 24 were identified to be from Au segments. Fig. 3 presents the representative AFM images of indentations in Au and Ni segments obtained with the same applied force ~35μN. The corresponding height profiles in Fig. 3c and f shows that permanent deformation and pile-ups near the indents were more clearly visible in Au segments than Ni ones. This result was found in line with the shape of the loading – unloading curves in Fig. 3g showing that a larger plastic work was dissipated in Au segments than Ni segments

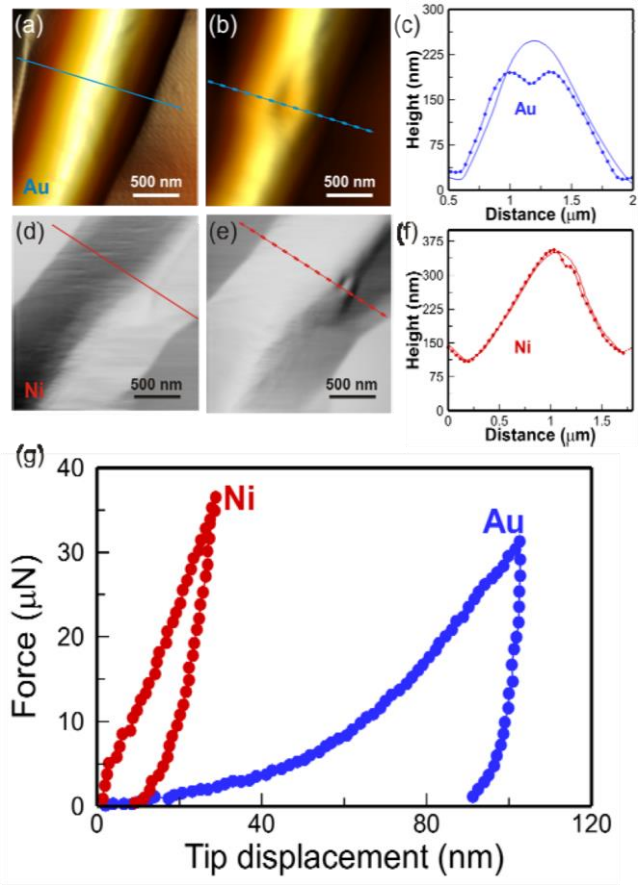

Figure 2.3: Representative nanoindentation response of Ni and Au segments in bimetallic nanowires. AFM images and line profiles obtained before and after indentation in (a)-(c) Au nanowire segment and (d)-(f) Ni segment. (g) Force-displacement curves for the indents shown in (b) and (e).

All hardness measurements from this work are presented in Fig. 4a as a function of the contact depth h_c normalized by the local diameter measured at the indentation site, Fig. 1b. We found that Au segments had an average hardness of 2.84 GPa with a standard deviation of ±0.68GPa for indentation forces between 17.1 μN and 39.27 μN. In contrast, Ni segments proved to be much harder with an average hardness of 12.57 GPa; however Fig. 4 also shows a larger standard deviation ±4.91 GPa for a similar range of forces. This finding suggested a difference in size effects between Ni and Au NW segments, although it was not clear at this stage of analysis whether this difference resulted from extrinsic ISE or intrinsic diameter effects.

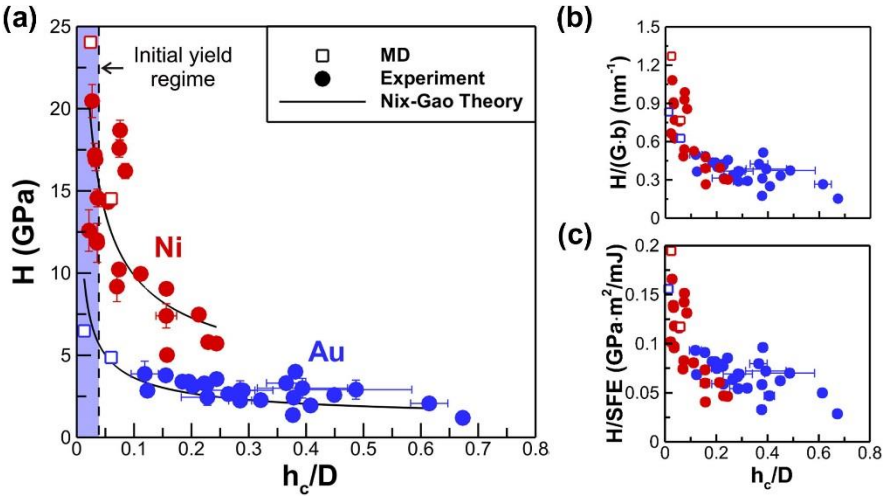

Figure 2.4: Nanoindentation size effects. (a) Hardness vs. normalized contact depth obtained in Ni and Au segments where D is the NW diameter. Nix–Gao theory from Eq. (3) with h* = D is shown using H0 = 2.97 and 1.09 GPa as fitting parameters in Ni and Au, respectively. An estimate of the initial yield regime based on the onset of plasticity predicted by MD simulation is indicated by a shaded area. Hardness of Ni and Au NWs normalized by (b) the product of shear modulus G and magnitude of Burgers vector b, and (c) the SFE as a function of normalized contact depth. In each figure, error bars include measurement uncertainties for both the contact depth due to pile-ups and the NW diameter.

Moreover, Fig. 5 presents the effect of material aging on the nanohardness of Ni NW segments over the course of several years. This figure clearly shows that the hardness was not sensitive to aging. Hence these experimental results ruled out the hypothesis that the

nanoindentation of Ni segments was influenced by the growth of an oxide shell, if any. This also confirms that the structure of the bimetallic Ni-Au NWs was very stable.

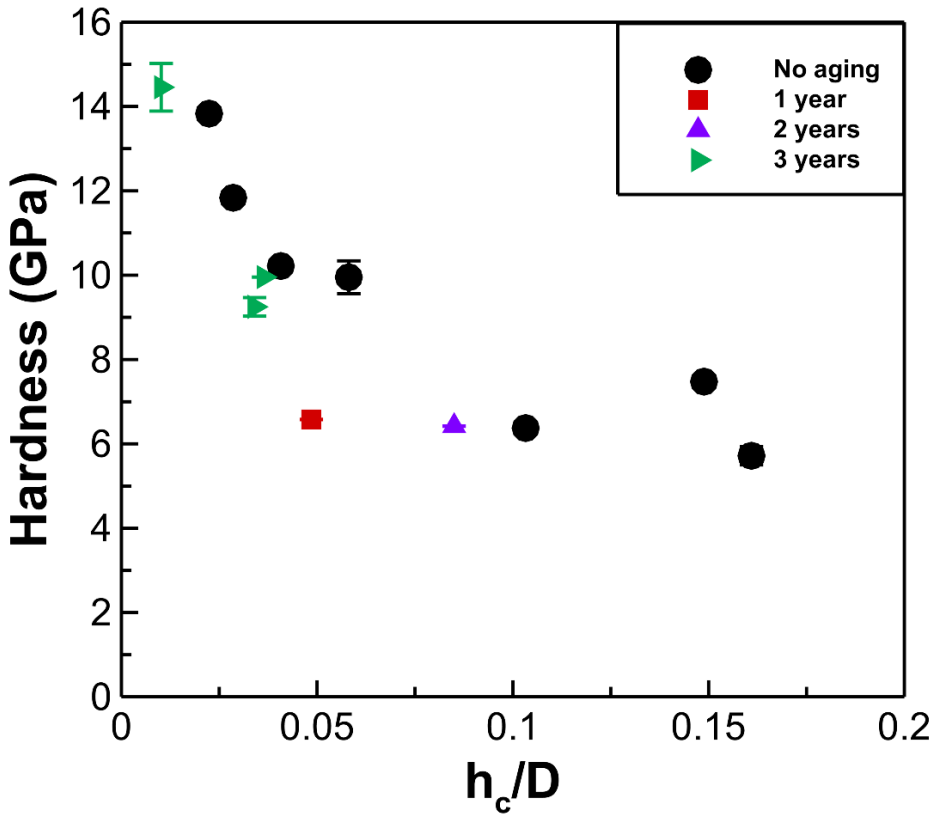

Figure 2.5: Influence of room-temperature aging and oxidation in air on hardness of Ni NW segments as a function of normalized contact depth. Aging effects on the nanoindentation response are found to be negligible.

2.4. Discussion

2.4.1. Data Interpretation in Nanoindentation of NWs on Flat Substrates

Although traditional depth-sensing instrumented indentation on flat substrates is a well-established technique, AFM nanoindentation of metallic NWs on flat substrates requires special attention. Because nanoindentation experiments are force-controlled, the interpretation of total displacements in NW indentation remains a major challenge. This is due to the strong non-linearity from the double-contact deformation at the tip – NW and

NW – substrate interfaces , as well as, from the lateral elastic expansion of the NW because of free surfaces . Also, considerations about how the NW is anchored to the substrate are of critical importance. Past theoretical studies have proved that free or fixed-end boundary conditions can directly influence the force – displacement nanoindentation response . Also, the AFM nanoindentation set-up used raises a question about the role of amine-aurophilic interaction at the NW – substrate interface. The mechanics of this type of interaction are not fully understood and challenging to quantify experimentally, but also proves to play a key role in preventing the NWs from rolling in our AFM nanoindentation experiments. As a result of these above limitations, we were not able to measure the elastic properties of the NW segments, despite our predictions that the elastic behavior of the NWs varies with the NW orientation, as shown in Fig. A.2b and c. Nonetheless, two unique features of AFM nanoindentation were deployed for the characterization of incipient plasticity in bimetallic NWs. First, non-contact high-resolution imaging of surface areas in AFM nanoindentation provided accurate tip positioning prior to indentation, along with a rapid account of permanent deformations after testing. In Fig. 2.3, qualitative differences in terms of plastic deformation processes have been observed between Au NW segments and Ni NW segments. This agrees well with our atomistic simulations showing in Fig. A.1 that the interaction mechanisms between newly-emitted dislocations and free surfaces are fundamentally different between Ni NWs and Au NWs during nanoindentation. Second, recent progress in AFM nanoindentation protocol using diamond probes mounted on AFM cantilevers has been shown to reduce the error in force measurement down to 2%, compared to 37% using the standard protocol . Therefore, the hardness measurement errors shown in Fig. 1.4 are in the determination of the contact depth h_c from digital image

analysis of indentation marks left in the NW surface, which could be as high as 10% for large contact depths due to the plastic pile-ups, and the diameter variations if the NW did not perfectly adhere to the substrate, although this error was found to be to less than 5% in this study, including the variation due to the irregular pores in the template. Furthermore, if we assume a random orientation of NWs from drop casting, the atomistic simulation results presented in Fig. A.2b – d give confidence that the NW orientation had little effect on hardness properties in bimetallic NWs experimentally. Rather, we found that the size and SFE of the materials played a larger role in the nanoindentation response and plastic behavior of the NWs.

2.4.2. Nanoindentation Size Effects

To understand the fundamental role that SFE plays on ISE in bimetallic NWs, we compared the hardness data in Fig. 2.4 to the classic Nix-Gao relation predicting the change in micro-hardness H with the contact depth h_c such that:

$$\left(\frac{H}{H_0}\right)^2 = 1 + \frac{h^*}{h_c}, \qquad (3)$$

where h^* is a characteristic length scale that generally depends on not only the properties of the indented material but also the indenter angle, and is typically of the order micrometers . H_0 is the size-independent hardness obtained for large depths ($h_c >> h^*$). A priori, the ISE observed in our AFM experiments should be influenced by the SFE only, since the cube-corner tip geometry was constant. However, an initial fitting of experimental and atomistic simulation results tended to work poorly and yielded unreasonable values for H_0 and h^* compared to literature values for thin films and coatings in Ni and Au . This was attributed to the fact that the plasticity of nanoindented NWs is governed by discrete

dislocation bursts rather than a continuous plastic flow, suggesting that the Nix-Gao relation used could either break down at small indentation depths or be associated with a SFE-independent characteristic length scale h^*.

We verified the later hypothesis by assigning the parameter h^* in the Nix-Gao relation as the diameter of the largest NW, which represents the physical limit for the extension of the plastic zone. Using this assumption, Fig. 2.4 shows an excellent fit between hardness data and the Nix-Gao relation for both Ni segments and Au segments when fitting values for H_0 are equal to 2.97 GPa and 1.09 GPa, respectively. These H_0 values are also significantly closer to those reported for nanoindentation of Ni and Au thin films mentioned above. In summary, we conclude that ISE observed in bimetallic Ni-Au NWs are SFE-independent and primarily linked to the NW diameter.

2.4.3. Hardness Dependence on NW Diameter

Fig. 2.4 points to two possible regimes of diameter-dependent hardness in bimetallic NWs, as a function of the normalized contact depth imposed by the tip. First, an initial yielding regime is predicted by MD simulations for $2\% \leq h_c/D \leq 5\%$, in which the plastic behavior of pristine, defect-free Ni NW segments is associated with the nucleation of dislocation loops and their absorption on opposite surfaces, as shown in Fig. A.1a – c. The range of contact depths corresponding to this regime is highlighted in grey color in Fig. 2.4 for clarity. Interestingly, Fig. 2.4 shows that one portion of hardness measurements in Ni NW segments lies in the initial yielding regime, whereas the other portion is outside. Prior to the first yielding event, surface dislocation sources manifest themselves by the presence of GNDs under the nanoindentation tip. Under these conditions, the study of Jennings et al. demonstrated that the stress required to emit new lattice dislocations from surface

sources is strongly strain-rate sensitive, and leads to a reduced dependence on sample diameter as the imposed strain-rate decreases. A log-log representation of our hardness *vs.* diameter data in Fig. 2.8a for Ni NW segments deformed with $h_c/D < 5\%$ supports this theory. More specifically, FCC metal nanopillars and NWs are understood to behave with an inverse relationship between strength and diameter according to a power-law scaling of the type D^{-n} with n typically varying between 0.4 and 1.0 . Yet this group of hardness measurements tend to exhibit a power-law scaling exponent of $n = 0.18$, significantly smaller than the values reported above. Also, it is worth noting that the statistical hardness distribution appears to be large, which qualitatively agrees with the occurrence of thermally-activated processes and a minimum energy barrier for surface dislocation nucleation.

Second, Fig.2. 8a also shows that Ni NW segments exhibit a size-dependence with a power-law scaling exponent of $n = 0.80$ when only the data falling outside the initial yielding regime, i.e. obtained with $h_c/D = 5\% \sim 7\%$, is considered. This result is in better agreement with scaling exponents reported in the literature, and suggests that the plastic deformation process in this case is associated with collective dislocation dynamics such as dislocation – dislocation interactions and dislocation multiplications, rather than surface dislocation nucleation. Our MD simulations have shown that this hypothesis is possible in the nanoindentation of Ni NWs with certain tilt rotations when newly-nucleated dislocations are blocked at the bottom boundary, thereby increasing the probability for immobile defects present in the crystal at large contact depths.

Furthermore, Fig. 2.4 shows that all hardness measurements in Au NW segments appear to fall chiefly outside the initial yield regime predicted by MD simulations. Fig. 2. 8b

presents a log-log plot of our hardness measurements in Au NW segments with h_c/D = 15% ~ 20%, showing a power-law scaling equal to n = 0.82 (we note that n = 0.80 was also found for other sets in Au segments at smaller and larger normalized contact depths).This phenomenon could be attributed to the pre-straining of several Au segments that were found to be plastically bent after synthesis as shown in Fig. 2.2c, presumably containing defects. Another possibility suggested by the MD simulation snapshots in Fig. A.2 is that the SFE affects the interaction processes between newly-nucleated dislocation loops and free surfaces. For Ni NW segments, it is possible to assume that the high SFE is responsible for confining the size of the loops inside the crystal, which promotes slip localization. In turn, dislocations resulting from localized slip in FCC metal NWs is more easily absorbed by opposite surfaces due to image forces . On the contrary, the low SFE in Au segments allows the dislocation loop to expand across the NW cross-section, truncating the dislocation arms, and thereby favoring the interaction with other crystal defects, more consistent with the idea of a collective dislocation behavior. However, the lack of experimental measurements in Au NW segments with shallow indentations at h_c/D < 5% precludes drawing a decisive conclusion. Nevertheless, our experiments yields some additional insight by suggesting that the SFE has limited influence on the collective dislocation dynamics and corresponding size-dependence, similar to the reports on the micropillar compression of a vast range of FCC metals.

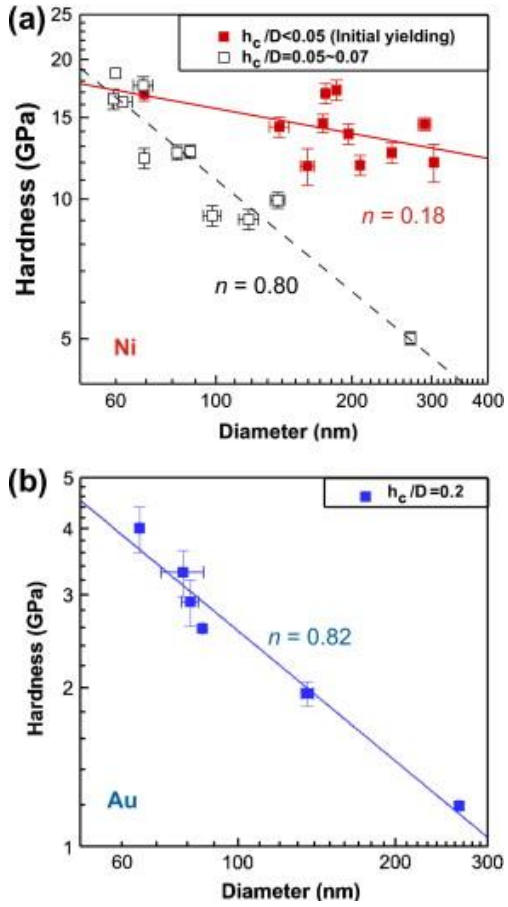

Figure 2.8: Power-law scaling of experimental hardness data with diameter in bimetallic nanowires. (a) Ni nanowire segments with normalized contact depths < 5% (solid symbols) and between 5% and 7% (open symbols). (b) Au nanowire segments with normalized contact depths ~ 20%.

2.4.3. Hardness Dependence on Material Properties

Following the analysis of Rester et al., it is clear that the H should be a function of both the SFE, the shear modulus, G, and the Burgers vector, b. The values used for the SFE were 123.6 and 41.6 mJ/m^2, for Ni and Au, respectively. The magnitude of G*b used was calculated to be 18.848 and 7.776 nm*GPa for Ni and Au, respectively. While, there is a probability of an initial dislocation density, in both metals, they should be on the order of the same magnitude, so this may be neglected as shown by Rester. It should be noted that while the MD simulations show a pristine NW and it is understood that electrodeposited

NWs will have some initial dislocation density, statistically it is very unlikely that this density is high enough to affect more than a few of our data points. In fact, given the relative lack of scattering shown in nickel points, which were found to consist of straight segments in electron microscopy, coupled with the much higher amount of scattering in the Au segments which were had a much higher chance of being pre-strained it is safe to make the assumption that the distribution of initial dislocations was widely spaced enough that it did not affect our measurements with the exception of the occasional bent Au segment. As a measure of control, we attempted to not indent within a micron of a bend to try to minimize the effects of high dislocation densities, we simply used bent segments as a visual guide to indent Au segments in general.

In order to understand the effects of these material properties on both the hardness and the size effects, H was normalized by both G*b and SFE were plotted versus the normalized contact depth. It should be noted that the ratios of both G and SFE for Ni and Au is approximately the same; around 2.9

These plots, shown in Figs.2. 4b-c, confirm that ISE are independent of both G*b and SFE. It also appears, initially, that H could be strongly dependent on either of these factors. However, the normalized H predicted by MD simulations show when normalized by G*b, the points are still significantly different even at depths beyond the initial yielding zone shown in Fig. 2.4a. Yet, when normalized by the SFE, the points beyond the initial yielding zone converge. This is consistent with the difference in yielding mechanisms due to the SFE, and suggests that the hardness, at least at higher levels of plasticity is largely governed by the SFE.

2.5. Conclusions

An experimental approach using AFM nanoindentation was successfully developed to examine the local plasticity and size-dependent hardness of bimetallic Ni-Au NWs with small dimensions and attached to chemically-functionalized flat substrates. Template-assisted electrodeposition was used to prepare single-crystalline bimetallic NWs with a growth direction of either [111] or [001] directions. Their structure was found stable during long-term aging, while the presence of oxide did not appear to affect the hardness of Ni NW segments. The hardness of individual NW segments was found larger in Ni than Au largely owing to the difference in SFE between these two metals; however a major finding predicted by MD simulations was that the interaction mechanisms between newly-emitted dislocations and free surface were fundamentally different between Ni and Au single-crystalline NWs. Furthermore, we have demonstrated that ISE observed in bimetallic Ni-Au NWs subjected to nanoindentation were primarily SFE-independent and only related to the geometrical limit imposed by the NW diameter on the plastic zone. The SFE was found to have limited influence on the power-law diameter-dependence of hardness of Au and Ni NW segments at large plastic deformation. Remarkably, however, the initial yielding of NW segments associated with the emission dislocation loops from surface sources, was found to exhibit little-to-no diameter-dependence. This combined experimental – atomistic simulation study therefore provides new insight into size effects on surface-mediated plasticity of geometrically-confined FCC metals, which is critically important for understanding the mechanical behavior of nanowire-based functional devices.

We recognize the value of expanding the study to include metals that have different ratios

of G and SFE. A continued study using Cu or Au NWs could help to concretely eluciate important relationships between NW nanoindentation hardness and intrinsic material properties.

References

1. Samardak A, Sukovatitsina E, Ognev A, et al. High-Density Nickel Nanowire Arrays for Data Storage Applications. JPCS, vol. 345: IOP Publishing, 2012. p.012011.
2. Lee S-H, Jung Y, Agarwal R. Highly Scalable Non-Volatile and Ultra-Low-Power Phase-Change Nanowire Memory, Nature Nanotech. 2007;2:626.
3. Rex M, Hernandez FE, Campiglia AD. Pushing the Limits of Mercury Sensors with Gold Nanorods, Anal. Chem.Analytical chemistry 2006;78:445.
4. Haes AJ, Stuart DA, Nie S, et al. Using Solution-Phase Nanoparticles, Surface-Confined Nanoparticle Arrays and Single Nanoparticles as Biological Sensing Platforms, J. Fluoresc. 2004;14:355.
5. Cui Y, Wei Q, Park H, et al. Nanowire Nanosensors for Highly Sensitive and Selective Detection of Biological and Chemical Species, Science 2001;293:1289.
6. Sudeep P, Joseph SS, Thomas KG. Selective Detection of Cysteine and Glutathione Using Gold Nanorods, J. Am. Chem. Soc 2005;127:6516.
7. Salem AK, Searson PC, Leong KW. Multifunctional Nanorods for Gene Delivery, Nature Mater. 2003;2:668.
8. Amir Parviz B, Ryan D, Whitesides GM. Using Self-Assembly for the Fabrication of Nano-Scale Electronic and Photonic Devices, IEEE Trans. Adv. Packag

2003;26:233.

9. Liu X, Wang D, Li Y. Synthesis and Catalytic Properties of Bimetallic Nanomaterials with Various Architectures, Nano Today 2012.
10. Tok JBH, Chuang F, Kao MC, et al. Metallic Striped Nanowires as Multiplexed Immunoassay Platforms for Pathogen Detection, Angew. Chem. Int. Ed. 2006;45:6900.
11. Keating CD, Natan MJ. Striped Metal Nanowires as Building Blocks and Optical Tags, Adv. Mater. 2003;15:451.
12. Nicewarner-Pena SR, Freeman RG, Reiss BD, et al. Submicrometer Metallic Barcodes, Science 2001;294:137.
13. Walton ID, Norton SM, Balasingham A, et al. Particles for Multiplexed Analysis in Solution: Detection and Identification of Striped Metallic Particles Using Optical Microscopy, Anal. Chem.Analytical chemistry 2002;74:2240.
14. Link S, El-Sayed MA. Size and Temperature Dependence of the Plasmon Absorption of Colloidal Gold Nanoparticles, J. Phys. Chem. B 1999;103:4212.
15. Diao J, Gall K, Dunn ML, et al. Atomistic Simulations of the Yielding of Gold Nanowires, Acta Mater. 2006;54:643.
16. Liang H, Upmanyu M, Huang H. Size-Dependent Elasticity of Nanowires: Nonlinear Effects, Phys. Rev. B 2005;71:241403.
17. Lucas M, Leach AM, McDowell MT, et al. Plastic Deformation of Pentagonal Silver Nanowires: Comparison between Afm Nanoindentation and Atomistic Simulations, Phys. Rev. B 2008;77:245420.

18. Weinberger CR, Jennings AT, Kang K, et al. Atomistic Simulations and Continuum Modeling of Dislocation Nucleation and Strength in Gold Nanowires, J. Mech. Phys. Solid. 2012;60:84.
19. Wang F, Liu Y, Yin X, et al. The Interface and Surface Effects of the Bicrystal Nanowires on Their Mechanical Behaviors under Uniaxial Stretching, J. Appl. Phys. 2010;108:074311.
20. Branicio PS, Rino J-P. Large Deformation and Amorphization of Ni Nanowires under Uniaxial Strain: A Molecular Dynamics Study, Phys. Rev. B 2000;62:16950.
21. Han J, Fang L, Sun J, et al. Length-Dependent Mechanical Properties of Gold Nanowires, J. Appl. Phys. 2012;112:114314.
22. Sansoz F, Dupont V. Nanoindentation and Plasticity in Nanocrystalline Ni Nanowires: A Case Study in Size Effect Mitigation, Scripta Materialia 2010;63:1136.
23. Wood EL, Sansoz F. Growth and Properties of Coherent Twinning Superlattice Nanowires, Nanoscale 2012;4:5268.
24. Park HS, Klein PA. Surface Cauchy-Born Analysis of Surface Stress Effects on Metallic Nanowires, Phys. Rev. B 2007;75:085408.
25. Wang JW, Sansoz F, Huang JY, et al. Near-Ideal Theoretical Strength in Gold Nanowires Containing Angstrom Scale Twins, Nat. Commun. 2013;4.
26. Zheng H, Cao AJ, Weinberger CR, et al. Discrete Plasticity in Sub-10-Nm-Sized Gold Crystals, Nat. Commun. 2010;1.
27. Zheng H, Wang JB, Huang JY, et al. In Situ Visualization of Birth and Annihilation

of Grain Boundaries in an Au Nanocrystal, Phys. Rev. Lett. 2012;109.

28. Seo J-H, Yoo Y, Park N-Y, et al. Superplastic Deformation of Defect-Free Au Nanowires Via Coherent Twin Propagation, Nano Lett. 2011;11:3499.
29. Lu Y, Huang JY, Wang C, et al. Cold Welding of Ultrathin Gold Nanowires, Nature Nanotech. 2010;5:218.
30. Lu Y, Song J, Huang JY, et al. Surface Dislocation Nucleation Mediated Deformation and Ultrahigh Strength in Sub-10-Nm Gold Nanowires, Nano Res. 2011;4:1261.
31. Lu Y, Song J, Huang JY, et al. Fracture of Sub-20nm Ultrathin Gold Nanowires, Adv. Funct. Mater. 2011;21:3982.
32. Deng C, Sansoz F. Size-Dependent Yield Stress in Twinned Gold Nanowires Mediated by Site-Specific Surface Dislocation Emission, Appl. Phys. Lett. 2009;95:091914.
33. Deng C, Sansoz F. Enabling Ultrahigh Plastic Flow and Work Hardening in Twinned Gold Nanowires, Nano Lett. 2009;9:1517.
34. Deng C, Sansoz F. Near-Ideal Strength in Gold Nanowires Achieved through Microstructural Design, ACS Nano 2009;3:3001.
35. Deng C, Sansoz F. Effects of Twin and Surface Facet on Strain-Rate Sensitivity of Gold Nanowires at Different Temperatures, Phys. Rev. B 2010;81:155430.
36. Deng C, Sansoz F. Fundamental Differences in the Plasticity of Periodically Twinned Nanowires in Au, Ag, Al, Cu, Pb and Ni, Acta Mater. 2009;57:6090.
37. Jiang J-W, Leach AM, Gall K, et al. A Surface Stacking Fault Energy Approach to

Predicting Defect Nucleation in Surface-Dominated Nanostructures, J. Mech. Phys. Solid. 2013;61:1915.

38. Wu B, Heidelberg A, Boland JJ. Mechanical Properties of Ultrahigh-Strength Gold Nanowires, Nature Mater. 2005;4:525.
39. Legros M, Gianola D, Motz C. Quantitative in Situ Mechanical Testing, MRS Bull. 2010;35.
40. Yue Y, Liu P, Zhang Z, et al. Approaching the Theoretical Elastic Strain Limit in Copper Nanowires, Nano Lett. 2011;11:3151.
41. Gianola DS, Sedlmayr A, Monig R, et al. In Situ Nanomechanical Testing in Focused Ion Beam and Scanning Electron Microscopes, Rev. Sci. Instrum. 2011;82:063901.
42. Peng C, Zhan Y, Lou J. Size-Dependent Fracture Mode Transition in Copper Nanowires, Small 2012;8:1889.
43. Mompiou F, Legros M, Sedlmayr A, et al. Source-Based Strengthening of Sub-Micrometer Al Fibers, Acta Mater. 2012;60:977.
44. Kiener D, Hosemann P, Maloy S, et al. In Situ Nanocompression Testing of Irradiated Copper, Nature Mater. 2011;10:608.
45. Lu Y, Peng C, Ganesan Y, et al. Quantitative in Situ Tem Tensile Testing of an Individual Nickel Nanowire, Nanotechnology 2011;22:355702.
46. Dou R, Derby B. The Strength of Gold Nanowire Forests, Scripta Mater. 2008;59:151.
47. Mordehai D, Lee S-W, Backes B, et al. Size Effect in Compression of Single-

Crystal Gold Microparticles, Acta Mater. 2011;59:5202.

48. Wang Z, Mook WM, Niederberger C, et al. Compression of Nanowires Using a Flat Indenter: Diametrical Elasticity Measurement, Nano Lett. 2012;12:2289.
49. Uchic MD, Dimiduk DM, Florando JN, et al. Sample Dimensions Influence Strength and Crystal Plasticity, Science 2004;305:986.
50. Rinaldi A, Peralta P, Friesen C, et al. Sample-Size Effects in the Yield Behavior of Nanocrystalline Nickel, Acta Mater. 2008;56:511.
51. Wu B, Heidelberg A, Boland JJ, et al. Microstructure-Hardened Silver Nanowires, Nano Lett. 2006;6:468.
52. Cimalla V, Röhlig C-C, Pezoldt J, et al. Nanomechanics of Single Crystalline Tungsten Nanowires, J. Nanomater. 2008;2008:44.
53. Zhang H, Tang J, Zhang L, et al. Atomic Force Microscopy Measurement of the Young's Modulus and Hardness of Single Lab 6 Nanowires, Appl. Phys. Lett. 2008;92:173121.
54. Oliver WC, Pharr GM. Improved Technique for Determining Hardness and Elastic Modulus Using Load and Displacement Sensing Indentation Experiments, J. Mater. Res. 1992;7:1564.
55. Choi Y, Van Vliet KJ, Li J, et al. Size Effects on the Onset of Plastic Deformation During Nanoindentation of Thin Films and Patterned Lines, J. Appl. Phys. 2003;94:6050.
56. Mordehai D, Kazakevich M, Srolovitz DJ, et al. Nanoindentation Size Effect in Single-Crystal Nanoparticles and Thin Films: A Comparative Experimental and

Simulation Study, Acta Mater. 2011;59:2309.

57. Soifer YM, Verdyan A, Kazakevich M, et al. Edge Effect During Nanoindentation of Thin Copper Films, Mater. Lett. 2005;59:1434.
58. Gouldstone A, Koh HJ, Zeng KY, et al. Discrete and Continuous Deformation During Nanoindentation of Thin Films, Acta Mater. 2000;48:2277.
59. Bansal S, Toimil-Molares E, Saxena A, et al. Nanoindentation of Single Crystal and Polycrystalline Copper Nanowires. ELEC COMP C, 2005. Proceedings. 55th: IEEE, 2005. p.71.
60. Feng G, Nix WD, Yoon Y, et al. A Study of the Mechanical Properties of Nanowires Using Nanoindentation, J. Appl. Phys. 2006;99:074304.
61. Li X, Gao H, Murphy CJ, et al. Nanoindentation of Silver Nanowires, Nano Lett. 2003;3:1495.
62. Minor A, Morris J, Stach E. Quantitative in Situ Nanoindentation in an Electron Microscope, Appl. Phys. Lett. 2001;79:1625.
63. McAllister QP, Gillespie Jr JW, VanLandingham MR. Nonlinear Indentation of Fibers, J. Mater. Res. 2012;27:197.
64. Nix WD, Gao HJ. Indentation Size Effects in Crystalline Materials: A Law for Strain Gradient Plasticity, J. Mech. Phys. Solid. 1998;46:411.
65. Dupont V, Sansoz F. Molecular Dynamics Study of Crystal Plasticity During Nanoindentation in Ni Nanowires, J. Mater. Res. 2009;24:948.
66. Sansoz F, Dupont V. Nanoindentation and Plasticity in Nanocrystalline Ni Nanowires: A Case Study in Size Effect Mitigation, Scripta Mater. 2010;63:1136.

67. Lian J, Wang J, Kim Y-Y, et al. Sample Boundary Effect in Nanoindentation of Nano and Microscale Surface Structures, J. Mech. Phys. Solid. 2009;57:812.
68. Bauer LA, Reich DH, Meyer GJ. Selective Functionalization of Two-Component Magnetic Nanowires, Langmuir 2003;19:7043.
69. Cortés A, Riveros G, Palma JL, et al. Single-Crystal Growth of Nickel Nanowires: Influence of Deposition Conditions on Structural and Magnetic Properties, J. Nanosci. Nanotechno. 2009;9:1992.
70. Daniel M-C, Astruc D. Gold Nanoparticles: Assembly, Supramolecular Chemistry, Quantum-Size-Related Properties, and Applications toward Biology, Catalysis, and Nanotechnology, Chem. Rev. 2003;104:293.
71. Sansoz F, Gang T. A Force-Matching Method for Quantitative Hardness Measurements by Atomic Force Microscopy with Diamond-Tipped Sapphire Cantilevers, Ultramicroscopy 2010;111:11.
72. Nečas D, Klapetek P. Gwyddion: An Open-Source Software for Spm Data Analysis, Central Cent. Eur. J. Phys. 2012;10:181.
73. McAllister QP, Gillespie JWJ, VanLandingham MR. Nonlinear Indentation of Fibers, J. Mater. Res. 2012;27:197.
74. Askari D, Feng G. Finite Element Analysis of Nanowire Indentation on a Flat Substrate, J. Mater. Res. 2012;27:586.
75. Qu S, Huang Y, Nix WD, et al. Indenter Tip Radius Effect on the Nix–Gao Relation in Micro- and Nanoindentation Hardness Experiments, J. Mater. Res. 2004;19:3423.

76. Zong Z, Lou J, Adewoye O, et al. Indentation Size Effects in the Nano-and Micro-Hardness of Fcc Single Crystal Metals, Mater. Sci. Eng. A 2006;434:178.
77. Graça S, Colaço R, Vilar R. Indentation Size Effect in Nickel and Cobalt Laser Clad Coatings, Surf. Coat. Technol. 2007;202:538.
78. Dietiker M, Nyilas RD, Solenthaler C, et al. Nanoindentation of Single-Crystalline Gold Thin Films: Correlating Hardness and the Onset of Plasticity, Acta Mater. 2008;56:3887.
79. Ma Z, Long S, Pan Y, et al. Indentation Depth Dependence of the Mechanical Strength of Ni Films, J. Appl. Phys. 2008;103:043512.
80. Greer JR, Oliver WC, Nix WD. Size Dependence of Mechanical Properties of Gold at the Micron Scale in the Absence of Strain Gradients, Acta Mater. 2005;53:1821.
81. Rester M, Motz C, Pippan R. Stacking Fault Energy and Indentation Size Effect: Do They Interact?, Scripta Materialia 2008;58:187.
82. Jennings AT, Li J, Greer JR. Emergence of Strain-Rate Sensitivity in Cu Nanopillars: Transition from Dislocation Multiplication to Dislocation Nucleation, Acta Mater. 2011;59:5627.
83. Dou R, Derby B. A Universal Scaling Law for the Strength of Metal Micropillars and Nanowires, Scripta Mater. 2009;61:524.
84. Sansoz F. Atomistic Processes Controlling Flow Stress Scaling During Compression of Nanoscale Face-Centered-Cubic Crystals, Acta Mater. 2011;59:3364.
85. Weinberger CR, Cai W. Surface-Controlled Dislocation Multiplication in Metal

Micropillars, Proc. Natl. Acad. Sci. USA 2008;105:14304.

CHAPTER 3: ATOMIC FORCE MICROSCOPY BASED NANOINDENTATION OF SILVER AND COPPER NANOWIRES SYNTHESIZED BY DIRECT ELECTRODEPOSITION

Abstract

Previous experiments regarding the nanoindentation of bimetallic Ni-Au NWs suggested that pre-straining may have an influence the yielding behavior of FCC metal NWs. In order to study this hypothesis, we use a newly-developed direct electrodeposition method to grow Cu and Ag NWs directly on glass slides which also act as a substrate for nanoindentation hardness testing to ensure that no defects from pre-straining are present. We first test Ag NWs which reveal strong indentation size effects and a nanoindentation hardness of 1.04 GPa, in good agreement with previous nanoindentation results from Ni and Au. We also demonstrate control over the surface structure of Cu NWs. The appearance of a corrugated surface under certain conditions suggests the formation the inclusion of superlattice twin boundaries. We find that Cu NWs that exhibit a highly corrugated surface have around 2.4 times the strength of Cu NWs with a smooth surface. This is well aligned with results from nanomechanical testing of Cu nanopillars with twinned and single crystalline microstructures.

3.1 Introduction

The plasticity of FCC metal NWs is complex and dramatically influenced by local variations in the materials properties, crystallography, and sample size. Thus, there is an

inherent need to reliably make NWs with controlled crystallography and uniform dimension, but is not yet fully realized in common NW synthetic techniques such as template-assisted electrodeposition. Wet-chemical techniques often produce nearly uniform NWs, but these often have a protecting ligand shell which may be undesirable. Also, processing steps used in the synthesis such as centrifugation, or dissolving the templates may result in straining the NWs which could alter their mechanical properties .

This chapter has two major focal points. The first objective is to explore an alternative synthetic route to produce Cu and Ag NWs by direct electrodeposition; a method of electrodeposition that uses a thin layer of liquid electrolyte to grow NWs without the need for a template. Cu NWs previously produced by this technique were able to grow quite long, and have been shown to contain densely packed twins, but it has not yet been adapted for Ag. Thus, Section 3.2, presents a parametric study to adapt the method by Zhong *et al.* [22] to produce Cu NWs and Ag NWs with focus on parameters affecting the microstructure. We find that the applied voltage can control the surface structure when the technique is used to produce Cu NWs. When the technique was adapted to synthesize Ag NWs, it was found that the use of an applied current instead of an applied voltage plays a key role on the branching.

The second objective focuses on the mechanical properties of NWs grown through direct electrodeposition as measured by the atomic force microscopy (AFM) nanoindentation technique. This technique is unique in that it can measure *local* plastic properties along the NW's length. This is crucial in order to understand both the effect of the experimental conditions as well as determining the uniformity of the NWs. Nanoindentation experiments

were carried out with the same methodology as in Chapter 2 of this thesis.

3.2 Direct Electrodeposition and Nanoindentation of Silver Nanowires.

3.2.1 Synthetic Methods

The synthetic set-up by Zhong et al. [22] was used to produce Ag NWs by direct electrodeposition, as illustrated in Fig. 3.1. This set-up consisted of two silver bezel wire electrodes (99.9% pure, 0.4 mm thick, ~1.5" in length. Starr Gems, Tucson, AZ) sandwiched between two glass slides and spaced 2 cm apart (unless otherwise specified), and tightly bound with vinyl electrical tape. This left a volume of ~100 µL to be filled by electrolyte solution. The temperature was controlled with a Peltier element (TEC1-12709 12 V 100W, EVERREDtronics, Shanghai, China) fixed to an aluminum heat sink. Thermocouples (K-type, Omega Engineering, Stamford, CT) were affixed to the Peltier element (TC1) and to the center of the top glass slide (TC2). The temperature of the Peltier had variance of less than 0.2 °C across its face. The Peltier element and electrochemical cell were powered with distinct power supplies (HP Harrison 6203B and Keithley SourceMeter 2420, respectively). The heat sink was submerged half way in an ice-water bath to assist the cooling efficiency of the Peltier element. A photograph of this set up is shown in the appendix.

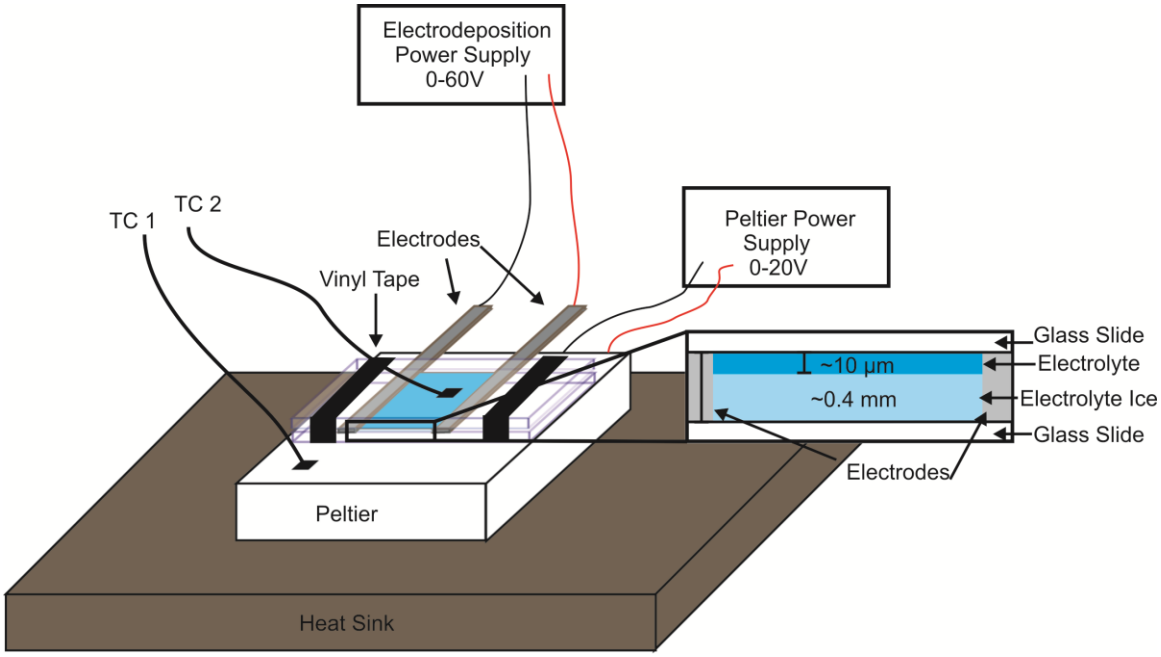

Figure 3.1: Direct electrodeposition set-up. The electrodeposition cell is comprised of two glass slides with metal electrodes and placed on a Peltier cooler. A binary electrolyte is injected in between the slides and partially frozen by the Peltier. Thermocouples (TC) are attached to the Peltier (TC1) and the top glass slide (TC2).

Standard glass microscope slides were used as both a growth substrate and a vessel in which to hold the electrolyte. Care was taken to ensure that the new slides were clean and free of particulate matter by a triple rinse with DI water. All glassware used for holding and mixing reagents was washed with *aqua regia* followed by acetone and DI water rinses. Each time, freshly made *aqua regia* was prepared by adding concentrated nitric acid to concentrated hydrochloric acid in a 3:1 volumetric ratio. Silver nitrate (99.995%, Alfa Aesar, Ward Hill MA) was chosen as an electrolyte due to its high solubility in water along with its relatively low toxicity compared to other common silver electrolytes such as potassium argentocyanide (KAgCN). A simple binary salt also limits adsorbed atoms and subsitutional atomic defects. The electrolyte was either freshly prepared, or stored in a vial wrapped with several layers of heavy-weight paper to reduce photodegredation. $AgNO_3$

solutions were discarded after two weeks of aging.

The electrolytic cell (shown in appendix) was constructed by placing two flat wire electrodes on the top of a plain glass microscope slide (Corning Glassware, Corning, NY or Celestron, Torrance, CA). These were held in place by carefully aligning a second glass slide on top of the wires and binding the two glass slides together tightly with vinyl electrical tape (3M, Maplewood, MN) on each end. It is critical that (1) the wires are pulled taunt and overlap on each end of the glass slide, creating a completely enclosed space between them, and (2) the gap in the glass on both the top and bottom ends of the cell left open. Tape was only used on the ends of the slides. Since the wire electrodes were reused several times (each time, the cathode and anode were switched, as the anode slowly erodes), they were cleaned by first soaking in a 5% sulfuric acid solution, followed by rinsing with DI water. The sides of the bezel wire were manually honed, as necessary, with fine abrasive paper. After the cell was completed, it was carefully filled with by *slowly* injecting ~100 µL of 0.05 M $AgNO_3$ (unless otherwise specified) with a micropipette. The bottom of the cell was then gently tapped on a folded paper towel to get rid of any trapped air, and topped up with more electrolyte solution, until it was completely filled. It is critical that no trapped air is present within the electrolyte. A thermocouple was stuck to the top of the glass slide and secured with conductive metal tape, which was then sealed with an additional layer of vinyl tape, as the adhesive on the metal tape tended to fail at lowered temperatures. The conductive metal tape was required in order to obtain an accurate temperature measurement; vinyl tape alone was too thermally insulating.

A very thin layer was water was then dropped on the surface of the Peltier element. This

acted to help hold the electrochemical cell in place. The cell was placed directly on the water, and the Peltier element was allowed to several degrees below freezing, until TC2 (top glass slide thermocouple) read 8-10°C, and then the voltage to the Peltier element was lowered to read ~-1°C and TC2 was allowed to slowly reach -0.5°C. The quick freezing allowed the water layer on the Peltier to freeze, holding the electrochemical cell in place. However, bringing TC2 to freezing too quickly resulted in imperfect freezing of the electrolyte (see discussion). The cell was allowed to freeze for ~15-30 minutes, and visually inspected for clarity of ice. If striations in the ice layer were present; the cell was removed from the Peltier and allowed to come back to room temperature, and refilled with electrolyte if necessary, and the freezing cycle was repeated until ice with perfect clarity was achieved. (Note: A white LED flashlight was shone on the sample at an angle to observe clarity of ice). After this, the anode and cathode were connected to the power supply with alligator clips. The desired potential or current was applied for a time of 20 minutes for the parametric study. TC2 was closely monitored at this time, and $V_{Peltier}$ was manually adjusted to compensate for any temperature change. After this, the alligator clips were removed, and the Peltier element was cooled to ~-10°C, and the electrolyte was completely frozen. The vinyl tape was then cut, and the top glass slide was *carefully* removed. The electrolyte ice as then allowed to melt and evaporate, leaving behind Ag NWs on the glass substrate.

3.2.2 Characterization Methods

Characterization of the produced nanostructures from both Cu and Ag experiments was

completed first by visual inspection, assisted with an optical microscope with 1600x magnification, which was easily accomplished without removing the tape affixing the two glass slides together. Dendritic growth was typically distinguishable by eye. Specimens containing NWs that appeared to be straight were the replaced on the Peltier element and cooled to well below freezing. Then the tape was removed and the top glass slide was carefully pulled off, and the specimen was allowed to dry in atmosphere.

AFM images of the NWs were taken with a tapping mode NSC-16 probe (Mikromasch, Sofia, Bulgaria) with a nominal radius of less than 8 nm using a Quesant universal scanning probe microscope with a closed-loop metrology scanner with a range of 40 μm x40 μm . The AFM was carefully calibrated with precisions of 6.2 nm, 7.8 nm and 0.1 nm for the X, Y and Z directions, respectively. The tips radius confirmed by imaging the tip with a TGT1 test grating (NT-MDT, Moscow, Russia) and measuring the tip with the tip characterization function in the software package SPIP (Image Metrology A/S, Hørsholm, Denmark). The two tips used had a radius of 7.3 and 7.6 nm, meaning this was the smallest features that could be detected. The AFM was used to both image and measure the diameters of the NWs, although the length was not able to be determined because they were longer than the scan area. The lengths were estimated from optical microscopy. The average diameter of the NW was determined by using a line profile tool in the software package Gwyddion. A profile was taken across the transverse axis of the NW, and measured from the peak to the bottom of the profile. The difference in height was taken to be the diameter of the NW, and 10 measurements over 40 μm of NW length were averaged.

Powder x-ray diffraction (XRD) spectra were obtained using a Rigaku Miniflex2 x-ray

diffractometer, after they were imaged by AFM. Samples were prepared for XRD analysis by growing NWs with a thin glass microscope coverslip as the substrate, and then allowing them to dry and applying a thin layer of layer of hairspray. The hairspray was used to ensure the samples were well adhered to the glass slide and would not fall off during characterization and also helped protect against oxidation. After this, samples with hairspray were discarded and not used for AFM or nanoindentation analysis.

3.2.3a AFM Nanoindentation methodology

The AFM nanoindentation methodology was carried out according to the procedure described in a previous study . A diamond indenter probe (Micro Start Technologies, Huntsville, TX) with a radius of 74.5 nm (measured as described above) was used to both image and indent the individual NWs. Each sample was indented on the glass substrate that it was grown on after characterization was completed with the previously mentioned methods. A total of 20 individual indentation points were obtained from10 Ag NWs.. NWs that had any obvious defect upon imaging, such as knobs, diameter deviations or bends were not indented.

Two NWs, grown near each other in the same run were indented multiple times along approximately 60 μm of their length (this was not the total length, only the length indentations were completed. These NWs were nearly identical in length and diameter, and indented with similar forces that were successively increased along the length.

3.2.3b Nanoindentation data analysis

The nanoindentation hardness was determined using the methodology described previously . Data from indents that either resulted in breakage of the wire (n=3), or were not able to be measured directly were discarded. These indents were characterized by a localized shear band, as seen in Fig 3.5, rather than the expected distributed plasticity. It was impossible to directly determine the value of h_c, the plastic indentation depth from this deformation. This data however, was treated according to Hertzian elastic theory by using the elastic portion of the loading curve to determine an estimate of the true indentation depth. This treatment is fully described in the appendix.

3.2.3 Results and Discussion

3.2.3a Synthesis

The successful synthesis of Ag NWs through electrodeposition was contingent on providing optimal conditions. In this study, we have successfully produced both thick NWs (D_{NW}=461.33±28.3 nm) and fine NWs (D_{nw}=141.70±49.2 nm) with applied currents of I=0.12 mA and 0.08 mA, respectively. The other conditions used will be discussed below. Generally, it was found that conditions that promoted fast growth yielded products that had some degree of branching, as shown in Table 3.1. The lengths in Table 3.1 were estimated from optical microscopy. The conditions were elevated temperature, concentration, and applied voltage or current. Branching also was found in cases that the electrolyte had not been frozen carefully and had either bubbles or striations, as shown in Fig. 3.3.

Table 3.1: Summary of products from 20 minutes of direct electrodeposition of Ag

	NWs (Fig. 3.2a,b)	Branched NWs (2c)	Dendrites (2d)	Branched μWs (2e)
TC2 (°C)	-0.5	-0.5	0-40	40-80
[$AgNO_3$] (M)	0-0.001	0.001-0.05	0.05-1	0.01-0.1
V_{app}(V)	N/A	0.5-0.9	2-20	N/A
I_{app} (mA)	0.08-0.12	0.12-0.15	N/A	0.13-0.2
Approximate length (μm)	200	350	500	500-800

Electrocrystallization of metals has been studied for a number of years, and literature on this topic has been treated more fully in chapter 1 of this thesis. Here, we discuss in more detail the conditions that give rise to the observed microstructures. The first, and most important condition that was found to give smooth nanowires without branching in Ag was the ice quality. If the electrolyte was frozen too quickly, the ice appeared cloudy, and exhibited striations. If there were striations (Fig. 3.3c) or even bubbles present, this strongly indicated that the ice had grain boundaries present. In the case of grain boundaries, the concentration of metal ion may be higher at the grain boundary due to the partitioning effect (Fig 3.3a). This, in turn, would disrupt the bilayer, and cause a branch. Furthermore, is possible to make the assumption that the grain boundaries in the ice may act as a template for the growth.

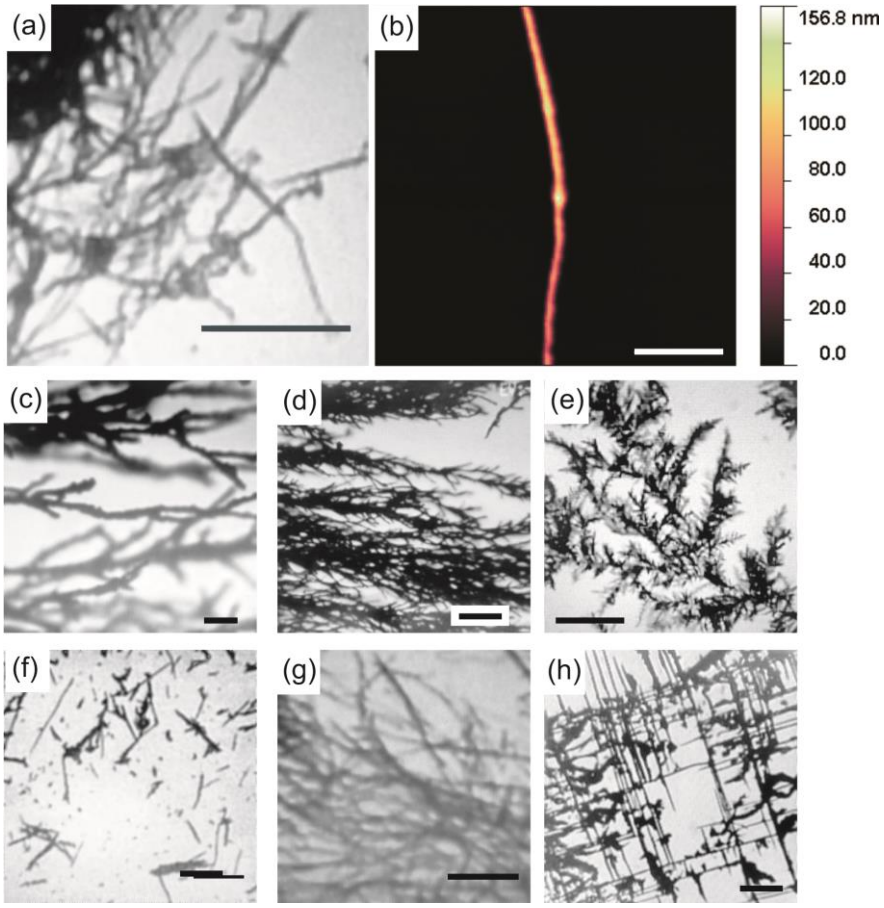

Figure 3.2: Silver nanostructures by direct electrodeposition. (a) Branched NWs obtained at 0.1 mA, scale bar is 10 µm. (b) AFM image of a smooth NW obtained at 0.8 mA, scale bar is 5 µm. (c) Lightly branched NWs obtained at 0.7 V, scale bar is 2 µm. (d) Highly branched growth obtained with 1.4 V, scale bar is 2 µm. (e) Dendritic growth obtained with 6 V, scale bar is 20 µm (f) Short NWs obtained at 0.08 mA, scale bar is 2 µm (g) smooth NWs obtained at 0.1 mA, scale bar is 5 µm, (h) branched µWs obtained at 0.2 mA, scale bar is 10 µm

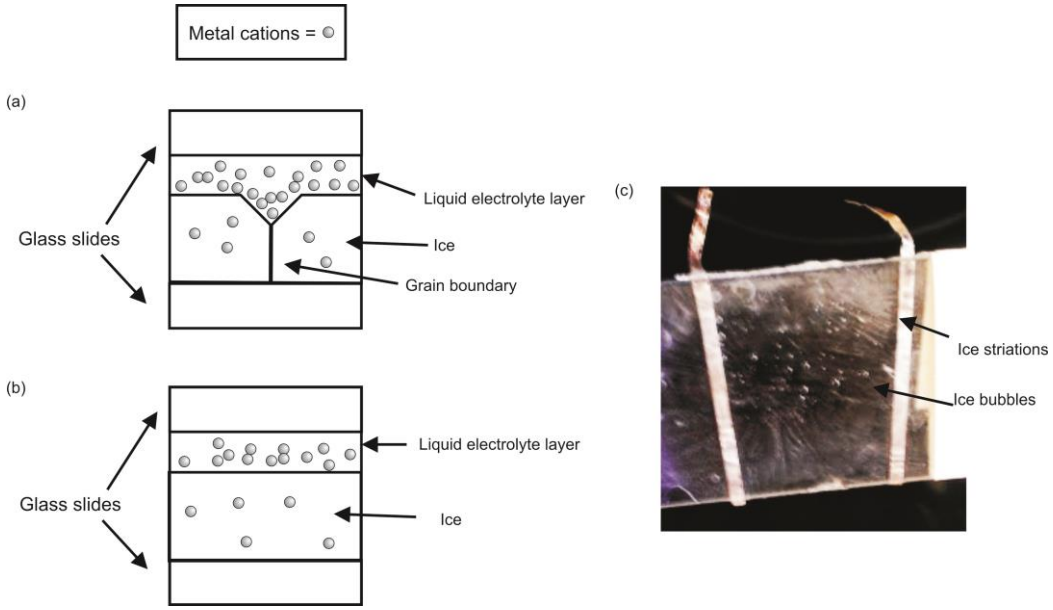

Figure 3.3: Partitioning effect in direct electrodeposition. (a) Grain boundaries (or air pockets) will lead to valleys in the surface of the ice with localized high concentrations of ions. Smooth ice (b) exhibits more uniform concentration, lowering the chances of dislocations in crystal growth. (c) Photograph showing striations due to the grain structure of ice.

Furthermore, we investigated the influence of the applied voltage and temperature. The most notable conclusion was that NWs would only form when a *constant current*, not voltage was applied. This result was surprising given the prevalence of potentiostatic conditions within template-assisted electrodeposition experiments, as well as, the successful synthesis of Cu NWs through direct electrodeposition with a constant V, reported by Zhong et al. [22]. In order to explain this apparent discrepancy, it is important to consider the fact that, in potentiostatic experiments, the variance of I, is dependent on the electrolyte's resistance, and varies with potential. Therefore, it is critical to use a 3-electrode cell with a standard electrode to be able to measure the true potential. The ohmic drop from solution resistance under applied current conditions, is constant under any

current. As these cells are currently small scale and consist of only µLs of volume, it is impractical to attempt a 3-electrode set-up. Also, a full study of the electronic characteristics of the electrolyte solution is beyond the scope of this thesis. However, our results suggest that local variations in the resistance of the electrolyte due to ionic concentration produce a much higher ohmic drop in $AgNO_3$ solutions than in $CuSO_4$, owing to the increased molar conductance of $AgNO_3$ solutions. The higher degree of branching in Ag when a potential is applied vs even high currents supports this hypothesis. In fact, increasing the current from 0.08 mA to 0.12 mA only increased the diameter of the NWs, not the degree of branching, whereas increasing the voltage from 4V to 8V increased both diameter and density of secondary growth patterns.

The temperature, as measured at TC2 also influenced the growth, although this may be due to the temperature governing the crystallization of the ice. Both the cooling rate and the stabilized temperature was important, although the cooling rate was more critical as it influenced the final ice structure. As the response of the Peltier element is extremely rapid, the electrochemical cell may be quickly cooled by applying a $V_{Peltier}$ such that TC1~-10°C, until TC2 ~10°C (~ 2-5 min) after which, TC1 must be adjusted to be ~-1°C, and the cell is allowed to reach -0.5°C (~10-12 min). Exact conditions to obtain perfect crystalline ice in the cell are not fully understood, although higher successes were found with very clean glass slides and slow freezing. The final equilibrium TC2 does not influence the ice structure, yet it does influence the thickness of the liquid electrolyte layer. According the study by Zhong et al. [29], working at -0.4°C should result in a liquid layer of ~10µm. Decreasing TC2 will shrink this layer and force ions to concentrate, resulting in fan-like

dendritic growth (appendix), and increasing TC2 resulted in a thicker liquid layer with a metal ion concentration gradient. This gradient then could lead to dislocations in growth causing bifurcations, as well as yield thicker growth which could not be measured through AFM.

The concentration of the electrolyte was also found to strongly affect the branching, and this is thought to be due to the increase in the length of the double layer [25]. In this system, the concentration was stabilized due to the fact that as metal ions were reduced from solution, Ag was electrowinned from the anode, replenishing the concentration. Ag is electrowinned efficiently enough that even at 0 M $AgNO_3$ concentration a few short NWs were formed within the 20 minutes the experiment ran, although these were very sparse and short. It was found that idea concentration of Ag NWs is 0.05 M, the same as the direct electrodeposition of Cu NWs.

From this study, it can be concluded that the critical factor in NW growth is stability in the electrolyte layer. This results in the need for perfect single crystalline ice with a concentration that is low enough to not promote dislocations as the NW is growing. By working just below the freezing temperature of the electrolyte solution the thickness of the electrolyte layer is controlled to be on the order of a few hundreds of nm, allowing for single layer growth. Conditions of -0.5°C, with applied current of 0.08 mA and [$AgNO_3$] for 20 minutes led to NWs with diameters of 141.70±49.2 nm (measured by AFM) and lengths ~500 μm (estimated by optical microscopy). While the diameter was fairly consistent, the length was not, and there were some lengths found to be as short as 10 μm, however mostly long NWs were observed. It is possible that the short NWs were branches,

which were very rarely observed (only 4-5 NWs out of several thousand in a batch had branches), that had fallen off through Oswaldt ripening

3.2.3b AFM nanoindentation

Nanoindentation experiments were used to determine the local plastic properties of the NW to give further insight into the interplay between sample size, material properties and indentation size effects on the mechanical behavior. A previous nanoindentation study on silver nanowires synthesized through wet-chemical reduction resulted in hardness values of 800 MPa, which is close to the bulk value, although tensile and bending tests show yield strengths between 0.71 and 4.8 GPa 28,29], which when considered by Tabor's relationship would be equivalent to hardness values of 2.1 to 14.4 GPa, much higher than the previous report of nanoindentation hardness in silver.

Unlike our previous experiments on nanoindentation of Ni and Au there were apparently two modes of plastic deformation at play. In the first mode, distributed plasticity, a footprint of the indenter probe was visible in the post-indentation AFM image, and the hardness was determined by using the h_c and $F_{max=}$ values, as in our previous experiments. The second mode, localized shearing, left behind no obvious indenter footprint but what appeared to be shear bands. These are shown below, in Fig. 3.4. Not only did this appear in the post-indentation imaging, it was apparent from the loading curves. These loading curves were characterized by an elastic loading followed by a sharp decrease in the measured applied force, after which there was a long plateau before finally increasing together.

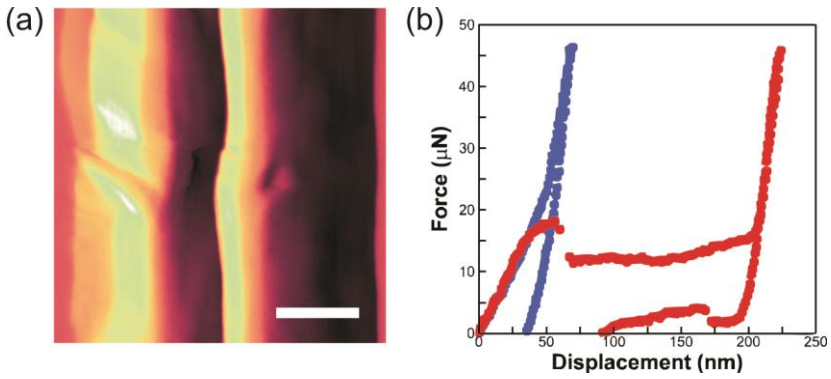

Figure 3.4: Plastic deformation in Ag NWs. (a) AFM derivative topography image shows the two modes of deformation in silver. Scale bar is 0.5 μm. (b) loading curves corresponding to each to the indents shown in part (a) The red curve corresponds to the indent on the right in (a) and the blue curve corresponds to the indent on the left in (a).

In order to understand the underlying causes of each observed mechanism we then analyzed the nanoindentation loading curves with special attention to the yield force required in each instance. The full treatment is shown in appendix A. However, the hardness values obtained through this treatment are estimates and were only used qualitatively. Another possibility explanation of these two behaviors is that the indentured tip was placed slightly off-center and slid along the side of the wire.

Another logical explanation of the shear banding effect is that could be due to the crystallographic orientation of the NWs. Chapter 1 of this thesis offers a more detailed discussion on the growth of NWs, although it is not uncommon to see a mix of growth orientations in NWs synthesized through templated electrodeposition . In the case of the two nanowires that grew side by side and were indented, it was found that the first NW deformed by shear banding after forces of 17.82 μN. Prior to reaching this force only a

very shallow indent was seen, although only in one case. At the next indent (F_{max}=28.79 μN), shear banding was observed, and observed consistently through the next four indents on that NW. On the NW next to it, which was of similar diameter and length, only distributed plasticity was observed. This NW was consistently indented following the first which deformed through localized shear banding. Two other NWs also exhibited localized shear banding, but they were not adjacent to any other NWs. As the crystallographic orientation in these wires is unknown, it is possible that the wires that deformed by slip banding were simply oriented different than the wires that deformed through distributed plasticity. This slip uniformly occurs at ~35° from the transverse axis of the NW, suggesting {111}. $< \overline{1}\ 10>$ slip with a NW growth direction of $[\ \overline{1}\ 10]$, although this is yet unconfirmed. Further studies are necessary to establish the reason for this observation of two modes of plastic deformation.

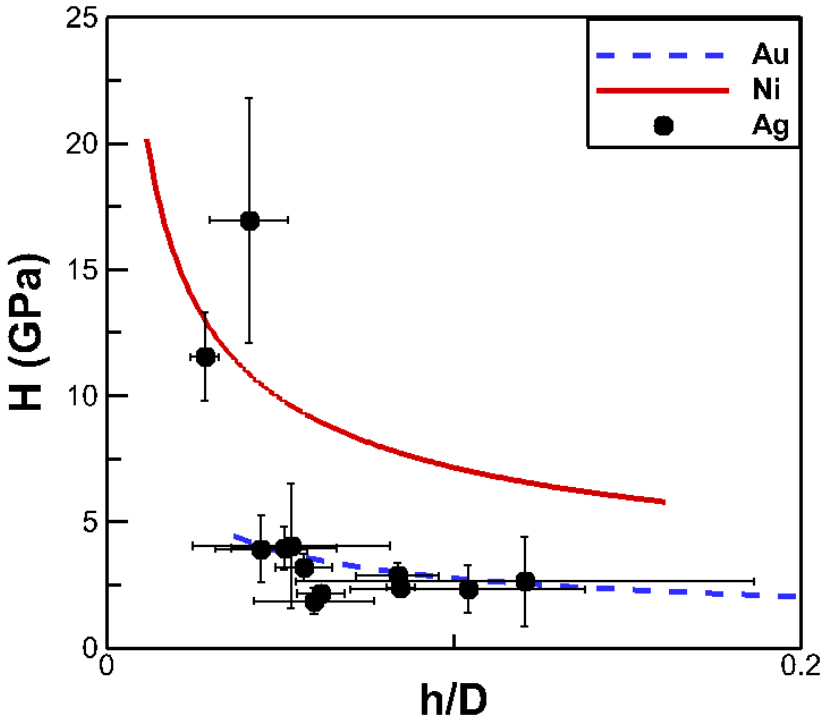

Figure 3.5: Size effects in FCC metal NWs. Ni (red line) and Au (blue line) are predicted from Nix-Gao theory based on a previous experiment, while Ag is from this experiment.

Fig. 3.5 compares the indentation size (ISE) effects observed in Ni-Au NWs with the new data from Ag NWs. NWs that deformed by shear banding are not included, although the hardness is presented as in the appendix. We again find that by limiting the Nix-Gao plastic length, h^*, to the diameter of the NW, strong size effects are observed. This treatment yields a nanoindentation hardness of 1.04 GPa, approximately 25% higher than that found in Ag NWs synthesized through wet-chemical synthesis techniques , yet lower than Au NWs, due to their differences in stacking fault energies. The observed ISE in Ag NWs follow closely that of Ni.

However, the plasticity of NWs is also dependent on materials properties such as SFE

and shear modulus, G. Due to similarities within the ratios of SFE and G with Ni and Au of ~3, the relative importance of each factor was unable to be determined. However, the ratios of Ni/Ag SFE and G*b are 7.7 and 2.18 respectively. In order to determine the contributions of SFE and G*b on the observed plasticity, we normalized the measured H values and normalized by both factors, shown in the appendix. From this treatment, we observe that SFE may have a larger role in governing the nanoindentation hardness, yet both materials properties do play some role.

3.3 Nanoindentation of Cu NWs with Controlled Microstructure.

3.3.1 Experimental Methods

3.3.1a Synthesis

Synthesis of Cu NWs was achieved following the method proposed by Zhong et al. . Fig. 3.1 shows a schematic of the experimental set-up used, which is identical to the experimental methods used to produce Ag NWs. Two 0.1 mm 99.9% pure copper wires (Alfa Aesar) used as both the cathode and anode were sandwiched between two standard glass microscopy slides (Corning Glassware, Corning, NY or Celestron, Inc., Torrance, CA) and held together with vinyl electrical tape (3M). The Cu wires were pickled in a 5% H_2SO_4 solution prior to use to remove any contamination, and rinsed with water before use. The construction and filling of the electrolyte cell followed exactly the procedure outlined in the section regarding the Ag NW synthesis. A micropipette was used to *slowly* fill the cell 100±20µL of 0.05M $CuSO_4$ solution in between the electrodes which were 2 cm apart. Thermocouples were attached on the Peltier (TC1) and top glass slide (TC2), and unless otherwise stated the temperature was measured at TC2. The temperature of the

glass slide was typically 0.3-0.4°C warmer than that of the Peltier element.

As with Ag NWs, it was imperative to obtain high ice quality upon freezing of the electrolyte. Following the procedure outlined in the Ag NW section, a thin layer of water was placed on the Peltier element to freeze the electrochemical cell in place before attaching the electrodes to the power supply. The glass slide was placed directly on the wet Peltier, and as the water froze, it held the glass slide in place. TC2 was quickly brought to around 10 °C, after which more controlled cooling was employed with 20 -30 minutes being needed to freeze the electrolyte. If visual inspection, assisted with a white LED light, revealed ice striations, the cell was cycled through freezing and thawing until the ice layer was clear, before TC2 was maintained at -0.3±0.1 °C.

Copper foil and tape were also explored as possible electrode materials; however, they did not yield reliable results. Voltages between 0.5V and 2V were employed to measure the effect on the surface structure of the NWs. Deposition was carried out for 20 minutes. A more detailed discussion of the merits of potentiostatic control vs galvanic control has been detailed in the section regarding Ag NWs, however due to the difference in molar conductivities between $AgNO_3$ and $CuSO_4$ it is expected that the ohmic drop is not as sensitive to experimental parameters in the Cu experiments. Therefore, it is predicted that it is not as vital to use a 3-electrode set up under these conditions.

It was found that electrodeposited Cu NWs did not adhered well to the glass substrate in contrast to the electrodeposited Ag NWs. In order to collect the NWs, the power supplied to the Peltier element was increased after electrodeposition until the temperature attained -5 °C to -10 °C to freeze the entire specimen, including the electrolyte liquid layer. After

the tape was removed, the ice containing the NWs was slid off the glass slide into a vial. Shaking of the vial was required to avoid NW clustering, which could possibly add some pre-straining to the NWs. Samples intended for AFM imaging and nanoindentation were also frozen, but the ice containing the NWs was simply left on the slide after the tape was removed. As the electrolyte began to thaw, the liquid was carefully pipetted away with limited NW disturbance. The remaining bit of liquid surrounding the nanowires was left to evaporate before AFM was done. If some NWs were found to adhere firmly to the glass slide, NWs were imaged directly on the glass substrate.

3.3.1b Characterization

The microstructure and mechanical characterization details followed those outlined in the Ag NW section. However, we note that electrodeposited Cu NWs were found to oxidize rather quickly; over the span of one night, they turned from black to blue-green color, so AFM nanoindentation was only conducted on relatively fresh batches of Cu NWs synthesized within a few hours. The NW structure was characterized by optical microscopy, and tapping mode AFM imaging with both a standard Si probe and the diamond-tipped sapphire cantilever AFM probe used for nanoindentation, as for Ag NWs. The NW diameter was measured by AFM using the difference in height from line profiles in the image analysis software Gwyddion .

AFM imaging with the large radius diamond probe was unable to pick up fine corrugated structures (see Appendix B), so we used the average spacing measured with an AFM probe with a radius of 7.4 nm, measured as described in the section regarding silver NWs. The

corrugation spacing was determined by using line profiles across six 5μm lengths for each voltage, and each peak to peak measurement was counted as one corrugation. We then apply this result to estimate the corrugation density, and measure the nanoindentation hardness of 3 NWs from each corrugation spacing.

3.3.2 Results and Discussion

Cu NWs of ~5 mm in length, Fig. 3.6a-b, were obtained within 20 minutes of electrodeposition at a top slide temperature of -0.3°C. These measurements agreed well with the growth rate of 3 $\mu m \cdot s^{-1}$ estimated by Zhong et al. under similar conditions. We likewise confirm that the temperature and potential play a dominant role in governing the final structure. Typically, increasing the voltage or decreasing the temperature, even by minor amounts resulted in fractal-like dendritic growth, Fig. 3.6c-d. Note that in Fig. 3.6c, the growth conditions were not far removed from those shown in Fig. 3.6a, yet the structures are remarkably different. A deviation of even half a degree in temperature TC2 led to dendritic growth. This has been discussed in detail in references.

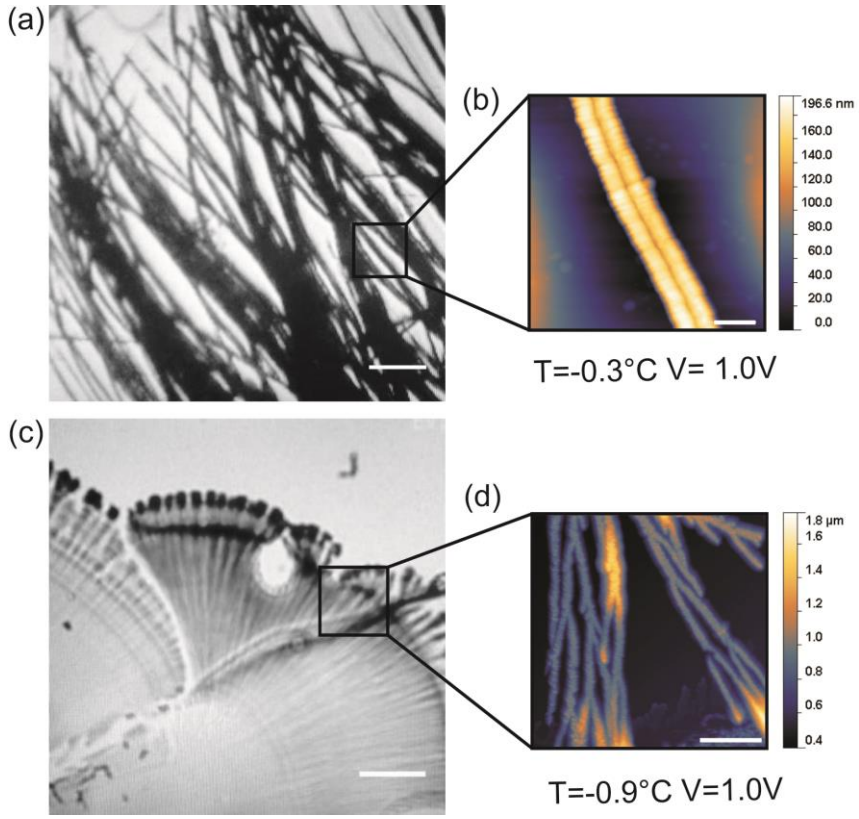

Figure 3.6: Copper nanostructures obtained by direct electrodeposition. (a) Optical micrograph and (b) AFM image of straight, unbranched NWs. Scale bars are 25 and 1µm, respecively (c) Optical micrograph and (d) AFM image of fractal-like dendritic nanostructures showing several bifurcations. Scale bars are 25 and 10 µm respectively.

While the form of the nanostructures (NW vs. dendrite) relied heavily on the temperature, it was found possible to produce straight Cu NWs over a large range of voltages between 0.2 V and 1.5 V. However, the applied voltage had a strong influence on the surface structure and diameter of the NWs. A high voltage (0.6-1.5 V) resulted in larger diameters (D_{NW} = 423.44±90.5 nm), and a surface characterized by the presence of ridges, or corrugations, as shown in Fig. 3.7a. Lowering the voltage to the lowest end (0.2-0.5 V)

yielded smaller NWs (D_{NW}=173.92±76.2 nm) with a smooth surface structure as shown in Fig. 3.7b. The diameter of straight Cu was found to vary from 91 nm and 521 nm over the range of voltages applied.

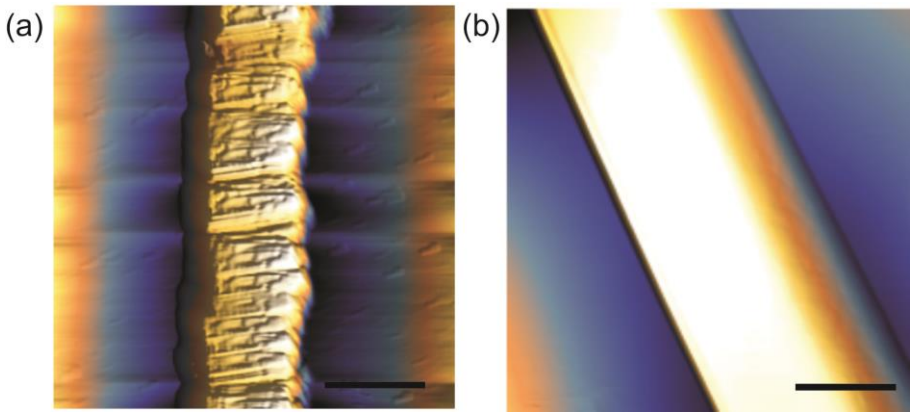

Figure 3.7: Derivitive topography of electrodeposited Cu NWs. (a) corrugated surface in a large NW grown at a voltage of 1.2V. A line profile showing the individual ridges is overlaid. Scale bar is 4µm. (b) Smooth surface of NW growth at 0.4V with line profile overlaid. Scale bars are 0.5 µm.

Powder XRD analysis of straight Cu NWs showed strong (111), (200) and (220) peaks, along with CuO peaks, see Appendix B. It could not be concluded, however, that these NWs were polycrystalline due to the possibility of the NWs being pulled and shifted in 3 dimensions as the sample was handled. Zhong et al. used selected area election diffraction (SAED) to conclude that the Cu NWs grown through direct electrodeposition with a (111) orientation, although no XRD analysis was presented. The authors also found that voltages as high as 2V successfully yielded NWs; however this result was not confirmed in the present study, perhaps due to minor differences in impurities, electrode spacing, or temperature fluctuations.

The lamellar morphology of the surface corrugations suggests the formation of TBs perpendicular to the NW length. The growth of lamellar twins in <111> oriented FCC NWs is generally accompanied by zigzag {111} surface facets with a similar morphology . This could be verified by conducting a high-resolution transmission electron microscopy (HRTEM) study of our Cu NWs, but such difficult experiments were beyond the scope of this thesis. Nevertheless, the AFM nanoindentation results presented below tend to support this hypothesis. Interestingly, we also find in Fig. 3.8 that the average corrugation density calculated from the peaks of the AFM line profiles is directly proportional to the applied voltage. A caveat, however, is that AFM imaging is limited by the size of the probe used. For non-indentation purposes, we utilized a standard tapping mode probe with a nominal radius of 8 nm (see silver section), so it is possible that this corresponds to the resolution limit in our twin spacing measurements using this method, see appendix for a more detailed discussion

.

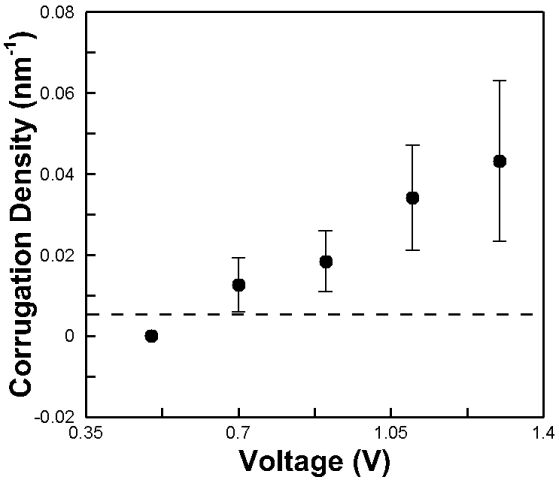

Figure 3.8: Corrugation density as a function of applied voltage in electrodeposited Cu NWs. Data below the dashed line corresponds to the appearance of smooth NWs.

. The NWs synthesized by Zhong et al. contained densely packed TB defects, which have been shown to strengthen NWs by helping to block emitted dislocations . These authors observed twin thicknesses as small as 0.5 nm whilst their NWs were of same diameter than in this study. While a complete study of the atomic structure and crystallography of these NWs has not been carried out, the appearance of twins in them does make sense. (Chapter 1 more thoroughly addresses possible mechanisms of 1-D growth)

. It is understood that the ohmic drop under potentiostatic control is very sensitive to the electrolyte environment. As linear growth occurs by the reduction of metal anions, there is a local starvation of metal cations near the growth front since they have been consumed to grow the NWs. Direct electrodeposition experiments have only been completed using a 2 electrode cell, so the instantaneous ohmic drop as metal cations were consumed could not

be accounted for, but this was manifested by a sudden change in current. This allows enough energy for twinning to occur, and this continues to cycle as the NW continues to grow. At low applied potentials, the decrease in current is not as severe, thus the energy barrier to form a TB, which is governed by the stacking fault energy (SFE) cannot be overcome by this localized disturbance, and perfect FCC stacking occurs. Contrary to the synthesis of electrodeposited Ag NWs, we were able to synthesize straight NWs without employing galvanostatic control. In fact, when the current was controlled, rather than the voltage, only smooth NWs were obtained. This offers more support that the ohmic drop is responsible for the formation of nanoscale twins in Cu.

Both theory and experiment have shown that the plasticity of Cu NWs is largely dependent on the microstructure. Jang et al. reported an average tensile strength for nanotwinned Cu nanopillars of 2.12 GPa, 1.5 times larger than that of single crystal nanopillars. Previous nanoindentation hardness studies on the ends of over-plated electrodeposited NWs were reported to have values of ~1.8 GPa for single crystalline while the hardness of polycrystalline Cu NWs was found as high as 2.1 GPa .

In this thesis, marked differences were observed in the AFM nanoindentation response as a function of the type of NWs. The nanoindentation behavior of smooth NWs was characterized by a large dissipation of plastic energy, opposed to the corrugated ones, as shown in Fig. 3.9a. No localized shear band deformation was observed, contrary to our previous study on Ag NWs.

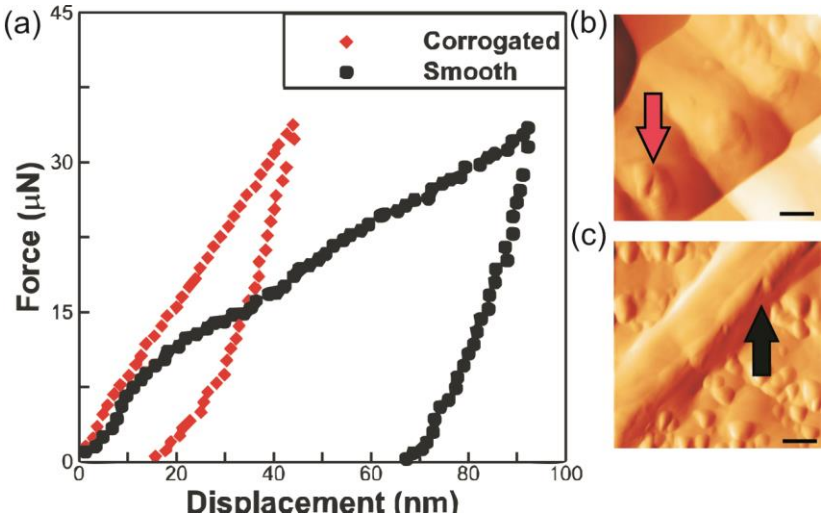

Figure 3.9: AFM nanoindentation response of electrodeposited Cu NWs. (a) Loading-unloading curves for smooth (black) and corrugated (red) Cu NWs. Corrugated NWs show a much higher hardness with less dissipated energy. (b) and (c) AFM derivative topography images of post indents corresponding to the loading curves of corrugated and smooth NWs in (a), respectively. Scale bars in both (b) and (c) are 500 nm.

Unlike our previous experiments on FCC metal NWs, indentation size effects were found to be negligible, as shown in Fig. 3.10a, whereas significant hardening in samples with corrugation was noted. We measured an average nanoindentation hardness of 1.60±0.57 GPa in smooth NWs, which is consistent with the nanoindentation hardness of single-crystalline Cu NWs . For NWs with corrugation, however, we find a 2.4 times increase in hardness to have an average of 3.85±0.53 GPa. This value shows a notable improvement over the nanoindentation of polycrystalline NWs reported by Bansal et al. , suggesting an additional strengthening effect over the enhancement of mechanical properties by nanocrystalline grain refinement.

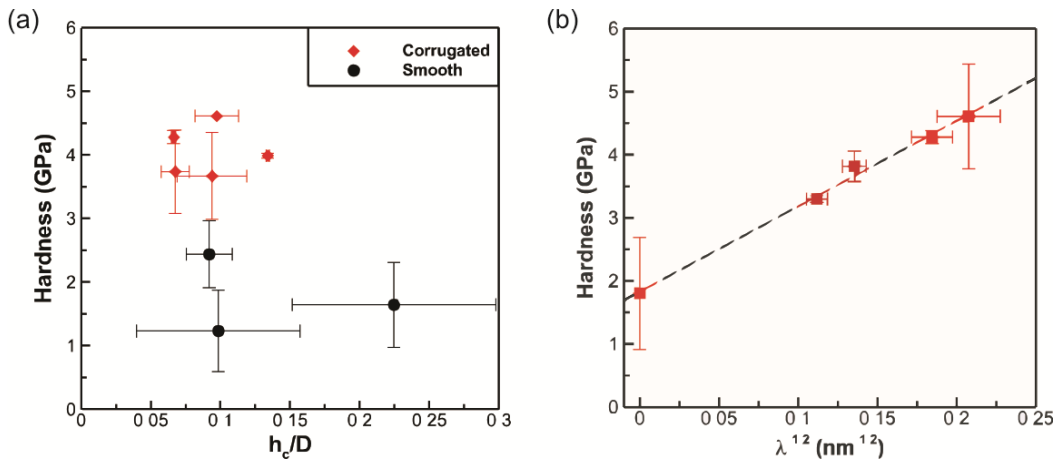

Figure 3.10: Effect of surface structure on the hardness of electrodeposited Cu NWs. (a) Hardness versus normalized indentation depth for both corrugated and smooth NWs. Error bars include 3 measurements each, except for the highest hardness which shows only 2. (b) The Hall-Petch relationship between H and the corrugation density, λ. The h_c/D values shown in (b) are 0.089±0.013.

Our AFM nanoindentation results are in good agreement with the literature on nanotwinned Cu nanopillars obtained by other methods. The increased strength with smaller twin spacing has been reported by Jang et al. in the case of twinned Cu nanopillars , as well as a comparable increases in strength between single crystalline and twinned Cu nanopillars . A striking finding in this thesis is that the hardness is found to increase with corrugation spacing which strongly support the hypothesis that strengthening is related to the presence of coherent TBs .The relationship between the surface structure of the NWs and the hardness can be described as a Hall-Petch relationship [47,48] as in Eq. 1, below, where H is the hardness, $H_0$is the hardness of NWs exhibiting smooth surfaces, λ is the corrugation density, and B is a strengthening coefficient that is material dependent.

$$H = H_0 + \frac{B}{\sqrt{\lambda}} \quad (1)$$

Past atomistic simulations in Cu showed that TBs exert a repulsive force on newly emitted dislocations, reaching a saddle point at the TB itself, which must be overcome by increasing the applied stress. Deng and Sansoz [40,50] have predicted that the repulsive force of a TB on a newly nucleated surface dislocation is also inversely proportional to the TB spacing, i.e. proportional to the TB density.

3.4. Conclusions:

We have presented an experimental method to control the growth of Ag and Cu NWs through direct electrodeposition. This methodology offers a more versatile way to produce large quantities of high quality, ultra-long NWs. Our data suggests that atomic defects within the NW can arise from minor local fluctuations of growth conditions, concentration gradients, ice grains or ohmic drops. The direct electrodeposition performed in this thesis was able to show good control over the microstructure of Cu NWs by varying the applied voltage.

We observed two types of plastic yielding in Ag NWs, distributed plasticity and localized shear band. Data from the first mode agrees very well with our previous observations on the nanoindentation testing of Ni and Au NWs. As a result, this work has further supported the conclusion that ISE in FCC metal NWs rely strongly on geometrical factors limited by the NWs diameter and initial dislocation density. At very low indentation depths, Ni and Ag exhibit very high hardness values, this is likely due to a small initial dislocation density.

There is not enough data in this thesis to conclude whether or not the expected power-law scaling is found in Ag at low indentation depths. A strong dependence of the nanoindentation hardness on the SFE was evidenced. The second observed type of yielding, localized shear bands, is not yet understood, although one possible explanation is that the NWs that deformed in this way had a different growth orientation. However, we cannot exclude the possibility that this was due to the nanoindenter tip sliding along the NW surface.

Previously reported strength data in nanotwinned Cu nanopillars were found in good agreement with the nanohardness results in smooth and corrugated NWs, supporting the idea that the microstructure of electrodeposited Cu NWs from single crystalline to nanotwinned has been successfully achieved. Furthermore, a major finding is the Hall-Petch relationship between H and λ in Cu NWs, which also agrees with the theory that TBs exert a repulsive force on newly nucleated dislocations as proposed in past atomistic simulation studies.

Future research should include a detailed electron microscopy analysis with special attention to the growth direction and presence of TBs or other growth defects. Also, computational and theoretical studies could help better understand the yield mechanism(s) in Ag and Cu NWs with either pristine or twinned microstructures.

References:

1. Wu, B., A. Heidelberg, and J.J. Boland, Mechanical properties of ultrahigh-strength gold nanowires. Nature Mater., 2005. 4(7): p. 525-529.

2. Shan, Z., et al., Mechanical annealing and source-limited deformation in submicrometre-diameter Ni crystals. Nature materials, 2007. 7(2): p. 115-119.

3. Park, H.S., K. Gall, and J.A. Zimmerman, Deformation of FCC nanowires by twinning and slip. Journal of the Mechanics and Physics of Solids, 2006. 54(9): p. 1862-1881.

4. Park, H.S., et al., Mechanics of crystalline nanowires. MRS bulletin, 2009. 34(03): p. 178-183.

5. Lian, J., et al., Sample boundary effect in nanoindentation of nano and microscale surface structures. J. Mech. Phys. Solid., 2009. 57(5): p. 812-827.

6. Legros, M., D. Gianola, and C. Motz, Quantitative In Situ Mechanical Testing. MRS Bull., 2010. 35.

7. Koh, S. and H. Lee, Molecular dynamics simulation of size and strain rate dependent mechanical response of FCC metallic nanowires. Nanotechnology, 2006. 17(14): p. 3451.

8. Ji, C. and H.S. Park, The coupled effects of geometry and surface orientation on the mechanical properties of metal nanowires. Nanotechnology, 2007. 18(30): p. 305704.

9. Huang, D., Q. Zhang, and P. Qiao, Molecular dynamics evaluation of strain rate and size effects on mechanical properties of FCC nickel nanowires. Computational Materials Science, 2011. 50(3): p. 903-910.

10. Wood, E.L. and F. Sansoz, Growth and properties of coherent twinning superlattice nanowires. Nanoscale, 2012. 4(17): p. 5268-5276.

11. Wood, E.L., et al., Size effects in bimetallic nickel–gold nanowires: Insight from atomic force microscopy nanoindentation. Acta Materialia, 2014. 66(0): p. 32-43.

12. Wang, J.W., et al., Near-ideal theoretical strength in gold nanowires containing angstrom scale twins. Nat. Commun., 2013. 4.

13. Sansoz, F., H. Huang, and D.H. Warner, An Atomistic Perspective on Twinning Phenomena in Nano-enhanced FCC Metals. JOM, 2008. 9: p. 79-84.

14. Sansoz, F. and V. Dupont, Nanoindentation and plasticity in nanocrystalline Ni nanowires: A case study in size effect mitigation. Scripta Materialia, 2010. 63(11): p. 1136-1139.

15. Deng, C. and F. Sansoz, Fundamental differences in the plasticity of periodically twinned nanowires in Au, Ag, Al, Cu, Pb and Ni. Acta Mater., 2009. 57(20): p. 6090-6101.

16. Deng, C. and F. Sansoz, Near-Ideal Strength in Gold Nanowires Achieved through Microstructural Design. ACS Nano, 2009. 3(10): p. 3001-3008.

17. Busbee, B.D., S.O. Obare, and C.J. Murphy, An Improved Synthesis of High-Aspect-Ratio Gold Nanorods. Advanced Materials, 2003. 15(5): p. 414-416.

18. Pérez-Juste, J., et al., Gold nanorods: synthesis, characterization and applications. Coordination Chemistry Reviews, 2005. 249(17): p. 1870-1901.

19. Cademartiri, L. and G.A. Ozin, Ultrathin Nanowires—A Materials Chemistry Perspective. Advanced Materials, 2009. 21(9): p. 1013-1020.

20. Benfield, R.E., et al., Structure and Bonding of Gold Metal Clusters, Colloids, and Nanowires Studied by EXAFS, XANES, and WAXS. The Journal of Physical Chemistry B, 2001. 105(10): p. 1961-1970.

21. Sakamoto, Y., et al., Synthesis of Platinum Nanowires in Organic−Inorganic Mesoporous Silica Templates by Photoreduction: Formation Mechanism and Isolation. The Journal of Physical Chemistry B, 2003. 108(3): p. 853-858.

22. Nečas, D. and P. Klapetek, Gwyddion: an open-source software for SPM data analysis. Central Cent. Eur. J. Phys., 2012. 10(1): p. 181-188.

23. Tabor, D., The hardness of metals. 2000: Oxford university press.

24. Kaischew, R. and E. Budevski, Surface processes in electrocrystallization. Contemporary Physics, 1967. 8(5): p. 489-516.

25. Tok, J.B.H., et al., Metallic striped nanowires as multiplexed immunoassay platforms for pathogen detection. Angew. Chem. Int. Ed., 2006. 45(41): p. 6900-6904.

26. Burton, W.K., N. Cabrera, and F.C. Frank, The Growth of Crystals and the Equilibrium Structure of their Surfaces. Philosophical Transactions of the Royal Society of London. Series A, Mathematical and Physical Sciences, 1951. 243(866): p. 299-358.

27. Burton, W., N. Cabrera, and F. Frank, Role of dislocations in crystal growth. Nature, 1949. 163(4141): p. 398-399.

28. Bierman, M.J., et al., Dislocation-Driven Nanowire Growth and Eshelby Twist. Science, 2008. 320(5879): p. 1060-1063.

29. Zhong, S., et al., Nanoscale Twinned Copper Nanowire Formation by Direct Electrodeposition. Small, 2009. 5(20): p. 2265-2270.

30. Zhang, Q., S.-J. Liu, and S.-H. Yu, Recent advances in oriented attachment growth and synthesis of functional materials: concept, evidence, mechanism, and future. Journal of Materials Chemistry, 2009. 19(2): p. 191-207.

31. Niederberger, M. and H. Colfen, Oriented attachment and mesocrystals: Non-classical crystallization mechanisms based on nanoparticle assembly. Physical Chemistry Chemical Physics, 2006. 8(28): p. 3271-3287.

32. Cho, K.-S., et al., Designing PbSe Nanowires and Nanorings through Oriented Attachment of Nanoparticles. Journal of the American Chemical Society, 2005. 127(19): p. 7140-7147.

33. Lee, H., et al., Focused patterning of nanoparticles by controlling electric field induced particle motion. Applied Physics Letters, 2009. 94(5): p. -.

34. Sun, S., et al., Magnetic field driven assembly of 1D-aligned silver superstructures. CrystEngComm, 2011. 13(15): p. 4827-4830.

35. Ding, C., et al., Growth of non-branching Ag nanowiresvia ion migrational-transport controlled 3D electrodeposition. CrystEngComm, 2012. 14(3): p. 875-879.

36. Bott, A.W., Controlled Current Techniques. epsilon. 47906: p. 1382.

37. Fang, J., et al., Silver nanowires growth via branch fragmentation of electrochemically grown silver dendrites. Chemical Communications, 2009(9): p. 1130-1132.

38. Li, X., et al., Nanoindentation of Silver Nanowires. Nano Lett., 2003. 3(11): p. 1495-1498.

39. Zhu, Y., et al., Size effects on elasticity, yielding, and fracture of silver nanowires: In situ experiments. Physical Review B, 2012. 85(4): p. 045443.

40. Vlassov, S., et al., Elasticity and yield strength of pentagonal silver nanowires: In situ bending tests. Materials Chemistry and Physics, 2014. 143(3): p. 1026-1031.

41. Wood, E., et al., Size effects in bimetallic nickel–gold nanowires: Insight from atomic force microscopy nanoindentation. Acta Materialia, 2014. 66: p. 32-43.

42. Lucas, M., et al., Plastic deformation of pentagonal silver nanowires: comparison between AFM nanoindentation and atomistic simulations. Phys. Rev. B, 2008. 77(24): p. 245420.

43. Jang, D., C. Cai, and J.R. Greer, Influence of Homogeneous Interfaces on the Strength of 500 nm Diameter Cu Nanopillars. Nano Letters, 2011. 11(4): p. 1743-1746.

44. Zhong, S., et al., Formation of nanostructured copper filaments in electrochemical deposition. Physical Review E, 2003. 67(6): p. 061601.

45. Wang, M., et al., Nanostructured Copper Filaments in Electrochemical Deposition. Physical Review Letters, 2001. 86(17): p. 3827-3830.

46. Wang, J., et al., Near-ideal theoretical strength in gold nanowires containing angstrom scale twins. Nature communications, 2013. 4: p. 1742.

47. Wang, B., et al., Controlled Growth and Phase Transition of Silver Nanowires with Dense Lengthwise Twins and Stacking Faults. Crystal Growth & Design, 2008. 8(8): p. 3073-3076.

48. Deng, C. and F. Sansoz, Enabling Ultrahigh Plastic Flow and Work Hardening in Twinned Gold Nanowires. Nano Lett., 2009. 9(4): p. 1517-1522.

49. Deng, C. and F. Sansoz, Effects of twin and surface facet on strain-rate sensitivity of gold nanowires at different temperatures. Phys. Rev. B, 2010. 81(15): p. 155430.

50. Deng, C. and F. Sansoz, Repulsive force of twin boundary on curved dislocations and its role on the yielding of twinned nanowires. Scripta Mater., 2010. 63(1): p. 50-53.

51. Cao, A., Y. Wei, and S.X. Mao, Deformation mechanisms of face-centered-cubic metal nanowires with twin boundaries. Applied physics letters, 2007. 90(15): p. 151909.

52. Afanasyev, K.A. and F. Sansoz, Strengthening in Gold Nanopillars with Nanoscale Twins. Nano Lett., 2007. 7(7): p. 2056-2062.

53. Jang, D., et al., Deformation mechanisms in nanotwinned metal nanopillars. Nature nanotechnology, 2012. 7(9): p. 594-601.

54. Bansal, S., et al. Nanoindentation of single crystal and polycrystalline copper nanowires. in ELEC COMP C, 2005. Proceedings. 55th. 2005. IEEE.

55. Deng, C. and F. Sansoz, Repulsive force of twin boundary on curved dislocations and its role on the yielding of twinned nanowires. Scripta Materialia, 2010. 63(1): p. 50-53.

56. Chen, Z., Z. Jin, and H. Gao, Repulsive force between screw dislocation and coherent twin boundary in aluminum and copper. Physical Review B, 2007. 75(21): p. 212104.

57. Zheng, XJ., Jiang, ZY., Xie, ZX., Zhang, SH., Mao, BW., and Zheng, LS., Growth of silver nanowires by an unconventional electrodeposition without template, Electrochemistry Communications, 2007.9(4)

CHAPTER 4: SUMMARY AND OUTLOOK

This thesis investigated the influence of sample size, microstructure and materials properties on the plasticity of FCC metal NWs by using AFM nanoindentation, and offered new insight into the interplay between experimental conditions and mechanical properties. An overall overview of major findings in this thesis is presented in the following.

4.1 Nanoindentation Methodology

An AFM was used for indenting FCC metal NWs. This technique was not new, however the experiment was modified to accommodate for indenting NWs rather than bulk materials or thin films. To indent bimetallic NWs, a substrate with a molecular "glue" was used to fix the NWs in place. It was found that NWs must be indented within 15 degrees from substrate normal in order to have reliable results.

4.2 Size Effects and Characteristic Plasticity Length Scales:

The initial treatment of nanoindentation hardness of bimetallic Ni-Au NWs by the classic Nix-Gao method yielded poor fitting. This was found to be due to free surface effects on 1-D materials versus thin films. By limiting a characteristic length value, $h_{c,}$ to the diameter of the NWs, the Nix-Gao curve was found for Au, Ni, and Ag. Furthermore, Ag and Ni showed an increase in hardness at very shallow indentations. Atomistic simulations performed by another student completed on Ni suggest that this could be due to an initial yielding zone, which was characterized by a statistical distribution of nanoindentation

hardness size effects. Au does not exhibit this phenomenon due to a high pre-existing defect density due to the handling of the NWs to free them from the templates and prepare them for nanoindenation.

4.3 Materials Properties Effects on the Indentation Hardness and ISE

While it was found that the nanoindentation hardness values of Ag, Au, and Ni are largely governed by their stacking fault energies, we observe that the indentation size effects (ISE) are largely independent from it. Similar conclusions were drawn about the dependence of the ISE on other materials properties. However it was supported through atomistic simulations conducted by another student with bimetallic NWs that the SFE largely governed the motion of dislocations through the NW. In Ni, dislocations tended to be emitted and glide through the NWs where they were absorbed on the opposing free surface. In Au, the dislocation loops tended to nucleate and be absorbed near the indenter tip. This was seen experimentally by large amounts of pileup in Au segments, whereas the Ni-segments were virtually free from pileup.

The observed ISE, predicted by Nix-Gao theory, rather seemed to be controlled largely by the density of preexisting dislocations. Ag NWs that exhibited distributed plasticity showed strong size effects, perhaps owing to either a very low initial defect density or the size effects observed were actually due only incipient plasticity in pristine NWs, not enough to cause the avalanche of dislocations.

4.4 Microstructural Concerns on the Yielding of FCC Metal NWs

All evidence in this thesis has proved that Ag NWs growth through direct electrodeposition were largely free of internal microstructural defects. This is evidenced by the mechanism of yielding through localized shear bands. It was noted that yield in these NWs occurred universally at 14 μN of force, where as those that exhibited distributed plasticity had a more statistical behavior, perhaps owing to varying densities of initial defects.

Analysis of the growth conditions used to produce Ag and Cu NWs showed that minor changes in the environment could cause dislocations to form during growth which could result in twinning or branching. We hypothesized that in Cu direct electrodeposition, the ohmic drop from fluctuations in ionic strength near the growth front, resulted in current spikes that allow the SFE barrier to be overcome by forming twin plane. Furthermore, we observed a linear dependence of hardness on the density of surface corrugations, which suggested TB-induced strengthening in Cu NWs.

4.5 Future Work

Direct electrodeposition of NWs has been shown to produce high quality NWs with tunable properties, with clear advantages over the traditional templated electrodeposition. The synthesis becomes scalable, and there are less handling steps so that the NWs are pristine for applications. The surface growth is not confined, so the surface structure of the NW may be altered. This research suggests that this could impart significant increases in strength.

However, more work is required in order to fully understand the deformation mechanics

and plasticity of the electrodeposited FCC metal NWs. The mechanism of strengthening in Cu NWs needs to be fully studied through electron microscopy to ascertain the growth direction and crystallographic structure. It would be highly desirable to image pre and post-indent NWs with TEM. Computational simulation studies should also be performed to understand the plastic deformation processes at atomic scale.

In Ag, more careful crystallographic studies need to be completed. SAED could prove to be invaluable. By understanding the crystallography and growth of the Ag NWs, the mechanism of deformation could be clearer. Atomistic simulations should also reveal if there is a stress threshold that triggers a massive dislocation avalanche.

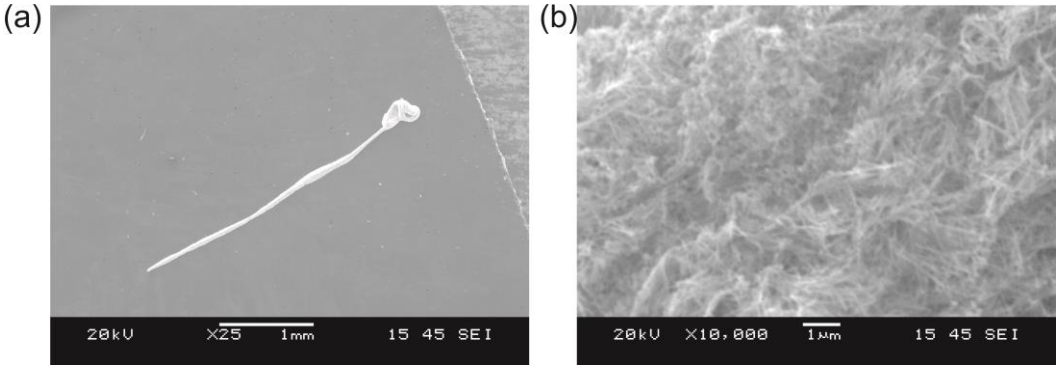

Figure 4.1: Silver nanoyarns.(a) a length of nanostructured yarn pulled from an electrolyte bath. (b) Magnified view showing texture of the yarn. SEM Image credit: Daniel Merkel

Finally, this work should further be explored for the possibility of creating ultra-strong meso-structures and composite materials. In Chapter 3, it was shown that well organized meshes of microwires can be obtained through these methods which could have applications in plasmonics. Furthermore, careful pulling the electrode from an electrolyte bath has produced silver nanowire yarns, as shown in Fig. 4.1. If these possess the same

increased strength as the individual NWs shown here, they could be of interest to the MEMs community.

APPENDIX A: SUPPORTING INFORMATION FOR CHAPTER 2

The following work represents results contributed by T. Avant and F. Sansoz from a collaborative work, Wood, E.L. et al. Acta Materialia, 66, 32-34, 2014. It is vital to the discussion and conclusions of Chapter 2, but does not represent work completed by the author of this thesis.

A.1 Atomistic Simulations of Deformation Processes and Hardness

Atomistic snapshots of the dislocation dynamics during the nanoindentation of single-crystalline [111]-oriented Ni and Au NWs are shown in Fig. A.1. The force-displacement curves corresponding to these simulations, Fig. A.2a, indicate that the NWs behaved elastically until the occurrence of discrete yielding steps resulting from sharp drops in contact force. Geometrically necessary dislocations (GNDs) were found to expand under the spherical tip with the increase in contact area; however their role on the mechanical response was considered to be inconsequential because they occurred prior to the first yielding step in Fig. A.2a. The relevant yielding mechanism in [111]-oriented Ni NWs was found to correspond to the emission of prismatic dislocation loops in the contact zone, followed by their escape from the crystal on the opposing surface at the bottom of the NW, Fig. A.1a-d and movie S1. Each of these single slip events led to a marked decrease in mean contact pressure, as shown in Fig. A.2b. By way of contrast, the plastic deformation of Au NWs was found to differ from the interaction mechanism between newly-emitted loops and the free surface predicted in Ni NWs. In this case, incipient plasticity resulted from the growth of GNDs into spiral dislocations, which were quickly absorbed by the

surface close to the tip after one or two rotations, Fig. A.1d-f. This yielding process did not produce any plastic deformation at the bottom of the Au NWs, as opposed to that predicted in Ni NWs, Fig. 6h and g, respectively.

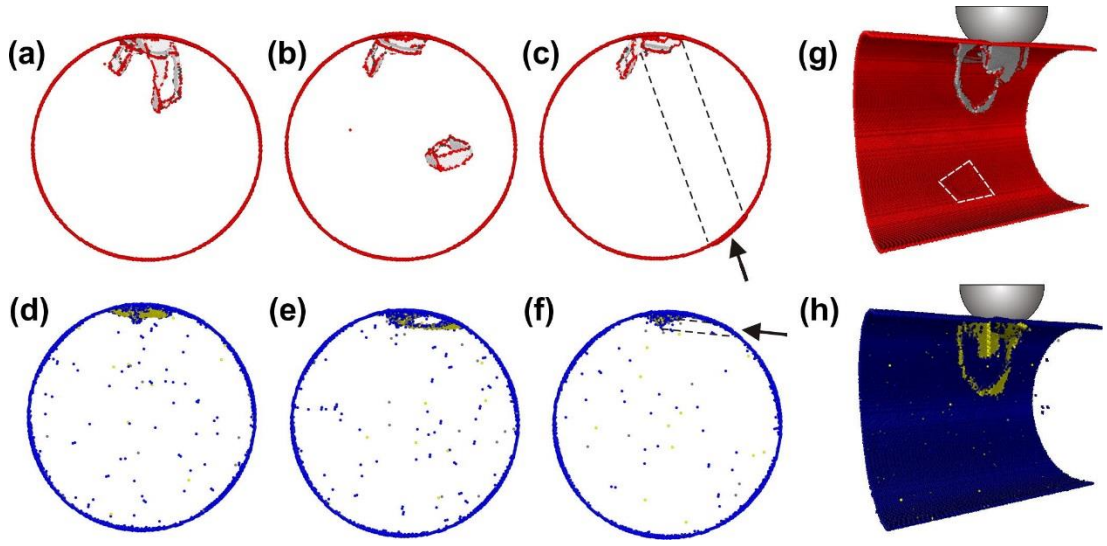

Figure A.1: MD simulations of spherical indentation in [111]-oriented single-crystalline FCC nanowires. (a)-(c) Nucleation, propagation and escape of a prismatic dislocation loop during a single yield event in Ni nanowires. (d)-(f) Emission and escape of a single-arm dislocation localized near the tip-nanowire contact in Au nanowires. Spherical tip in the upper region is not shown. Deformation microstructures obtained with a contact depth of 1.8 nm in (g) Ni nanowire and (h) Au nanowire. Bottom area highlighted by a dashed line in (g) represents the free surface zone where prismatic loops have escaped during nanoindentation.

Also, the simulated nanoindentation of [001]-oriented NWs showed a change in elastic response at shallow contact depths, but proved to exhibit no significant difference in plastic deformation mechanisms and the yielding contact pressure required to emit the first dislocations, Fig. A.2c. Furthermore, testing the effect of loading direction with different NW tilt angles, which is relevant to the interpretation of AFM nanoindentation experiments, allowed us to conclude that the NW rotation also had little influence on the yielding contact pressure and deformation mechanisms in [111]-oriented Au NWs and Ni NWs, except for the Ni NW with a 30° tilt angle resulting in a higher yield point, Fig. A.2d.

It is worth noting, however, that for the Ni NW with 30° rotation, newly-emitted dislocation loops were blocked by the fixed boundary in the lower part of the NW, and found to remain in the crystal; thereby increasing in yield contact pressure. Similarly, several dislocation arms were predicted to be pinned at the bottom boundary in Au NWs after large plastic deformation, suggesting the possible accumulation of crystal defects in AFM experiments on heavily deformed Au NWs. Furthermore, Fig. 2.4 shows good hardness agreement between the predictions from atomistic simulations and the experimental measurements from AFM nanoindentation. This result is surprising considering that the strain-rates are different by several order of magnitudes, but not uncommon because this phenomenon has also been observed previously by Sansoz and Stevenson in the AFM nanoindentation of nanocrystalline Ni films. Fig. 2.4 also shows that the data in Au NW segments were collected with much larger normalized contact depths in experiments compared to those from simulations, while some experimental and simulation data tend to overlap in Ni NW segments.

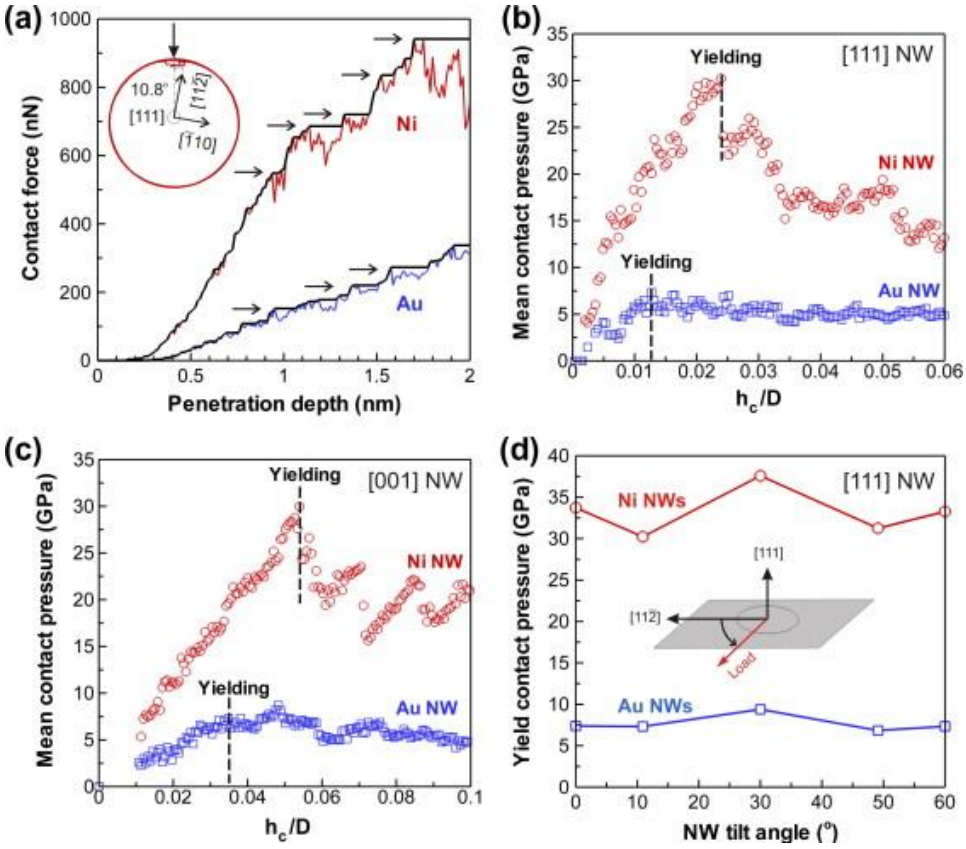

Figure A.2: Hardness of Ni and Au nanowires simulated by MD (a) Contact force evolution as a function of penetration depth with crystal orientations shown in inset. Each horizontal arrow indicates a single yield event. Effects of stacking-fault energy on mean contact pressure in (b) [111]-oriented nanowires and (c) [001]-oriented nanowires. (d) Change in contact pressure at initial yield point as a function of nanowire tilt angle with respect to the [112] crystallographic direction in [111]-oriented Ni nanowires.

APPENDIX B: SUPPORTING INFORMATION FOR CHAPTER 3

B.1 Silver

B.1.1 Synthesis

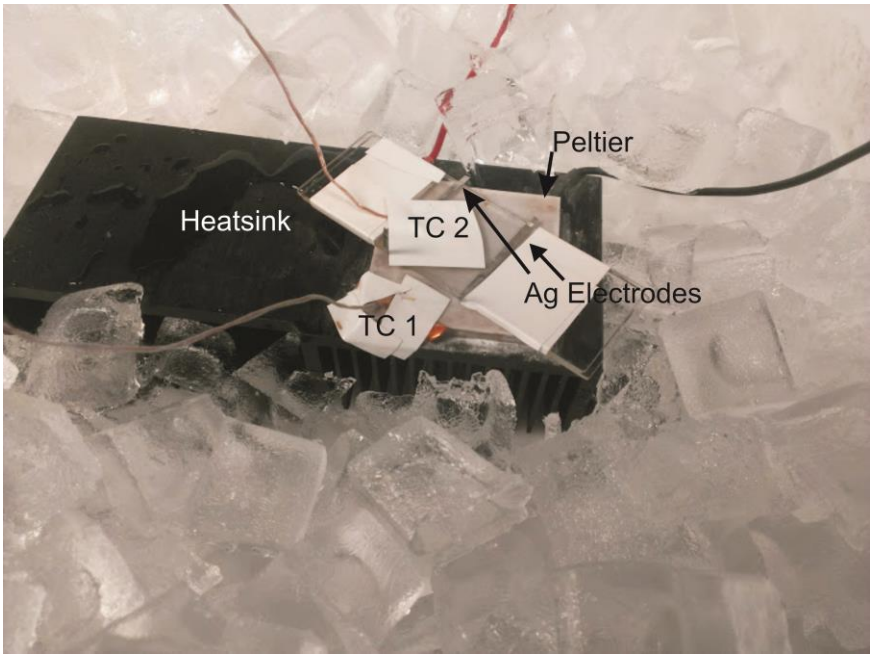

Figure B.1: Photograph of direct electrodeposition set up. Thermocouples were affixed with conductive tape, and secured with vinyl tape. White vinyl tape bound the edges of the glass slide which was fixed to the Peltier element with a thin layer of frozen water. The set up was contained within a polystyrene cooler (not shown).

The parametric study of Ag NW growth was conducted by investigating the effects of electrodes, electrolyte concentration and composition, applied voltage or current, and the temperature. Each parameter was varied individually.

Electrodes of Cu tape (brand, unknown), Pd, Ni, and Cu foils (ESPI Metals, Ashland, OR)

were cut to similar dimensions as the Ag bezel wire, and used in the same manner as both cathode and anodes, in all possible cathode/anode combinations (Table B.1). The spacing of the electrode was also studied, moving the cathode and anode to distances between 0.5 and 3" (Table B.2).

The electrolyte concentration was varied by diluting freshly prepared stock 1 M AgNO3 with DI water to concentrations between 0 M and 0.1 M. (Table B.3)

The effect of supporting electrolytes such as citrate buffer and boric acid was also investigated. Citrate buffer solution was prepared by mixing 2 molar solutions of citric acid and trisodium citrate in a 4:21 volume ratio. This acted as a buffer in the range of pH of 0.1 M $AgNO_3$ (~5.5) and stabilized the solutions pH against the possible formation of H_2 gas in solution. Boric acid is often used to help alleviate internal stress and suppress hydrogen formation in metal electroplating. A 2 M boric acid solution was prepared at 40°C, to increase the solubility. 1 M $AgNO_3$ and 2 M citrate buffer or boric acid were mixed and diluted until [$AgNO_3$]=0.05M and the supporting electrolyte was between 0.05 and 1.5M. (Table B.4).

The effect of temperature was investigated by applying voltages to the Peltier element to vary TC2 between -10 to 60°C, after which the temperature was further raised to 80°C by placing the heat sink in a warm water (50°C) bath (Table B.5).

The effects of applied potential (V) or current (I) were investigated by applying potentials between 0.1 V and 40 V (table B.6), although no growth was observed until 0.5V. Applied currents between 0.01 and 1 mA were investigated, although no growth was seen until 0.08 mA

B.1.2 Nanoindentation Analysis

We could not directly measure the plastic indentation depth, h_c, in Ag NWs that deformed *via* localized slip band formation, thus we could not readily measure the hardness of the NWs. Instead, we estimate the hardness of these points using Hertz elastic theory. The elastic portion of each loading curve (Fig. 3.6a) is fitted such that:

$$F = Ch^{\frac{3}{2}} \tag{1}$$

where *F* is the applied force, measured from the curve, and *C* is a fitting constant, and *h* is . E can then be obtained using:

$$E = \frac{3(1-\nu^2)}{4\sqrt{R}}\text{C} \tag{2}$$

where R is the reduced radius:

$$\frac{1}{R} = \frac{1}{R_{NW}} + \frac{1}{R_{indenter}} \tag{3}$$

The value of the Young's modulus, *E*, is then used to find the reduced Young's modulus:

$$\frac{1}{E^*} = \frac{1-\nu_{NW}^2}{E_{NW}} + \frac{1-\nu_{indenter}^2}{E_{indenter}} \tag{4}$$

From which we can relate the applied load, *F* to the indentation contact depth, *hc*, using eq. 5.

$$F = \frac{4}{3}\sqrt{RE^*}h_c^{\frac{3}{2}} \quad (5)$$

From Eq. 5, we are able to estimate the hardness, using

$$H = \frac{F}{A_c} \quad (6)$$

where A_c is the plastic contact area, and related to our indenter tip by the equation

$$A_c = 422.9951889975h_c + 422.9951889975h_c^2 \quad (7)$$

Table B.1: Materials properties for Ag indentation

	E (GPa)	ν	R (nm)
Diamond probe	1150	0.07	74.5
Ag NW	Experimentally determined	0.03	Experimentally determined.

B.1.3 Silver Synthetic Results

The powder XRD of Ag NWs, as grown on a glass coverslip is shown below and appears to be not well crystalized, although the (111) diffraction peak is present. The sample was imaged under AFM to ensure they were NWs, and had an average diameter of 140.2 ±10.6 nm, no AFM nanoindentation analysis was completed on this particular sample. The NWs were grown with an applied current of 0.8 mA. The observed XRD spectra may be due to a lack of crystallization, or perhaps not enough sample present, as the NWs were grown in a thin layer. Further XRD studies are planned.

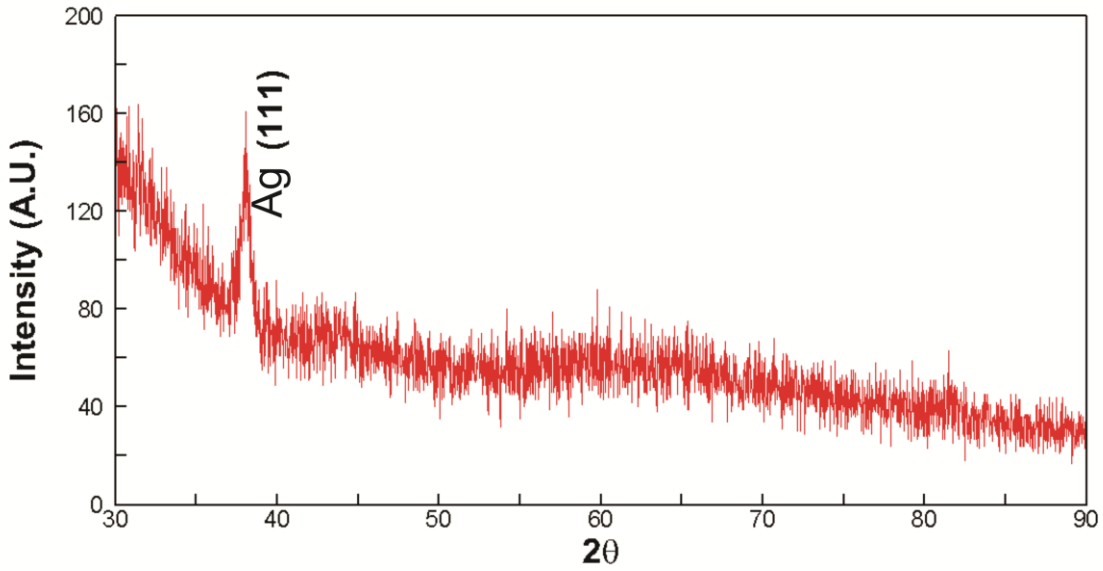

Figure B.2: Powder XRD of Ag NWs

TableB.2 Effect of electrode choices. Red represent cathode, black represents anode. Experimental conditions were T=-0.5°C, V=0.7 V, [AgNO3] =0.1 M, no supporting electrolyte.

	Ag	Cu	Ti	Pd	Ni
Ag	Branched NW	Branched µW	No Growth	Branched NW	No Growth
Cu	Branched µW	Branched µW	No Growth	Branched µW	No Growth
Ti	No Growth	No Growth	No Growth	No Growth	No Growth
Pd	Dendritic NW	Dendritic NW	No Growth	Dendritic NW	No Growth
Ni	No Growth	No Growth	No Growth	No Growth	No Growth

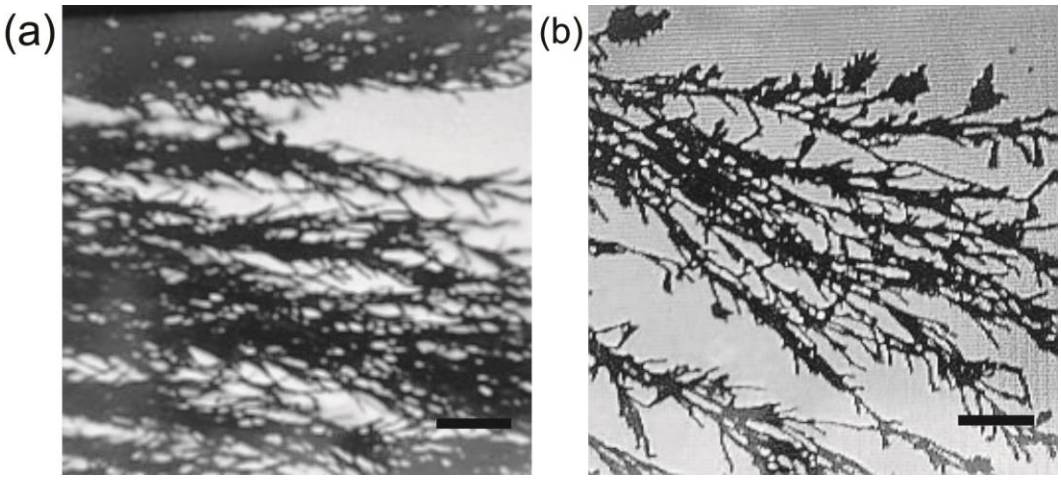

Figure B.3: Effect of electrodes (a) Ag anode, Pd cathode. (b) Ag cathode and anode. Experimental conditions were identical T=-0.5°C, V=0.7V, and [$AgNO_3$]=0.1 M. Scale bars are 40 µm

Table B.3: Effect of electrode spacing. Conditions were Ag electrodes, V=0.7V, T=-0.5 C

Distance (cm)	0.5	1	1.5	2	2.5	3
	Lightly branched dendrites	Lightly branched dendrites	Lightly branched dendrites	Lightly branched dendrites	Lightly branched dendrites	Lightly branched dendrites

Table B.3: Effect of Concentration. Conditions were Ag electrodes, T=-0.5°C, V=9V

[$AgNO_3$] (M)	0 to $1x10^{-4}$	$1x10^{-3}$	1 to $2x10^{-2}$	3 to$4x10^{-2}$	$5x10^{-2}$	$6\text{-}8x10^{-2}$	8 to 10 $x10^{-2}$
Results	Few short NWs	Few short branched NWs	Short branched NWs	Fine branched NWs	Branched NWs	Dendrites	Dense thick dendrites

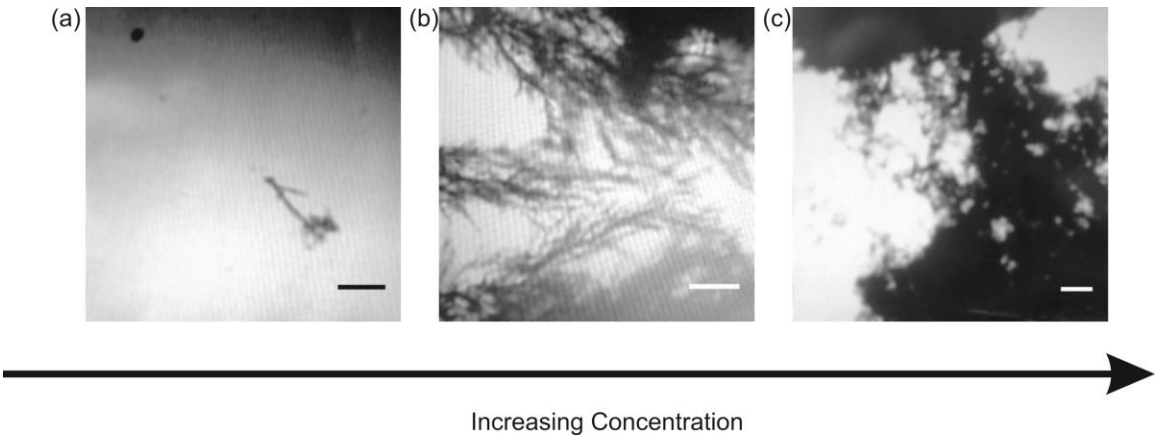

Figure B.4: Effect of increasing concentration. Conditions were Ag electrodes, T=-0.5°C, V=0.9V. (a) 0.0001 M(b)0.05 M, (c) 0.1 M Scale bars on (a) and (b) are 2 µm, (c) 20 µm

Table B.4 Effects of supporting electrolyte. Conditions were T=-0.05°C, [$AgNO_3$] =0.05M, V=0.7 V

[Citric Acid] (M)	0.01	0.05	1	1.5
	Lightly branched	Lightly branched with holes	Lightly branched with more holes	Excess gas produced-no results
[Boric Acid](M)	0.01	0.05	1	1.5
	Lightly branched	Few branches	Precipitated-No result	Precipitated-No result

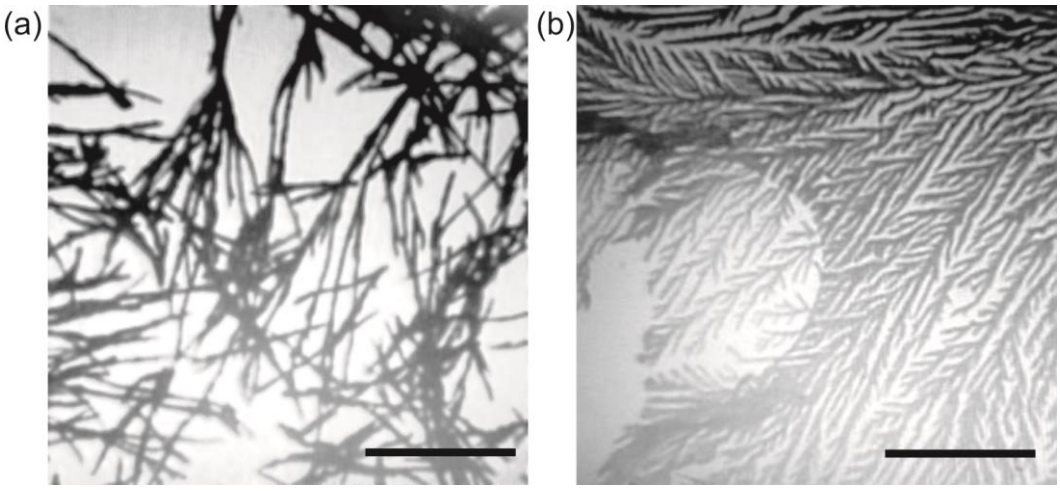

Figure B.5: Effect of supporting electrolyte. Conditions were T=-0.5° C, [$AgNO_3$] =0.05M, V=0.7V. (a) 0.05M boric acid (b) 0.05 M citric acid. Scale bars are 10 and 20 µm in (a) and (b) respectively.

Table B.6: Effect of temperature. Conditions were Ag electrodes, [$AgNO_3$]=0.1M, V=0.7V

Temperature (°C)	-10	-5	-0.5	0-40	40-60
Results	No growth	Fine fan-like dendrites	Branched NW	Dendritic NW	Branched µW

Table B.7: Effect of applied V. Conditions were T=-0.05°C, [$AgNO_3$] =0.05M with Ag electrodes

Voltage	0.5-0.9	2-10	30	40
	Branched NW	Dentrites	Film	No results

Table B.8: Effect of using applied current. Conditions were T=-0.05°C, [$AgNO_3$] =0.05 M with Ag electrodes

Current (mA)	0.01-0.08	0.08-0.12	0.15-0.2
Result	No Growth	Fine NWs	Branched µW

B.1.4. Silver Nanoindentation Hardness Results

The nanoindentation hardness, calculated by Hertz elastic theory, is shown below in Fig. B.8. The error is due to a range of fitting constants that yielded acceptable fits. With the exception of one point, all were below the measured indentation hardness when NWs yielded with distributed plasticity, providing further support for pre-existing strain causing hardening in these NWs.

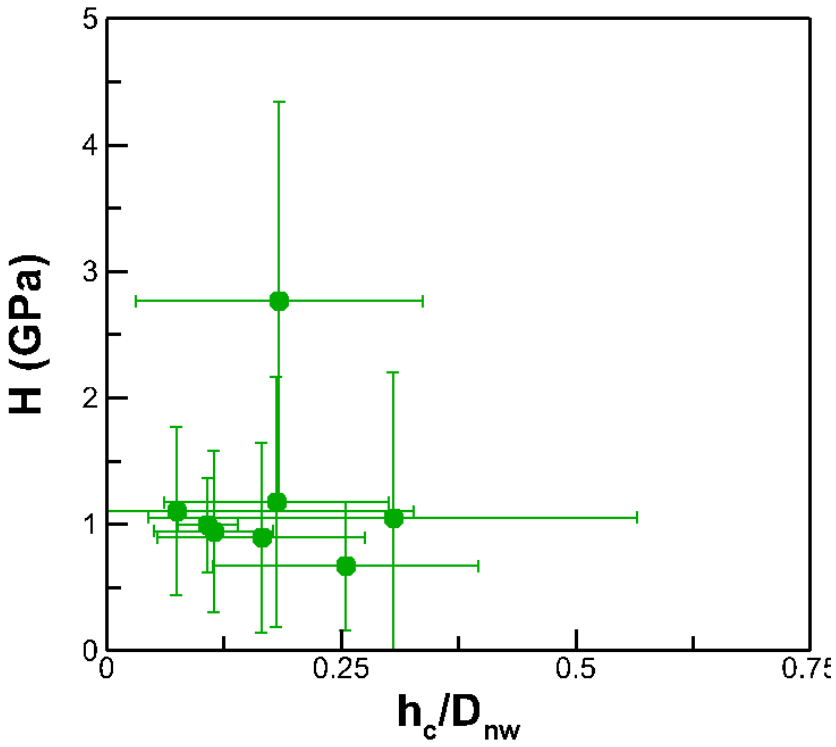

Figure B.7: Nanoindentation hardness is Ag calculated from Hertz elastic theory.

As shown in Fig. B.8 below, the nanoindentation hardness is not entirely governed by either the shear modulus, or the SFE, yet is influenced by each. Normalization by SFE yielded slightly better convergence, suggesting that this is perhaps a dominant factor, the interplay between materials properties and mechanical strength cannot be determined with these experiments. We find that the experimental E_{NW} varies somewhat but is around

71.4±14.3 GPa, which agrees reasonably well with other work.

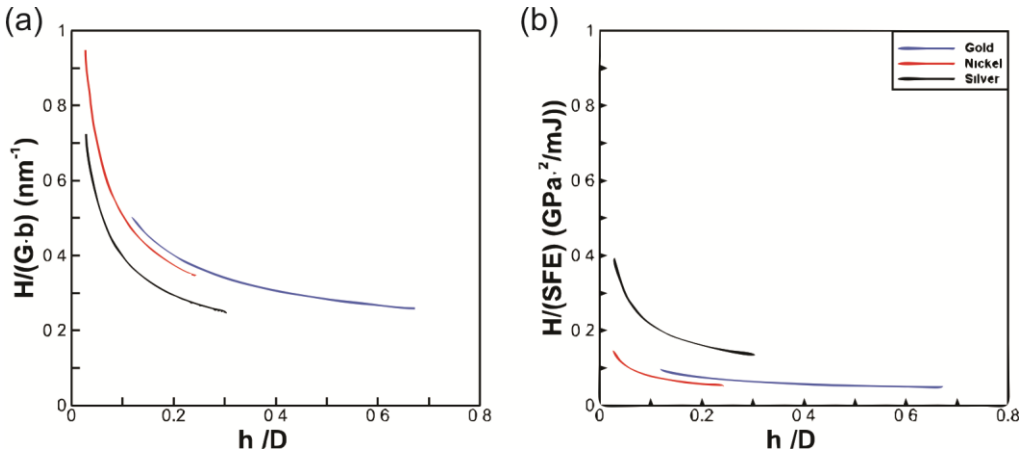

Figure B.8: Influence of materials properties on nanodindentation hardness (a) the effect of shear modulus and (b) SFE. Normalizing the nanoindenation hardness by SFE apparently yields better convergence.

Table B.9: Materials properties of FCC Metals

	G (GPa)	*b* (nm)	SFE (mJ m^{-2})
Ni	75	0.249	123.6
Au	27	0.288	41.6
Ag	30	0.289	16

B.2 Copper

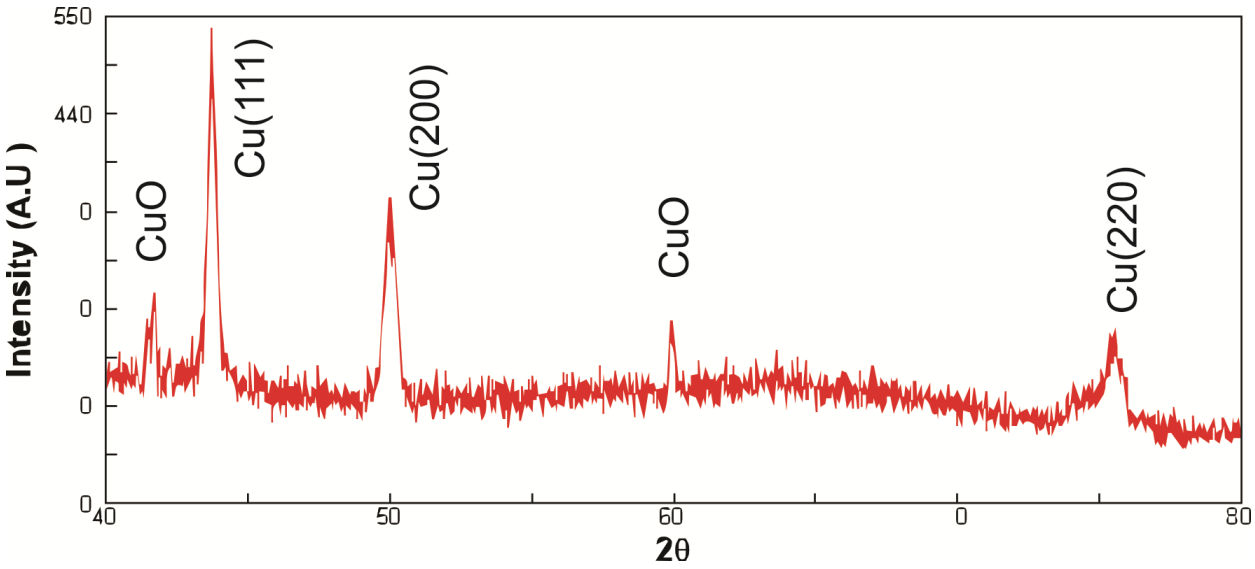

Figure B.9: Powder XRD of Cu NWs. Rapid oxidation occurred on as grown Cu NWs. It is also thought that the NWs may have formed three dimensional bundles.

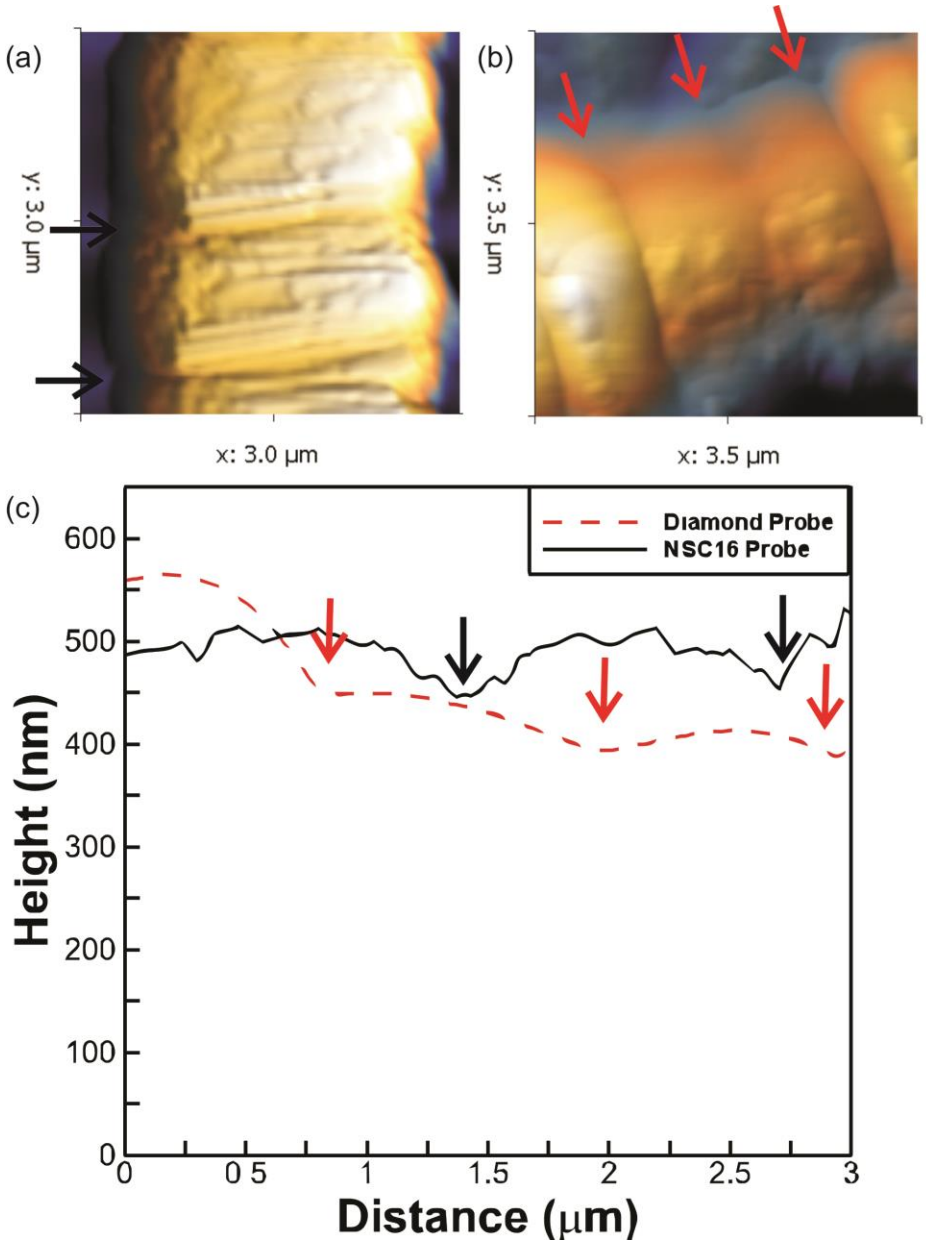

Figure B.10: Effect of tip radius on apparent microstructure. (a) NW image with standard tapping mode probe showing dense straight ridges along with larger corrugations spaces microns apart. (b) A NW from the same batch showing only the large corrugated structure due to the increased diameter (74.5 nm) of the indenter probe. (c) Line profiles of both NWs showing similar spacing of large corrugations (indicated by arrows).

B.3 AFM imaging

Atomic force microscopy is a powerful technique, but one that is limited to the probe that is being used. In our nanoindentation experiments, we both image and indent with a well characterized diamond probe with a radius of 74.5 nm, as measured by scanning a grating made up of well characterized Si spikes, as mentioned in the section regarding silver. However, our Cu NWs show corrugation spacing that is much smaller than the probe, so these NWs appear to be smooth with only troughs larger than the probe being imaged (Fig. C.2). Because nanoindentation is a time intensive process (each indent takes about 1 hour) we cannot image NWs with a higher resolution probe, calibrate the AFM nanoindenter tip with a fused quartz standard and perform nanoindentation, so the corrugation spacing is measured on NWs that are grown under identical conditions, and this corrugation spacing is what is used

References

1. Sansoz F, Stevenson KD. Relationship between Hardness and Dislocation Processes in a Nanocrystalline Metal at the Atomic Scale, Phys. Rev. B 2011;83:224101.
2. Tsuru Y, Nomura M, Foulkes FR. Effects of Boric Acid on Hydrogen Evolution and Internal Stress in Films Deposited from a Nickel Sulfamate Bath, Journal of Applied Electrochemistry 2002;32:629.
3. Sansoz F, Gang T. A Force-Matching Method for Quantitative Hardness

Measurements by Atomic Force Microscopy with Diamond-Tipped Sapphire Cantilevers, Ultramicroscopy 2010;111:11.

4. Zhu Y, Qin Q, Xu F, et al. Size Effects on Elasticity, Yielding, and Fracture of Silver Nanowires: In Situ Experiments, Physical review B 2012;85:045443.
5. Deng C, Sansoz F. Fundamental Differences in the Plasticity of Periodically Twinned Nanowires in Au, Ag, Al, Cu, Pb and Ni, Acta Mater. 2009;57:6090.

.

Bibliography

Afanasyev, Konstantin A. and Frederic Sansoz. "Strengthening in Gold Nanopillars with Nanoscale Twins." *Nano Lett.* 7, no. 7 (2007): 2056-2062.

Afanasyev, Konstantin A. and Frederic Sansoz. "Strengthening in Gold Nanopillars with Nanoscale Twins." *Nano Letters* 7, no. 7 (2007): 2056-2062.

Amir Parviz, B, Declan Ryan and George M Whitesides. "Using Self-Assembly for the Fabrication of Nano-Scale Electronic and Photonic Devices." *IEEE Trans. Adv. Packag* 26, no. 3 (2003): 233-241.

Askari, Davood and Gang Feng. "Finite Element Analysis of Nanowire Indentation on a Flat Substrate." *J. Mater. Res.* 27, no. 03 (2012): 586-591.

Bansal, S, E Toimil-Molares, A Saxena and Rao R Tummala. "Nanoindentation of Single Crystal and Polycrystalline Copper Nanowires." In *ELEC COMP C, 2005. Proceedings. 55th*, 71-76: IEEE, 2005.

Bauer, Laura Ann, Daniel H. Reich and Gerald J. Meyer. "Selective Functionalization of Two-Component Magnetic Nanowires." *Langmuir* 19, no. 17 (2003): 7043-7048.

Benfield, Robert E., Didier Grandjean, Michael Kröll, Raphael Pugin, Thomas Sawitowski and Günter Schmid. "Structure and Bonding of Gold Metal Clusters, Colloids, and Nanowires Studied by Exafs, Xanes, and Waxs." *The Journal of Physical Chemistry B* 105, no. 10 (2001): 1961-1970.

Bernardi, M., S. N. Raja and S. K. Lim. "Nanotwinned Gold Nanowires Obtained by Chemical Synthesis." *Nanotechnology* 21, no. 28 (2010): 285607.

Bott, Adrian W. "Controlled Current Techniques." *epsilon* 47906: 1382.

Branicio, Paulo S and José-Pedro Rino. "Large Deformation and Amorphization of Ni Nanowires under Uniaxial Strain: A Molecular Dynamics Study." *Phys. Rev. B* 62, no. 24 (2000): 16950.

Burek, Michael J. and Julia R. Greer. "Fabrication and Microstructure Control of Nanoscale Mechanical Testing Specimens Via Electron Beam Lithography and Electroplating." *Nano Letters* 10, no. 1 (2009): 69-76.

Busbee, B. D., S. O. Obare and C. J. Murphy. "An Improved Synthesis of High-Aspect-Ratio Gold Nanorods." *Advanced Materials* 15, no. 5 (2003): 414-416.

Cademartiri, Ludovico and Geoffrey A. Ozin. "Ultrathin Nanowires—a Materials Chemistry Perspective." *Advanced Materials* 21, no. 9 (2009): 1013-1020.

Cao, A. J., Y. G. Wei and Scott X. Mao. "Deformation Mechanisms of Face-Centered-Cubic Metal Nanowires with Twin Boundaries." *Applied Physics Letters* 90, no. 15 (2007): 151909.

Cao, AJ, YG Wei and Scott X Mao. "Deformation Mechanisms of Face-Centered-Cubic Metal Nanowires with Twin Boundaries." *Applied physics letters* 90, no. 15 (2007): 151909.

Cao, Ajing and E. Ma. "Sample Shape and Temperature Strongly Influence the Yield Strength of Metallic Nanopillars." *Acta Materialia* 56, no. 17 (2008): 4816-4828.

Cao, Ajing, Yueguang Wei and En Ma. "Grain Boundary Effects on Plastic Deformation and Fracture Mechanisms in Cu Nanowires: Molecular Dynamics Simulations." *Physical Review B* 77, no. 19 (2008): 195429.

Chen, Zhiming, Zhaohui Jin and Huajian Gao. "Repulsive Force between Screw Dislocation and Coherent Twin Boundary in Aluminum and Copper." *Physical Review B* 75, no. 21 (2007): 212104.

Choi, Yoonjoon, Krystyn J Van Vliet, Ju Li and Subra Suresh. "Size Effects on the Onset of Plastic Deformation During Nanoindentation of Thin Films and Patterned Lines." *J. Appl. Phys.* 94, no. 9 (2003): 6050-6058.

Cimalla, Volker, Claus-Christian Röhlig, Jörg Pezoldt, Merten Niebelschütz, Oliver Ambacher, Klemens Brückner, Matthias Hein, Jochen Weber, Srdjan Milenkovic and Andrew Jonathan Smith. "Nanomechanics of Single Crystalline Tungsten Nanowires." *J. Nanomater.* 2008, (2008): 44.

Cortés, Andrea, Gonzalo Riveros, Juan L Palma, Juliano C Denardin, Ricardo E Marotti, Enrique A Dalchiele and Humberto Gomez. "Single-Crystal Growth of Nickel Nanowires: Influence of Deposition Conditions on Structural and Magnetic Properties." *J. Nanosci. Nanotechno.* 9, no. 3 (2009): 1992-2000.

Cui, Yi, Qingqiao Wei, Hongkun Park and Charles M. Lieber. "Nanowire Nanosensors for Highly Sensitive and Selective Detection of Biological and Chemical Species." *Science* 293, no. 5533 (2001): 1289-1292.

Daniel, Marie-Christine and Didier Astruc. "Gold Nanoparticles: Assembly, Supramolecular Chemistry, Quantum-Size-Related Properties, and Applications

toward Biology, Catalysis, and Nanotechnology." *Chem. Rev.* 104, no. 1 (2003): 293-346.

Deng, C. and F. Sansoz. "Fundamental Differences in the Plasticity of Periodically Twinned Nanowires in Au, Ag, Al, Cu, Pb and Ni." *Acta Materialia* 57, no. 20 (2009): 6090-6101.

Deng, C. and F. Sansoz. "Fundamental Differences in the Plasticity of Periodically Twinned Nanowires in Au, Ag, Al, Cu, Pb and Ni." *Acta Mater.* 57, no. 20 (2009): 6090-6101.

Deng, Chuang and Frederic Sansoz. "Enabling Ultrahigh Plastic Flow and Work Hardening in Twinned Gold Nanowires." *Nano Lett.* 9, no. 4 (2009): 1517-1522.

Deng, Chuang and Frederic Sansoz. "Enabling Ultrahigh Plastic Flow and Work Hardening in Twinned Gold Nanowires." *Nano Letters* 9, no. 4 (2009): 1517-1522.

Deng, Chuang and Frederic Sansoz. "Near-Ideal Strength in Gold Nanowires Achieved through Microstructural Design." *ACS Nano* 3, no. 10 (2009): 3001-3008.

Deng, Chuang and Frederic Sansoz. "Size-Dependent Yield Stress in Twinned Gold Nanowires Mediated by Site-Specific Surface Dislocation Emission." *Appl. Phys. Lett.* 95, no. 9 (2009): 091914-3.

Deng, Chuang and Frederic Sansoz. "Effects of Twin and Surface Facet on Strain-Rate Sensitivity of Gold Nanowires at Different Temperatures." *Physical Review B* 81, no. 15 (2010): 155430.

Deng, Chuang and Frederic Sansoz. "Effects of Twin and Surface Facet on Strain-Rate Sensitivity of Gold Nanowires at Different Temperatures." *Phys. Rev. B* 81, no. 15 (2010): 155430.

Deng, Chuang and Frederic Sansoz. "Repulsive Force of Twin Boundary on Curved Dislocations and Its Role on the Yielding of Twinned Nanowires." *Scripta Mater.* 63, no. 1 (2010): 50-53.

Deng, Chuang and Frederic Sansoz. "Repulsive Force of Twin Boundary on Curved Dislocations and Its Role on the Yielding of Twinned Nanowires." *Scripta Materialia* 63, no. 1 (2010): 50-53.

Diao, Jiankuai, Ken Gall and Martin L Dunn. "Yield Strength Asymmetry in Metal Nanowires." *Nano Letters* 4, no. 10 (2004): 1863-1867.

Diao, Jiankuai, Ken Gall, Martin L Dunn and Jonathan A Zimmerman. "Atomistic Simulations of the Yielding of Gold Nanowires." *Acta Mater.* 54, no. 3 (2006): 643-653.

Dietiker, Marianne, Ralph D Nyilas, Christian Solenthaler and Ralph Spolenak. "Nanoindentation of Single-Crystalline Gold Thin Films: Correlating Hardness and the Onset of Plasticity." *Acta Mater.* 56, no. 15 (2008): 3887-3899.

Ding, Chunhua, Cuifeng Tian, Ralph Krupke and Jixiang Fang. "Growth of Non-Branching Ag Nanowires Via Ion Migrational-Transport Controlled 3d Electrodeposition." *CrystEngComm* 14, no. 3 (2012).

Dou, R and B Derby. "The Strength of Gold Nanowire Forests." *Scripta Mater.* 59, no. 2 (2008): 151-154.

Dou, R and B Derby. "A Universal Scaling Law for the Strength of Metal Micropillars and Nanowires." *Scripta Mater.* 61, no. 5 (2009): 524-527.

Dupont, V. and F. Sansoz. "Molecular Dynamics Study of Crystal Plasticity During Nanoindentation in Ni Nanowires." *J. Mater. Res.* 24, no. 3 (2009): 948-956.

Fang, Jixiang, Horst Hahn, Ralph Krupke, Frank Schramm, Torsten Scherer, Bingjun Ding and Xiaoping Song. "Silver Nanowires Growth Via Branch Fragmentation of Electrochemically Grown Silver Dendrites." *Chemical Communications*, no. 9 (2009): 1130-1132.

Fang, Jixiang, Horst Hahn, Ralph Krupke, Frank Schramm, Torsten Scherer, Bingjun Ding and Xiaoping Song. "Silver Nanowires Growth Via Branch Fragmentation of Electrochemically Grown Silver Dendrites." *Chemical Communications*, no. 9 (2009).

Feng, Gang, William D Nix, Youngki Yoon and Cheol Jin Lee. "A Study of the Mechanical Properties of Nanowires Using Nanoindentation." *J. Appl. Phys.* 99, no. 7 (2006): 074304-074304-10.

Fu, J, N Singh, KD Buddharaju, SHG Teo, C Shen, Y Jiang, CX Zhu, MB Yu, GQ Lo and N Balasubramanian. "Si-Nanowire Based Gate-All-around Nonvolatile Sonos Memory Cell." *Electron Device Letters, IEEE* 29, no. 5 (2008): 518-521.

Gall, Ken, Jiankuai Diao and Martin L. Dunn. "The Strength of Gold Nanowires." *Nano Letters* 4, no. 12 (2004): 2431-2436.

Gianola, Daniel S, Andreas Sedlmayr, R Monig, Cynthia A Volkert, Ryan C Major, Edward Cyrankowski, SAS Asif, Oden L Warren and Oliver Kraft. "In Situ Nanomechanical Testing in Focused Ion Beam and Scanning Electron Microscopes." *Rev. Sci. Instrum.* 82, no. 6 (2011): 063901-063901-12.

Gouldstone, A., H. J. Koh, K. Y. Zeng, A. E. Giannakopoulos and S. Suresh. "Discrete and Continuous Deformation During Nanoindentation of Thin Films." *Acta Mater.* 48, no. 9 (2000): 2277-2295.

Graça, S, R Colaço and R Vilar. "Indentation Size Effect in Nickel and Cobalt Laser Clad Coatings." *Surf. Coat. Technol.* 202, no. 3 (2007): 538-548.

Greer, J. R., W. C. Oliver and W. D. Nix. "Size Dependence of Mechanical Properties of Gold at the Micron Scale in the Absence of Strain Gradients." *Acta Mater.* 53, no. 6 (2005): 1821-1830.

Haes, Amanda J, Douglas A Stuart, Shuming Nie and Richard P Van Duyne. "Using Solution-Phase Nanoparticles, Surface-Confined Nanoparticle Arrays and Single Nanoparticles as Biological Sensing Platforms." *J. Fluoresc.* 14, no. 4 (2004): 355-367.

Halder, A. and N. Ravishankar. "Ultrafine Single-Crystalline Gold Nanowire Arrays by Oriented Attachment." *Advanced Materials* 19, no. 14 (2007): 1854-1858.

Han, Jing, Liang Fang, Jiapeng Sun, Ying Han and Kun Sun. "Length-Dependent Mechanical Properties of Gold Nanowires." *J. Appl. Phys.* 112, no. 11 (2012): 114314-114314-7.

Hong, Xun, Dingsheng Wang and Yadong Li. "Kinked Gold Nanowires and Their Spr/Sers Properties." *Chemical Communications* 47, no. 35 (2011).

Huang, Dan, Qing Zhang and Pizhong Qiao. "Molecular Dynamics Evaluation of Strain Rate and Size Effects on Mechanical Properties of Fcc Nickel Nanowires." *Computational Materials Science* 50, no. 3 (2011): 903-910.

Huang, Xiaoqing and Nanfeng Zheng. "One-Pot, High-Yield Synthesis of 5-Fold Twinned Pd Nanowires and Nanorods." *Journal of the American Chemical Society* 131, no. 13 (2009): 4602-4603.

Hui, Pan, Sun Han, Poh Cheekok, Feng Yuanping and Lin Jianyi. "Single-Crystal Growth of Metallic Nanowires with Preferred Orientation." *Nanotechnology* 16, no. 9 (2005): 1559.

Hyde, Brian, Horacio D Espinosa and Diana Farkas. "An Atomistic Investigation of Elastic and Plastic Properties of Au Nanowires." *Jom* 57, no. 9 (2005): 62-66.

Hyde, Brian, Horacio Espinosa and Diana Farkas. "An Atomistic Investigation of Elastic and Plastic Properties of Au Nanowires." *JOM* 57, no. 9 (2005): 62-66.

Jang, Dongchan, Can Cai and Julia R. Greer. "Influence of Homogeneous Interfaces on the Strength of 500 Nm Diameter Cu Nanopillars." *Nano Letters* 11, no. 4 (2011): 1743-1746.

Jang, Dongchan, Xiaoyan Li, Huajian Gao and Julia R Greer. "Deformation Mechanisms in Nanotwinned Metal Nanopillars." *Nature nanotechnology* 7, no. 9 (2012): 594-601.

Jennings, Andrew T., Ju Li and Julia R. Greer. "Emergence of Strain-Rate Sensitivity in Cu Nanopillars: Transition from Dislocation Multiplication to Dislocation Nucleation." *Acta Mater.* 59, no. 14 (2011): 5627-5637.

Ji, Changjiang and Harold S Park. "The Coupled Effects of Geometry and Surface Orientation on the Mechanical Properties of Metal Nanowires." *Nanotechnology* 18, no. 30 (2007): 305704.

Jiang, Jin-Wu, Austin M. Leach, Ken Gall, Harold S. Park and Timon Rabczuk. "A Surface Stacking Fault Energy Approach to Predicting Defect Nucleation in Surface-Dominated Nanostructures." *J. Mech. Phys. Solid.* 61, no. 9 (2013): 1915-1934.

Karim, S., M. E. Toimil-Molares, F. Maurer, G. Miehe, W. Ensinger, J. Liu, T. W. Cornelius and R. Neumann. "Synthesis of Gold Nanowires with Controlled Crystallographic Characteristics." *Applied Physics A: Materials Science & Processing* 84, no. 4 (2006): 403-407.

Keating, Christine D and Michael J Natan. "Striped Metal Nanowires as Building Blocks and Optical Tags." *Adv. Mater.* 15, no. 5 (2003): 451-454.

Kiener, D, P Hosemann, SA Maloy and AM Minor. "In Situ Nanocompression Testing of Irradiated Copper." *Nature Mater.* 10, no. 8 (2011): 608-613.

Koh, SJA and HP Lee. "Molecular Dynamics Simulation of Size and Strain Rate Dependent Mechanical Response of Fcc Metallic Nanowires." *Nanotechnology* 17, no. 14 (2006): 3451.

Kovtyukhova, Nina I and Thomas E Mallouk. "Nanowires as Building Blocks for Self-Assembling Logic and Memory Circuits." *Chemistry-A European Journal* 8, no. 19 (2002): 4354-4363.

Lee, Se-Ho, Yeonwoong Jung and Ritesh Agarwal. "Highly Scalable Non-Volatile and Ultra-Low-Power Phase-Change Nanowire Memory." *Nature Nanotech.* 2, no. 10 (2007): 626-630.

Legros, M, DS Gianola and C Motz. "Quantitative in Situ Mechanical Testing." *MRS Bull.* 35, (2010).

Li, Xiaodong, Hongsheng Gao, Catherine J. Murphy and K. K. Caswell. "Nanoindentation of Silver Nanowires." *Nano Lett.* 3, no. 11 (2003): 1495-1498.

Li, Yat, Fang Qian, Jie Xiang and Charles M Lieber. "Nanowire Electronic and Optoelectronic Devices." *Materials today* 9, no. 10 (2006): 18-27.

Li, Z, Y Chen, X Li, TI Kamins, K Nauka and R Stanley Williams. "Sequence-Specific Label-Free DNA Sensors Based on Silicon Nanowires." *Nano Letters* 4, no. 2 (2004): 245-247.

Lian, Jie, Junlan Wang, Yu-Young Kim and Julia Greer. "Sample Boundary Effect in Nanoindentation of Nano and Microscale Surface Structures." *J. Mech. Phys. Solid.* 57, no. 5 (2009): 812-827.

Liang, Haiyi, Moneesh Upmanyu and Hanchen Huang. "Size-Dependent Elasticity of Nanowires: Nonlinear Effects." *Phys. Rev. B* 71, no. 24 (2005): 241403.

Liang, Haiyi, Moneesh Upmanyu and Hanchen Huang. "Size-Dependent Elasticity of Nanowires: Nonlinear Effects." *Physical Review B* 71, no. 24 (2005): 241403.

Liang, Hongyan, Huaixin Yang, Wenzhong Wang, Jianqi Li and Hongxing Xu. "High-Yield Uniform Synthesis and Microstructure-Determination of Rice-Shaped Silver Nanocrystals." *Journal of the American Chemical Society* 131, no. 17 (2009): 6068-6069.

Ling, Tao, Huimin Yu, Xiaohua Liu, Zhongyao Shen and Jing Zhu. "Five-Fold Twinned Nanorods of Fcc Fe: Synthesis and Characterization." *Crystal Growth & Design* 8, no. 12 (2008): 4340-4342.

Link, Stephan and Mostafa A El-Sayed. "Size and Temperature Dependence of the Plasmon Absorption of Colloidal Gold Nanoparticles." *J. Phys. Chem. B* 103, no. 21 (1999): 4212-4217.

Liu, Xiangwen, Dingsheng Wang and Yadong Li. "Synthesis and Catalytic Properties of Bimetallic Nanomaterials with Various Architectures." *Nano Today*, (2012).

Lu, L., X. Chen, X. Huang and K. Lu. "Revealing the Maximum Strength in Nanotwinned Copper." *Science* 323, no. 5914 (2009): 607-610.

Lu, Lei, Yongfeng Shen, Xianhua Chen, Lihua Qian and K. Lu. "Ultrahigh Strength and High Electrical Conductivity in Copper." *Science* 304, no. 5669 (2004): 422-426.

Lu, Y., J. Y. Huang, C. Wang, S. H. Sun and J. Lou. "Cold Welding of Ultrathin Gold Nanowires." *Nature Nanotech.* 5, no. 3 (2010): 218-224.

Lu, Y., J. Song, J. Y. Huang and J. Lou. "Fracture of Sub-20nm Ultrathin Gold Nanowires." *Adv. Funct. Mater.* 21, no. 20 (2011): 3982-3989.

Lu, Y., J. Song, J. Y. Huang and J. Lou. "Surface Dislocation Nucleation Mediated Deformation and Ultrahigh Strength in Sub-10-Nm Gold Nanowires." *Nano Res.* 4, no. 12 (2011): 1261-1267.

Lu, Yang and Jun Lou. "Quantitative in-Situ Nanomechanical Characterization of Metallic Nanowires." *JOM Journal of the Minerals, Metals and Materials Society* 63, no. 9 (2011): 35-42.

Lu, Yang, Cheng Peng, Yogeeswaran Ganesan, Jian Yu Huang and Jun Lou. "Quantitative in Situ Tem Tensile Testing of an Individual Nickel Nanowire." *Nanotechnology* 22, no. 35 (2011): 355702.

Lu, Yang, Jun Song, Jian Huang and Jun Lou. "Surface Dislocation Nucleation Mediated Deformation and Ultrahigh Strength in Sub-10-Nm Gold Nanowires." *Nano Research* 4, no. 12 (2011): 1261-1267.

Lucas, Marcel, Austin M Leach, Matthew T McDowell, Simona E Hunyadi, Ken Gall, Catherine J Murphy and Elisa Riedo. "Plastic Deformation of Pentagonal Silver Nanowires: Comparison between Afm Nanoindentation and Atomistic Simulations." *Phys. Rev. B* 77, no. 24 (2008): 245420.

Ma, Zengsheng, Shiguo Long, Yong Pan and Yichun Zhou. "Indentation Depth Dependence of the Mechanical Strength of Ni Films." *J. Appl. Phys.* 103, no. 4 (2008): 043512-043512-6.

Marco, Bernardi, N. Raja Shilpa and Lim Sung Keun. "Nanotwinned Gold Nanowires Obtained by Chemical Synthesis." *Nanotechnology* 21, no. 28 (2010): 285607.

Martin, Charles R. "Nanomaterials: A Membrane-Based Synthetic Approach." *Science* 266, no. 5193 (1994): 1961-1966.

Maurer, F., J. Brötz, S. Karim, M.E. Toimil-Molares, C. Trautmann and H. Fuess. "Preferred Growth Orientation of Metallic Fcc Nanowires under Direct and Alternating Electrodeposition Conditions." *Nanotechnology* 18, no. 13 (2007): 135709.

McAllister, Quinn P, John W Gillespie Jr and Mark R VanLandingham. "Nonlinear Indentation of Fibers." *J. Mater. Res.* 27, no. 1 (2012): 197.

McAllister, Quinn P., John W. Jr. Gillespie and Mark R. VanLandingham. "Nonlinear Indentation of Fibers." *J. Mater. Res.* 27, no. 01 (2012): 197-213.

Minor, AM, JW Morris and EA Stach. "Quantitative in Situ Nanoindentation in an Electron Microscope." *Appl. Phys. Lett.* 79, no. 11 (2001): 1625-1627.

Mompiou, Frédéric, Marc Legros, Andreas Sedlmayr, Daniel S Gianola, Daniel Caillard and Oliver Kraft. "Source-Based Strengthening of Sub-Micrometer Al Fibers." *Acta Mater.* 60, no. 3 (2012): 977-983.

Mordehai, Dan, Michael Kazakevich, David J Srolovitz and Eugen Rabkin. "Nanoindentation Size Effect in Single-Crystal Nanoparticles and Thin Films: A Comparative Experimental and Simulation Study." *Acta Mater.* 59, no. 6 (2011): 2309-2321.

Mordehai, Dan, Seok-Woo Lee, Björn Backes, David J Srolovitz, William D Nix and Eugen Rabkin. "Size Effect in Compression of Single-Crystal Gold Microparticles." *Acta Mater.* 59, no. 13 (2011): 5202-5215.

Motoyama, M., Y. Fukunaka, T. Sakka and Y. H. Ogata. "Initial Stages of Electrodeposition of Metal Nanowires in Nanoporous Templates." *Electrochimica Acta* 53, no. 1 (2007): 205-212.

Nečas, David and Petr Klapetek. "Gwyddion: An Open-Source Software for Spm Data Analysis." *Central Cent. Eur. J. Phys.* 10, no. 1 (2012): 181-188.

Nicewarner-Pena, Sheila R, R Griffith Freeman, Brian D Reiss, Lin He, David J Peña, Ian D Walton, Remy Cromer, Christine D Keating and Michael J Natan. "Submicrometer Metallic Barcodes." *Science* 294, no. 5540 (2001): 137-141.

Nix, W. D. and H. J. Gao. "Indentation Size Effects in Crystalline Materials: A Law for Strain Gradient Plasticity." *J. Mech. Phys. Solid.* 46, no. 3 (1998): 411-425.

Oliver, Warren Carl and George Mathews Pharr. "Improved Technique for Determining Hardness and Elastic Modulus Using Load and Displacement Sensing Indentation Experiments." *J. Mater. Res.* 7, no. 6 (1992): 1564-1583.

Pan, Hui, Han Sun, Cheekok Poh, Yuanping Feng and Jianyi Lin. "Single-Crystal Growth of Metallic Nanowires with Preferred Orientation." *Nanotechnology* 16, no. 9 (2005): 1559.

Park, Harold S, Wei Cai, Horacio D Espinosa and Hanchen Huang. "Mechanics of Crystalline Nanowires." *MRS bulletin* 34, no. 03 (2009): 178-183.

Park, Harold S, Ken Gall and Jonathan A Zimmerman. "Deformation of Fcc Nanowires by Twinning and Slip." *Journal of the Mechanics and Physics of Solids* 54, no. 9 (2006): 1862-1881.

Park, Harold S and Patrick A Klein. "Surface Cauchy-Born Analysis of Surface Stress Effects on Metallic Nanowires." *Phys. Rev. B* 75, no. 8 (2007): 085408.

Peng, Cheng, Yongjie Zhan and Jun Lou. "Size-Dependent Fracture Mode Transition in Copper Nanowires." *Small* 8, no. 12 (2012): 1889-1894.

Pérez-Juste, Jorge, Isabel Pastoriza-Santos, Luis M Liz-Marzán and Paul Mulvaney. "Gold Nanorods: Synthesis, Characterization and Applications." *Coordination Chemistry Reviews* 249, no. 17 (2005): 1870-1901.

Pérez-Juste, Jorge, Isabel Pastoriza-Santos, Luis M. Liz-Marzán and Paul Mulvaney. "Gold Nanorods: Synthesis, Characterization and Applications." *Coordination Chemistry Reviews* 249, no. 17–18 (2005): 1870-1901.

Petrova, Hristina, Jorge Perez-Juste, Zhenyuan Zhang, Jing Zhang, Tom Kosel and Gregory V. Hartland. "Crystal Structure Dependence of the Elastic Constants of Gold Nanorods." *Journal of Materials Chemistry* 16, no. 40 (2006).

Qu, S., Y. Huang, W.D. Nix, H. Jiang, F. Zhang and K.C. Hwang. "Indenter Tip Radius Effect on the Nix–Gao Relation in Micro- and Nanoindentation Hardness Experiments." *J. Mater. Res.* 19, no. 11 (2004): 3423-3434.

Ramgir, Niranjan S, Yang Yang and Margit Zacharias. "Nanowire-Based Sensors." *Small* 6, no. 16 (2010): 1705-1722.

Rester, M, C Motz and R Pippan. "Stacking Fault Energy and Indentation Size Effect: Do They Interact?" *Scripta Materialia* 58, no. 3 (2008): 187-190.

Rex, Matthew, Florencio E Hernandez and Andres D Campiglia. "Pushing the Limits of Mercury Sensors with Gold Nanorods." *Anal. Chem.Analytical chemistry* 78, no. 2 (2006): 445-451.

Rinaldi, A, P Peralta, C Friesen and K Sieradzki. "Sample-Size Effects in the Yield Behavior of Nanocrystalline Nickel." *Acta Mater.* 56, no. 3 (2008): 511-517.

Sakamoto, Yuzuru, Atsushi Fukuoka, Takanori Higuchi, Noriyuki Shimomura, Shinji Inagaki and Masaru Ichikawa. "Synthesis of Platinum Nanowires in Organic−Inorganic Mesoporous Silica Templates by Photoreduction: Formation Mechanism and Isolation." *The Journal of Physical Chemistry B* 108, no. 3 (2003): 853-858.

Salem, Aliasger K., Peter C. Searson and Kam W. Leong. "Multifunctional Nanorods for Gene Delivery." *Nature Mater.* 2, no. 10 (2003): 668-671.

Samardak, AS, EV Sukovatitsina, AV Ognev, LA Chebotkevich, R Mahmoodi, SM Peighambari, MG Hosseini and F Nasirpouri. "High-Density Nickel Nanowire Arrays for Data Storage Applications." In *JPCS*, 345, 012011: IOP Publishing, 2012.

Sansoz, F., H. Huang and D. H. Warner. "An Atomistic Perspective on Twinning Phenomena in Nano-Enhanced Fcc Metals." *JOM* 9, (2008): 79-84.

Sansoz, Frederic. "Atomistic Processes Controlling Flow Stress Scaling During Compression of Nanoscale Face-Centered-Cubic Crystals." *Acta Mater.* 59, no. 9 (2011): 3364-3372.

Sansoz, Frederic and Virginie Dupont. "Nanoindentation and Plasticity in Nanocrystalline Ni Nanowires: A Case Study in Size Effect Mitigation." *Scripta Mater.* 63, no. 11 (2010): 1136-1139.

Sansoz, Frederic and Virginie Dupont. "Nanoindentation and Plasticity in Nanocrystalline Ni Nanowires: A Case Study in Size Effect Mitigation." *Scripta Materialia* 63, no. 11 (2010): 1136-1139.

Sansoz, Frederic and Travis Gang. "A Force-Matching Method for Quantitative Hardness Measurements by Atomic Force Microscopy with Diamond-Tipped Sapphire Cantilevers." *Ultramicroscopy* 111, no. 1 (2010): 11-19.

Sansoz, Frederic and Kevin D. Stevenson. "Relationship between Hardness and Dislocation Processes in a Nanocrystalline Metal at the Atomic Scale." *Phys. Rev. B* 83, no. 22 (2011): 224101.

Sauer, G., G. Brehm, S. Schneider, K. Nielsch, R. B. Wehrspohn, J. Choi, H. Hofmeister and U. Gösele. "Highly Ordered Monocrystalline Silver Nanowire Arrays." *Journal of Applied Physics* 91, no. 5 (2002): 3243-3247.

Seo, Jong-Hyun, Youngdong Yoo, Na-Young Park, Sang-Won Yoon, Hyoban Lee, Sol Han, Seok-Woo Lee, Tae-Yeon Seong, Seung-Cheol Lee and Kon-Bae Lee. "Superplastic Deformation of Defect-Free Au Nanowires Via Coherent Twin Propagation." *Nano Lett.* 11, no. 8 (2011): 3499-3502.

Shan, ZW, Raja K Mishra, SA Syed Asif, Oden L Warren and Andrew M Minor. "Mechanical Annealing and Source-Limited Deformation in Submicrometre-Diameter Ni Crystals." *Nature materials* 7, no. 2 (2007): 115-119.

Shankar, M Ravi and Alexander H King. "How Surface Stresses Lead to Size-Dependent Mechanics of Tensile Deformation in Nanowires." *Applied physics letters* 90, no. 14 (2007): 141907.

Shen, Ming, Yukou Du, Ping Yang and Long Jiang. "Morphology Control of the Fabricated Hydrophobic Gold Nanostructures in W/O Microemulsion under Microwave Irradiation." *Journal of Physics and Chemistry of Solids* 66, no. 10 (2005): 1628-1634.

Shen, Xiao Shuang, Guan Zhong Wang, Xun Hong, Xing Xie, Wei Zhu and Da Peng Li. "Anisotropic Growth of One-Dimensional Silver Rod−Needle and Plate−Belt Heteronanostructures Induced by Twins and Hcp Phase." *Journal of the American Chemical Society* 131, no. 31 (2009): 10812-10813.

Soifer, Ya M, A Verdyan, M Kazakevich and E Rabkin. "Edge Effect During Nanoindentation of Thin Copper Films." *Mater. Lett.* 59, no. 11 (2005): 1434-1438.

Sudeep, PK, ST Shibu Joseph and K George Thomas. "Selective Detection of Cysteine and Glutathione Using Gold Nanorods." *J. Am. Chem. Soc* 127, no. 18 (2005): 6516-6517.

Sun, Shaodong, Dongchu Deng, Chuncai Kong, Yunxia Zhang, Xiaoping Song, Bingjun Ding and Zhimao Yang. "Magnetic Field Driven Assembly of 1d-Aligned Silver Superstructures." *CrystEngComm* 13, no. 15 (2011): 4827-4830.

Sun, X. M and Y. D Li. "Cylindrical Silver Nanowires: Preparation, Structure, and Optical Properties." *Advanced Materials* 17, no. 21 (2005): 2626-2630.

Sun, Yugang, Byron Gates, Brian Mayers and Younan Xia. "Crystalline Silver Nanowires by Soft Solution Processing." *Nano Letters* 2, no. 2 (2002): 165-168.

Sun, Yugang, Brian Mayers, Thurston Herricks and Younan Xia. "Polyol Synthesis of Uniform Silver Nanowires: A Plausible Growth Mechanism and the Supporting Evidence." *Nano Letters* 3, no. 7 (2003): 955-960.

Tabor, David. *The Hardness of Metals*: Oxford university press, 2000.

Tan, Ming and Xinqi Chen. "Growth Mechanism of Single Crystal Nanowires of Fcc Metals (Ag, Cu, Ni) and Hcp Metal (Co) Electrodeposited." *Journal of The Electrochemical Society* 159, no. 1 (2012): K15-K20.

Tian, Mingliang, Jinguo Wang, James Kurtz, Thomas E. Mallouk and M. H. W. Chan. "Electrochemical Growth of Single-Crystal Metal Nanowires Via a Two-Dimensional Nucleation and Growth Mechanism." *Nano Letters* 3, no. 7 (2003): 919-923.

Toimil Molares, M. E., V. Buschmann, D. Dobrev, R. Neumann, R. Scholz, I. U. Schuchert and J. Vetter. "Single-Crystalline Copper Nanowires Produced by Electrochemical Deposition in Polymeric Ion Track Membranes." *Advanced Materials* 13, no. 1 (2001): 62-65.

Tok, Jeffrey B-H, Frank Chuang, Michael C Kao, Klint A Rose, Satinderpall S Pannu, Michael Y Sha, Gabriela Chakarova, Sharron G Penn and George M Dougherty. "Metallic Striped Nanowires as Multiplexed Immunoassay Platforms for Pathogen Detection." *Angew. Chem. Int. Ed.* 45, no. 41 (2006): 6900-6904.

Tsuru, Y., M. Nomura and F. R. Foulkes. "Effects of Boric Acid on Hydrogen Evolution and Internal Stress in Films Deposited from a Nickel Sulfamate Bath." *Journal of Applied Electrochemistry* 32, no. 6 (2002): 629-634.

Uchic, Michael D., Dennis M. Dimiduk, Jeffrey N. Florando and William D. Nix. "Sample Dimensions Influence Strength and Crystal Plasticity." *Science* 305, no. 5686 (2004): 986-989.

Vlassov, Sergei, Boris Polyakov, Leonid M Dorogin, Mikk Antsov, Magnus Mets, Madis Umalas, Rando Saar, Rünno Lõhmus and Ilmar Kink. "Elasticity and Yield Strength of Pentagonal Silver Nanowires: In Situ Bending Tests." *Materials Chemistry and Physics* 143, no. 3 (2014): 1026-1031.

Walter, EC, RM Penner, H Liu, KH Ng, MP Zach and F Favier. "Sensors from Electrodeposited Metal Nanowires." *Surface and interface analysis* 34, no. 1 (2002): 409-412.

Walter, Erich C., Michael P. Zach, Frédéric Favier, Benjamin J. Murray, Koji Inazu, John C. Hemminger and Reginald M. Penner. "Metal Nanowire Arrays by Electrodeposition." *ChemPhysChem* 4, no. 2 (2003): 131-138.

Walton, Ian D., Scott M. Norton, Arjuna Balasingham, Lin He, Dominador F. Oviso, Dimpy Gupta, Paul A. Raju, Michael J. Natan and R. Griffith Freeman. "Particles for Multiplexed Analysis in Solution: Detection and Identification of Striped Metallic Particles Using Optical Microscopy." *Anal. Chem.Analytical chemistry* 74, no. 10 (2002): 2240-2247.

Wang, Biao, Guang Tao Fei, Ye Zhou, Bing Wu, Xiaoguang Zhu and Lide Zhang. "Controlled Growth and Phase Transition of Silver Nanowires with Dense Lengthwise Twins and Stacking Faults." *Crystal Growth & Design* 8, no. 8 (2008): 3073-3076.

Wang, Chao, Yujie Wei, Hongyuan Jiang and Shouheng Sun. "Bending Nanowire Growth in Solution by Mechanical Disturbance." *Nano Letters* 10, no. 6 (2010): 2121-2125.

Wang, Fenying, Yunhong Liu, Xing Yin, Nan Wang, Dongxu Wang, Yajun Gao and Jianwei Zhao. "The Interface and Surface Effects of the Bicrystal Nanowires on Their Mechanical Behaviors under Uniaxial Stretching." *J. Appl. Phys.* 108, no. 7 (2010): 074311-074311-8.

Wang, J. W., F. Sansoz, J. Y. Huang, Y. Liu, S. H. Sun, Z. Zhang and S. X. Mao. "Near-Ideal Theoretical Strength in Gold Nanowires Containing Angstrom Scale Twins." *Nat. Commun.* 4, (2013).

Wang, Jian and Hanchen Huang. "Novel Deformation Mechanism of Twinned Nanowires." *Applied physics letters* 88, no. 20 (2006): 203112.

Wang, Jiangwei, Frederic Sansoz, Jianyu Huang, Yi Liu, Shouheng Sun, Ze Zhang and Scott X Mao. "Near-Ideal Theoretical Strength in Gold Nanowires Containing Angstrom Scale Twins." *Nature communications* 4, (2013): 1742.

Wang, Jinguo, Mingliang Tian, Thomas E. Mallouk and Moses H. W. Chan. "Microtwinning in Template-Synthesized Single-Crystal Metal Nanowires." *The Journal of Physical Chemistry B* 108, no. 3 (2003): 841-845.

Wang, Mu, Sheng Zhong, Xiao-Bo Yin, Jian-Ming Zhu, Ru-Wen Peng, Yuan Wang, Ke-Qin Zhang and Nai-Ben Ming. "Nanostructured Copper Filaments in Electrochemical Deposition." *Physical Review Letters* 86, no. 17 (2001): 3827-3830.

Wang, X. W., G. T. Fei, X. J. Xu, Z. Jin and L. D. Zhang. "Size-Dependent Orientation Growth of Large-Area Ordered Ni Nanowire Arrays." *Journal of Physical Chemistry B* 109, no. 51 (2005): 24326-24330.

Wang, Zhao, William M Mook, Christoph Niederberger, Rudy Ghisleni, Laetitia Philippe and Johann Michler. "Compression of Nanowires Using a Flat Indenter: Diametrical Elasticity Measurement." *Nano Lett.* 12, no. 5 (2012): 2289-2293.

Weinberger, Christopher R, Andrew T Jennings, Keonwook Kang and Julia R Greer. "Atomistic Simulations and Continuum Modeling of Dislocation Nucleation and Strength in Gold Nanowires." *J. Mech. Phys. Solid.* 60, no. 1 (2012): 84-103.

Weinberger, Christopher R. and Wei Cai. "Surface-Controlled Dislocation Multiplication in Metal Micropillars." *Proc. Natl. Acad. Sci. USA* 105, no. 38 (2008): 14304-14307.

Weinberger, Christopher R. and Wei Cai. "Orientation-Dependent Plasticity in Metal Nanowires under Torsion: Twist Boundary Formation and Eshelby Twist." *Nano Letters* 10, no. 1 (2009): 139-142.

Wen, Yuhua, Yang Zhang and Zizhong Zhu. "Size-Dependent Effects on Equilibrium Stress and Strain in Nickel Nanowires." *Physical Review B* 76, no. 12 (2007): 125423.

Wood, E. L., T. Avant, G. S. Kim, S. K. Lee, Z. Burchman, J. M. Hughes and F. Sansoz. "Size Effects in Bimetallic Nickel–Gold Nanowires: Insight from Atomic Force Microscopy Nanoindentation." *Acta Materialia* 66, no. 0 (2014): 32-43.

Wood, EL, T Avant, GS Kim, SK Lee, Z Burchman, JM Hughes and F Sansoz. "Size Effects in Bimetallic Nickel–Gold Nanowires: Insight from Atomic Force Microscopy Nanoindentation." *Acta Materialia* 66, (2014): 32-43.

Wood, Erin L and Frederic Sansoz. "Growth and Properties of Coherent Twinning Superlattice Nanowires." *Nanoscale* 4, no. 17 (2012): 5268-5276.

Wu, Bin, Andreas Heidelberg and John J Boland. "Mechanical Properties of Ultrahigh-Strength Gold Nanowires." *Nature Mater.* 4, no. 7 (2005): 525-529.

Wu, Bin, Andreas Heidelberg, John J Boland, John E Sader, XiaoMing Sun and YaDong Li. "Microstructure-Hardened Silver Nanowires." *Nano letters* 6, no. 3 (2006): 468-472.

Wu, Bin, Andreas Heidelberg, John J. Boland, John E. Sader, Sun and Li. "Microstructure-Hardened Silver Nanowires." *Nano Lett.* 6, no. 3 (2006): 468-472.

Wu, Hsiang-Yang, Hsin-Cheng Chu, Tz-Jun Kuo, Chi-Liang Kuo and Michael H. Huang. "Seed-Mediated Synthesis of High Aspect Ratio Gold Nanorods with Nitric Acid." *Chemistry of Materials* 17, no. 25 (2005): 6447-6451.

Yue, Yonghai, Pan Liu, Ze Zhang, Xiaodong Han and En Ma. "Approaching the Theoretical Elastic Strain Limit in Copper Nanowires." *Nano Lett.* 11, no. 8 (2011): 3151-3155.

Zhang, Han, Jie Tang, Lin Zhang, Bai An and Lu-Chang Qin. "Atomic Force Microscopy Measurement of the Young's Modulus and Hardness of Single Lab 6 Nanowires." *Appl. Phys. Lett.* 92, no. 17 (2008): 173121-173121-3.

Zhang, Jun Jie, Ji Hui Yin and Xiao Chun Ma. "Molecular Dynamics Study of Size Effect on Uniaxial Tension of Single Crystal Cu Nanowires." *Advanced Materials Research* 160, (2011): 682-686.

Zhang, Yongfeng and Hanchen Huang. "Do Twin Boundaries Always Strengthen Metal Nanowires?" *Nanoscale Research Letters* 4, no. 1 (2008): 34 - 38.

Zhao, Yuxin, Ying Zhang, Yanpeng Li and Zifeng Yan. "Soft Synthesis of Single-Crystal Copper Nanowires of Various Scales." *New Journal of Chemistry* 36, no. 1 (2012): 130-138.

Zheng, H., A. J. Cao, C. R. Weinberger, J. Y. Huang, K. Du, J. B. Wang, Y. Y. Ma, Y. N. Xia and S. X. Mao. "Discrete Plasticity in Sub-10-Nm-Sized Gold Crystals." *Nat. Commun.* 1, (2010).

Zheng, H., J. B. Wang, J. Y. Huang, A. J. Cao and S. X. Mao. "In Situ Visualization of Birth and Annihilation of Grain Boundaries in an Au Nanocrystal." *Phys. Rev. Lett.* 109, no. 22 (2012).

Zheng, He, Ajing Cao, Christopher R. Weinberger, Jian Yu Huang, Kui Du, Jianbo Wang, Yanyun Ma, Younan Xia and Scott X. Mao. "Discrete Plasticity in Sub-10-Nm-Sized Gold Crystals." *Nat Commun* 1, (2010): 144.

Zhong, Sheng, Thomas Koch, Mu Wang, Torsten Scherer, Stefan Walheim, Horst Hahn and Thomas Schimmel. "Nanoscale Twinned Copper Nanowire Formation by Direct Electrodeposition." *Small* 5, no. 20 (2009): 2265-2270.

Zhong, Sheng, Yuan Wang, Mu Wang, Min-Zhe Zhang, Xiao-Bo Yin, Ru-Wen Peng and Nai-Ben Ming. "Formation of Nanostructured Copper Filaments in Electrochemical Deposition." *Physical Review E* 67, no. 6 (2003): 061601.

Zhu, Jianwei, Daning Shi, Jijun Zhao and Baolin Wang. "Coupled Effects of Size and Uniaxial Force on Phase Transitions in Copper Nanowires." *Nanotechnology* 21, no. 18 (2010): 185703.

Zhu, Ting and Ju Li. "Ultra-Strength Materials." *Progress in Materials Science* 55, no. 7 (2010): 710-757.

Zhu, Yong, Qingquan Qin, Feng Xu, Fengru Fan, Yong Ding, Tim Zhang, Benjamin J. Wiley and Zhong Lin Wang. "Size Effects on Elasticity, Yielding, and Fracture of Silver Nanowires: In Situ Experiments." *Physical Review B* 85, no. 4 (2012): 045443.

Zong, Z, J Lou, OO Adewoye, AA Elmustafa, F Hammad and WO Soboyejo. "Indentation Size Effects in the Nano-and Micro-Hardness of Fcc Single Crystal Metals." *Mater. Sci. Eng. A* 434, no. 1 (2006): 178-187.